AI-AEC-12744
GENERAL, MISCELLANEOUS,
AND PROGRESS REPORTS

QUARTERLY TECHNICAL PROGRESS REPORT

AEC UNCLASSIFIED PROGRAMS

JULY-SEPTEMBER 1968

The preceding Quarterly Progress Report was:

AI-AEC-12721 Fiscal Year 1968

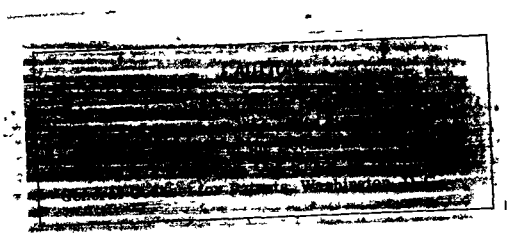

ATOMICS INTERNATIONAL

A DIVISION OF NORTH AMERICAN ROCKWELL CORPORATION

CONTRACT: AT(04-3)-701
ISSUED:

DISCLAIMER

DISTRIBUTION

This report has been distributed according to the category "General, Miscellaneous, and Progress Reports," as given in the Standard Distribution for Unclassified Scientific and Technical Reports, TID-4500.

CONTENTS

UNCLASSIFIED TOPICAL REPORTS PUBLISHED
JULY-SEPTEMBER 1968

AEC Task	AEC UC Distr	Report No.	Title	Authors
5-A	32	NAA-SR 11980	Storage of Microscopic Cross-Section Data in the AIENDF Vol II	R. F. Berland and
6-C	80	AI-AEC 12687	LMFBR Fission Product Contamination and Control Studies - A Status Report	W. P. Kunkel et. al.
8	80	AI-AEC 12572	Retirement of the Sodium Reactor Experiment	R. R. Eggleston
10-A	37	AI-AEC 12700	Evaluation of an Electrochemical Oxygen Meter	E. W. Murbach and N. W. Heath
10-C	25	AI-AEC 12694	Biaxial Stress-Rupture Properties of Austenitic Stainless Steels in Static Sodium	W. T. Lee
11-A	25	AI-AEC 12726	Self-Diffusion of uranium and Carbon in Uranium Monocarbide	G. G. Bentle and G. Ervin, Jr.
11-C	25	NAA-SR 12486	Graphite Crystal Growth	S. B. Austerman, J. M. Wagner, and S. M. Myron

R

Program: Reactor Physics		
AEC Task: 5-A, Reactor Physics, Cross Section Analysis		
Project Manager: H. A. Morewitz		
Reporting Period: July-September 1968		
General Order: 7701	Subaccount: 13130	AEC Category: 04-40-01-03.1

Principal Scientists: H. Alter, C. L. Dunford

I. PROJECT OBJECTIVES

The objectives of this project include the evaluation, production, and maintenance of an up-to-date set of basic nuclear data; production and evaluation of multigroup constants; and the improvement of present day methods of neutronic calculations as related to microscopic and macroscopic nuclear data.

To accomplish these objectives, existing experimental and theoretical information on nuclear data will be surveyed, analyzed, and compiled. Automated methods will be developed for manipulating and evaluating large amounts of available nuclear data and for the periodic updating of compiled data. Nuclear model calculations will be developed, extended, and used to help fill gaps in the data. The optical model analyses have two prime goals: to develop and test improved nuclear optical models for energy regions of interest to the fast reactor program and to develop sufficient confidence in the results of theoretical calculations so that they may be used confidently to predict neutron cross section data where no experimental data are available. An automated system will be developed and maintained for the ready production of multigroup constants, and spectra generating techniques for production of realistic multigroup constants will be developed and incorporated into the system. The objectives of this project are related to Tasks 9-1.2, 9-1.3, and 9-3.6 as outlined in the LMFBR Physics Program Plan, WASH-1109, Volume 9.

II. MAJOR ACCOMPLISHMENTS DURING FISCAL YEAR 1969

The coding and checkout of SCORE, VERSION II, was completed during this report period.

III. PROGRESS DURING REPORT PERIOD

During this report period, the recoding efforts associated with the present version of SCORE were completed. This includes an overlay structure for SCORE which allows execution with a memory size of less than 180,000 bytes. The system has been divided into five major independent segments to facilitate creation of the overlay structure. These segments are SCISRS data retrieval, SCISRS data manipulation, ENDF/B data retrieval and overlay, curve fitting, and resonance parameter analysis. In the process of recoding to create the overlay structure, many former coding inefficiencies were detected and eliminated. The presentation of information for many options was also improved. Care was taken to improve the ease with which the evaluator may use SCORE. With this objective in mind, routines were written to prevent termination of the execution of SCORE caused by input of unacceptable or incomplete data.

The graphics subroutines have been modified to handle variable address IBM 2250 buffers such as the IBM 2250 Model III. In the process of this conversion, the program was modified to increase buffer storage to 8K if available. If that much is not available, 4K is used as an alternative. The extension to 8K buffer allows more data points to be displayed at one time; however, it has been noticed that some picture flutter is introduced when a large number of data points is plotted due to the increase in display generation time.

Documentation for the present version of SCORE continues. As soon as the documentation is complete, the code will be deposited in the Argonne Code Center. A working version of SCORE has been sent to AWRE Aldermaston at their request. We hope to obtain useful feedback from Aldermaston as well as other potential users of the SCORE data evaluation system.

During this report period, the efforts associated with the ENDF/B Phase II data testing were concentrated in two areas: one area dealt with converting ENDF/B microscopic data into the AIENDF format, processing this data with the AI multigroup codes GRISM and AILMOE, and calculating required parameters with the diffusion theory code CAESAR; the other area involved the direct use of the ENDF/B data tapes, the processing codes DAMMET, ETOE, and MC^2 to produce multigroup constants for use in the diffusion theory code CAESAR. The former method has been successfully applied to the analysis of

ZPR-3-48, the latter method has not been carried to completion because of problems in the MC^2 calculation.

Preliminary results for the analysis for the ZPR-3-48 "Benchmark" calculation (Phase II data testing) are given in Table 1. Problem specifications were essentially those outlined by W. G. Davey in his letters of June 21 and August 30, 1968, with the following exceptions.

1) Multigroup libraries were generated with GRISM. A concurrent effort involving ENDF/B data files directly, DAMMET, ETOE, and MC^2 has not as yet been completely successful.

2) Plutonium 242 was omitted; there is only a small fraction present and the CAESAR diffusion theory code is presently number of isotope limited to 20.

3) Aluminum data was used in place of magnesium for silicon.

4) Ten groups of down-scattering were used.

5) A temperature of 300°K was used for all resonance calculations.

6) The CAESAR convergence criterion was 0.00002; the calculation would not converge with $\epsilon = 0.00001$.

The partial results obtained to date are compared with the corresponding experimental values in the following table.

TABLE 1

COMPARISON OF CALCULATED AND MEASURED PARAMETERS FOR THE ZPR-3-48 (Data – ENDF/B; Processing Code – GRISM, AILMOE, Diffusion Theory Code CAESAR)

Quantity	Calculated	Experimental
K	0.9758	1.0
F24/F25	0.199	0.204
F26/F25	0.0697	0.0670
F/28/F25	0.0322	0.0307
F49/F25	0.928	0.976
F40/F25	0.234	0.243
C28/F25	0.145	0.138
C(Boron-10)/F25	1.295	-

The concurrent effort involving the updated ENDF/B data tapes (numbers 114, 115, 116, and 117), and the processing codes DAMMET, ETOE, and MC^2 has not as yet been run successfully. The data tapes were processed by the latest version of the DAMMET code which was made operational on the Control Data Corporation 6600 computer. A large list of isotopic data was placed on magnetic tape in Binary Mode 2. The latest version of the ETOE code was made fully operational and was used to process several isotopes to check out the program. A number of programming changes were necessary to make the program operational on the CDC computer. A library of isotopes needed for the analysis of ZPR-3-48 and ZPR-3-11 were processed by using the ETOE code. This microscopic data library will be fed into MC^2 when it is made operational. MC^2 punched card output will be processed into multigroup libraries for use in Atomics International diffusion theory codes via a routine that has been written.

All data and format errors for natural copper and its two principle isotopes, thus far detected by the various ENDF/B checking codes, have been corrected. A final check, including the automated plotting of the pertinent ENDF/B data files, disclosed additional errors which are currently being corrected. A rough draft of a report documenting the copper data has been completed.

IV. EVALUATION OF EFFORT TO DATE

The recoding and optimizing of the SCORE program to allow execution in a core memory of approximately 180,000 bytes eliminated the major objection of too large a core storage, thus allowing for wider program use. In the process of recoding to create the present overlay structure, many former coding inefficiencies were eliminated and the presentation of information for many options improved. An overall result is that, for the data evaluator, the ease with which he uses SCORE has been enhanced.

In the ENDF/B Phase II data testing, a dual benchmark testing effort is underway. One route is the DAMMET-ETOE-MC^2 diffusion theory procedure (in use by ANL and LASL); the other involves the generation of data tapes in the AIENDF format from the ENDF/B tapes, then processing with the AI codes

GRISM and AILMOE to produce multigroup sets for the diffusion code CAESAR. Initial results from CAESAR give k = 0.976 which is in reasonable agreement with results from ANL, k = 0.973 and LASL, k = 0.970. Both of the latter results were obtained by using DAMMET-ETOE-MC^2 as the processing mechanism. Thus, for the first time since the beginning of ENDF/B data testing, a degree of consistency has developed in the task of data evaluation and testing.

V. NEXT REPORT PERIOD ACTIVITIES

Documentation for SCORE and for the evaluation of copper and its principle isotopes will be completed. The testing of ENDF/B data on ZPR-3-48 and ZPR-3-11 will be completed, and the evaluation of critical assemblies, yet to be specified by the data testing subcommittee of CSEWG, will be continued.

Program:	Civilian Power, LMFBR		
AEC Task:	5-B, Reactor Physics, Fast Reactor Physics Experiments		
Project Manager:	H. A. Morewitz		
Reporting Period:	July-September 1968		
General Order: 7701	Subaccount: 14610	AEC Category: 04-01-61-02.1	

Principal Investigators: T. H. Springer, R. J. Tuttle, H. N. Royden

I. PROJECT OBJECTIVES

The objectives of this project are to (a) determine reactivity, temperature, and Doppler coefficients of various materials in a variety of fast reactor spectra, (b) investigate effects due to different geometric arrangements of such materials, including the variation of the surface-to-mass ratio, (c) provide experimental results for the purpose of checking theoretical predictions, and (d) develop improved experimental and theoretical methods for treatment of problems in the field of fast reactor physics. The objectives of this project correspond to Task 9-2 of the LMFBR Program Plan Section 9 (WASH-1109).

II. MAJOR ACCOMPLISHMENTS DURING FISCAL YEAR 1969

The interaction of a heated blanket with a heated sample has been measured in an LMFBR spectrum and shown to be small, thus justifying small-sample Doppler coefficient measurements.

The temperature coefficient of reactivity of a U^{235} sample was found to be positive but small in Core 17.

III. PROGRESS DURING REPORT PERIOD

Experimentation is continuing in ECEL Core 17. The test region of this core, which includes sodium, provides a spectrum (U-235/U-238 median fission energy = 94 kev) simulating that of a typical sodium-cooled, oxide-fueled FBR.

The temperature coefficient of reactivity for a series of samples placed in blankets of similar and dissimilar materials (See Table 1) have been measured. The results are similar to those obtained in the relatively soft spectrum of

Core 15 (18 kev U-235/U-238 mfe), although the magnitude of the effect as measured in Core 17 is somewhat reduced as a result of the harder spectrum: typically, the change in reactivity in the sample between two arbitrary temperatures in the interval from 20 to 800°C is 10% less when a blanket of the same material is heated than when the blanket is at room temperature.

TABLE 1

HEATED BLANKET EXPERIMENT

Sample	Blanket	Temperature (°C)
Th	Th	20
Th	Th	400
Th	U^{238}	20
Th	U^{238}	400
U^{238}	Th	20
U^{238}	Th	400
U^{238}	U^{238}	20
U^{238}	U^{238}	400
U^{238}	U^{235}	20
U^{238}	U^{235}	400
U^{235}	U^{235}	20
U^{235}	U^{235}	400
U^{235}	U^{238}	20
U^{235}	U^{238}	400
$U^{235}O_2$	U^{235}	20
$U^{235}O_2$	U^{235}	400

A measurement of the temperature coefficient of U^{235} metal in the unperturbed Core 17 yielded a slightly positive value; that is, the sample becomes more reactive as the temperature increases. Inasmuch as the expansion coefficient of reactivity of U^{235} is probably negative in this spectrum, a decidedly positive Doppler is inferred. (From a practical standpoint, however, a typical FBR fuel element would have a negative coefficient of reactivity since it contains a large fraction of U^{238}.) Temperature-coefficient measurements were also done with three PuO_2 samples having different isotopic compositions.

An extensive series of measurements of the central flux spectrum was conducted with proton-recoil counters. Variations in the position and the surrounding material were made to determine the effect of these variables on the measured spectrum. The results show good agreement with those of the AILMOE calculations. Details are discussed in the Integral Reactor Physics Experiments section of this report (Task 5-D).

Preliminary calculations on the feasibility of measuring reactivity effects of burnup in irradiated samples indicate that total reactivity changes in samples with burnups of the order of 2% are readily measurable and that the fission-product contribution can probably be determined from auxiliary ECEL measurements on U-235 and U-238 samples, and an independent burnup determination.

Detailed analyses of past and proposed measurements of the effective capture-to-fission ratio in fast reactor critical assemblies are proceeding. Preliminary results indicate that the method used by Adamson et al (ZEBRA-6) and Andersson et al (FRO-5, 8) is very sensitive to errors in the basic data used in calculating the several correction factors. Since errors in these correction factors are correlated through the flux calculations, quadratic combination of individual estimated errors is not appropriate. For example, the uncertainties in the FRO measurements due only to the calculated corrections are indicated by this analysis to be approximately twice that quoted as the total experimental uncertainty.

TRIX calculations for U-238 using the new unresolved-resonance routine were compared with the optical-model calculations of Dunford. Identical nuclear parameters were used in both calculations. The TRIX results ranged between 0 and 11% higher than the optical-model results between 1 and 100 kev. Detailed analysis showed that the discrepancy is due primarily to contributions from neutrons with angular momenta greater than zero. Above the inelastic level at 45 kev, the $\ell = 0$ and $\ell = 2$ contributions fall more rapidly in the TRIX results; whereas, the slopes of the $\ell = 1$ contribution are nearly the same. A more sophisticated approach to the calculations of the $\ell = 0$ angular-momentum barrier penetrability and outgoing inelastic-scattering width is being taken to reduce the discrepancies.

Correction of the nuclear unit radius used by the TRIX code for calculating penetrabilities for neutrons with orbital angular momentum greater than zero has produced good agreement between TRIX and optical-model calculations on U-238 below the first inelastic level. A model for the inelastic-scattering level width, which sums over each outgoing channel using the correct penetrability, was coded for TRIX and is being checked out.

Three new boron reactivity samples were prepared, and these and older samples were neutron radiographed to determine the actual dimensions. These samples will be used to measure the infinitely-dilute boron reactivity.

Central worths were measured for a number of samples of fissile, fertile, coolant, control, and structural materials. These included U-235 (7 different surface/mass ratios), PuO_2 (3 S/M's), Th, Na, C, Li-6, Li-7, Ta, W, stainless steel, Nb, Al, and Inconel. For the fissile samples, the variation of reactivity with S/M is needed to determine the thermal-expansion part of the temperature coefficient of reactivity; for tantalum, this variation provides potentially useful information on control-rod worth. Lithium, tungsten, and niobium are possible coolant or structural materials in thermionic reactors. Aluminum and Inconel are structural materials used in our experiments.

IV. EVALUATION OF EFFORT TO DATE

The measurements in heated blankets provide a basis for estimating hot reactor hot-sample effects. Techniques for measuring flux spectra with proton-recoil counters in this reactor have been successfully developed. Progress has been made towards extending the current experimental techniques to measurements of burnup effects and the effective capture-to-fission ratio. Modifications to the TRIX code have further improved calculations of resonance self-shielding.

V. NEXT REPORT PERIOD ACTIVITIES

Additional Doppler-effect and reactivity measurements will be made. Measurements of neutron importance will be made with a spontaneous fission source and three photoneutron sources, if these sources are ready. Reaction rate measurements will be made with boron-10 and lithium-6 counters. The analysis of capture-to-fission ratio measurements will be completed.

Program:	General Reactor Technology		
AEC Task:	5-D, Reactor Physics, Integral Experiments		
Project Manager:	H. A. Morewitz		
Reporting Period:	July-September 1968		
General Order: 7701	Subaccount: 13210	AEC Category:	04-40-01-02.1

Principal Investigator: R. K. Paschall

I. PROJECT OBJECTIVES

The purpose of the fast reactor physics program is to supply data pertinent to both the safe and economic design and operation of fast power reactors. Safety and economics often compete in good reactor design and very conservative estimates are usually made in the area of safety because of the paucity of precise physics data. This program is designed to study these specific areas and confirm the nuclear parameters and calculational methods used on conceptual evaluation and preliminary design.

The large volume of coolant (50%) and structural material (15%) in current fast reactor designs make increasingly important the accurate knowledge of light element scattering cross sections which affect the magnitude of both the Doppler and sodium-void effects. Also of concern is the resonance shielding for various mixtures of the light elements.

A series of integral experiments are being performed using coolant material (sodium) and the predominant structural material (iron). The measurements seek to determine the differential neutron spectrum in large volumes of sodium, in a large quantity of pure iron, and in appropriate mixtures of these materials, for both isotopic and reactor neutron sources. The resulting neutron spectra will be compared to predictions based on Monte Carlo calculations in order to check the scattering cross sections presently used. The use of a reactor as a neutron source will allow, in addition, reactivity measurements of the sodium void as well as direct studies of spectral changes occurring during this voiding. The objectives of this project correspond to Task 9-2.11 of the LMFBR Program Plan, Section 9 (WASH-1109).

II. MAJOR ACCOMPLISHMENTS DURING FISCAL YEAR 1969

1. Analysis of the proton-recoil neutron spectrum measurements in a large volume of sodium was completed.

2. Analysis of the proton-recoil neutron spectrum measurements in a large volume of sodium and stainless steel was completed (Task 24b).

3. Calculations (using the ANISN and MODISK codes) for experiments (1) and (2) were completed and good comparisons were obtained between measured and calculated data.

4. Proton-recoil spectrum measurements were completed in the center of ECEL reactor core 17.

5. A study of the neutron energy distribution in a beam of neutrons emanating from a 2-in. by 2-in. square hole in ECEL core 17 extending along a radius from the core center outward was performed by using a series of polyethylene, paraffin and lead shields, and collimators. Over the energy range ~90 to 400 kev, good agreement with the spectrum measured at the core center was found, although the magnitude was lower by several orders.

III. PROGRESS DURING REPORT PERIOD

a. NEUTRON SPECTRA IN SODIUM AND IN Na, SS, Fe-Ni ASSEMBLIES

Analysis of the proton-recoil neutron spectrum measurements in the large volume of sodium was completed. Figure 1 shows the experimental arrangement. Ten slabs of sodium, each 12.5-in. thick (12-in. of Na between 0.25-in. Al walls) by 5-ft^2 were stacked together to give a volume 125-in. thick by 5-ft^2. A 24-in. diameter fission plate between the 5-ft^2 graphite thermal column of the STIR reactor and sodium provided the fission neutrons. Two lead plates 1-in. thick by 5-ft^2 were placed between the fission plate and the sodium. This attenuated the gamma flux without changing the neutron spectrum by any measurable amount. The spectrometer detectors were located in the center of one of the slabs which has a 2-in. diameter by 36-in. deep hole in it. This slab was interchanged with the others to allow the detectors to be placed with 15.9, 79.4, 142.9, 206.4, and 269.9 cm of sodium and aluminum between them and the fission plate.

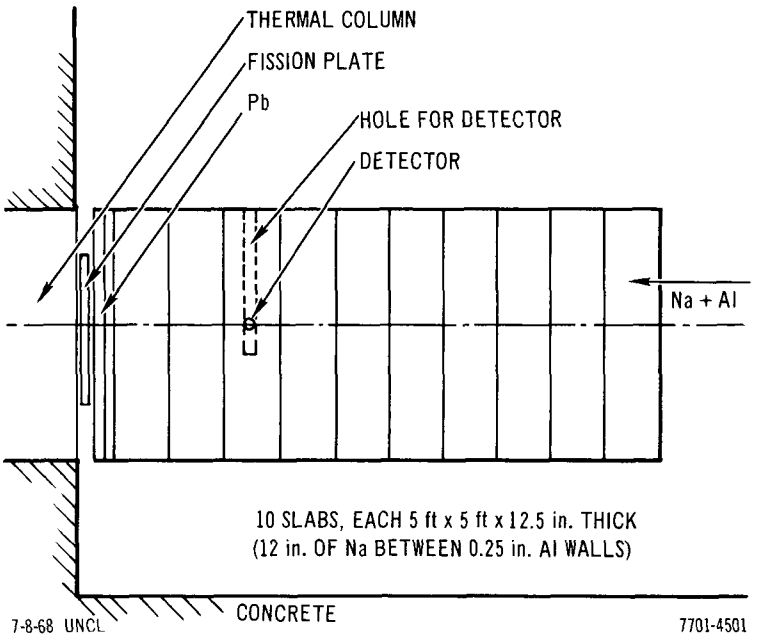

Figure 1. Experimental Arrangement for Neutron Spectrum Measurements in Sodium

New calculations were completed by using the ANISN and MODISK codes. A group structure was used with $\Delta\mu = 0.693$ for most of the groups from 10^{-8} to 10 Mev. The neutron cross sections were updated for these groups and weighted with spectra obtained from AILMOE calculations. Aluminum, used to contain the sodium, was included in the calculations. Figure 2 shows the measured and calculated results. The agreement is satisfactory, but the calculations are generally lower than the measurements, with the difference increasing with distance from the fission plate.

A detector filled with 1 atm of hydrogen was used to obtain data from 1 to 300 kev. Two parameter analysis was needed to separate the gamma background from the neutron events below 60 kev. If the gamma to neutron ratio was too large, useful results could not be obtained below about 6 kev (as was the case in the 1st, 7th, and 9th slabs). Some data were taken with a detector filled with 1 atm of methane (and some He^3 added for calibration with slow neutrons). These data, at least up to 600 kev, were satisfactory in the first sodium slab. Poor results were obtained in the other slabs because of too many slow neutron interactions with the He^3 (even though the detector was cadmium covered).

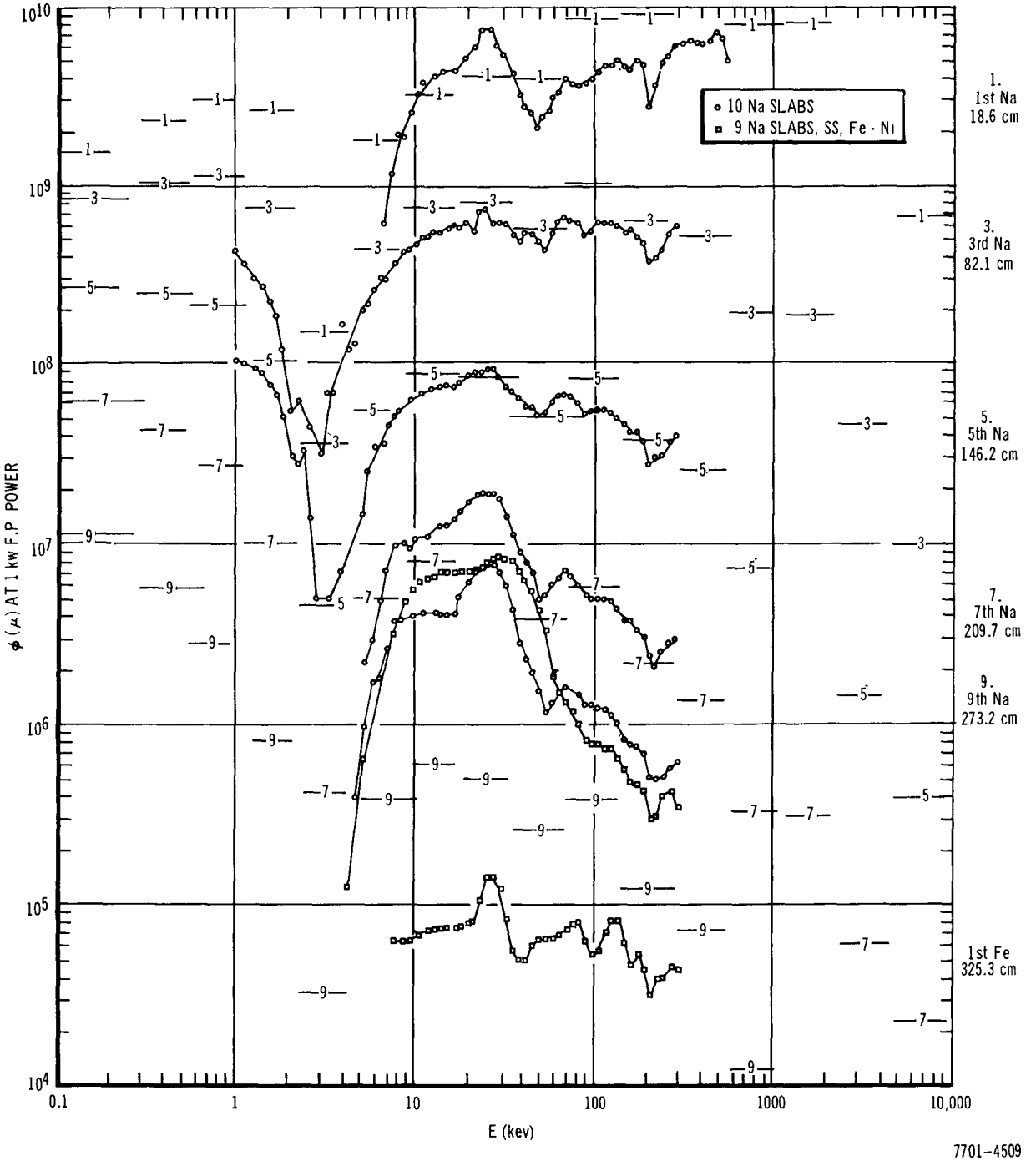

Figure 2. Neutron Spectra in Na, SS, and Fe-Ni Assemblies

Additional proton-recoil spectrum studies which were carried on under the sponsorship of the general FBR portion of the FFTF shielding program (Task 24b) were performed using the techniques and procedures developed in this program. The work, which utilized the same large slabs of Na but included additional slabs of stainless steel and iron/nickel is included in this report for the sake of completeness as well as to illustrate the state of development of the proton-recoil spectrometer.

An arrangement was made of 9 sodium slabs followed by 12-in. of stainless steel slabs followed by 21-in. of an iron-nickel slab mixture. Some shielding was placed behind and along the sides of the arrangement to remove the room return neutrons. Spectrum measurements were made in the 9th Na slab (273.2 cm from the source) and in the 1st Fe-Ni slab (325.3 cm from the source). The results are shown in Figure 2. Associated foil measurements, however, showed that room-return background was a very significant fraction of the measured results. Therefore, a new arrangement was made with only 5 sodium slabs followed by the metal mixture. Also, considerably more shielding was added all around the assembly. Then, spectrum measurements were made in the 5th Na slab (146.2 cm from the source) and at 167.8, 184.3, 198.3, and 228.8 cm from the source in the metal. A detector filled with 2.63 atm of methane (and 5% N_2 for calibrating) was used to obtain data to 1.2 Mev. The N_2 was much more satisfactory than He^3 for a calibrating gas where epicadmium neutrons were present.

Calculations,* similar to those for the pure sodium, were made for the sodium-steel mixture. Originally, the steel cross sections were weighted with the AILMOE spectra calculated for sodium. This, however, caused the calculations to deviate from the measurements by as much as a factor of 40 in the farthest detector position. When the steel cross sections were weighted with AILMOE spectra calculated in iron, the results shown in Figure 3 were obtained. The agreement with measurements was considerably improved. Figures 4, 5, and 6 show the neutron attenuation through the 10 sodium slabs; and through the 5 Na slabs, SS, Fe-Ni combination at 13, 106, and 840 kev, respectively. Although the magnitude differs between the measurements and

*Supported by North American Rockwell

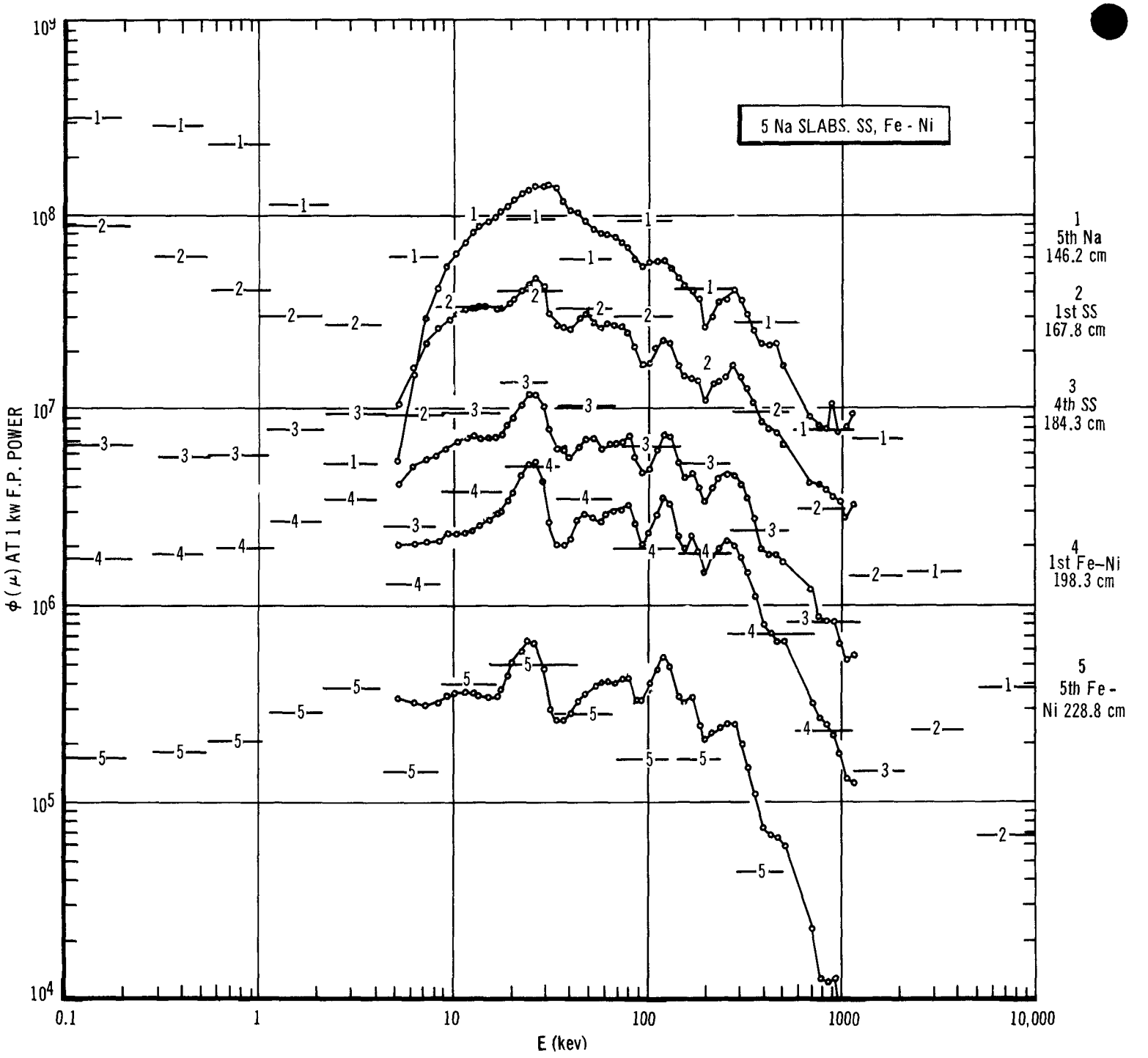

Figure 3. Neutron Spectra in Na, SS, and Fe-Ni Assemblies

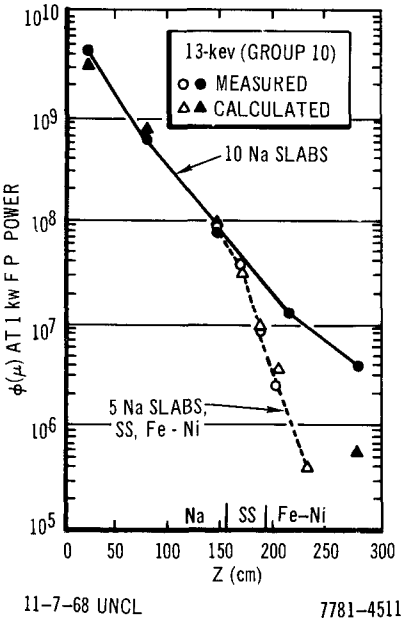

Figure 4. Neutron Attenuation in Na, SS, and Fe-Ni

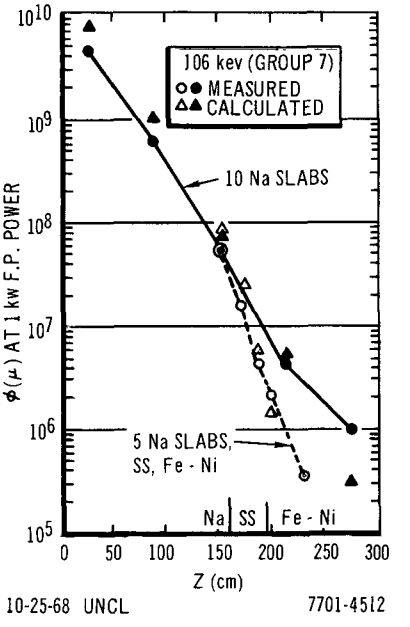

Figure 5. Neutron Attenuation in Na, SS, and Fe-Ni

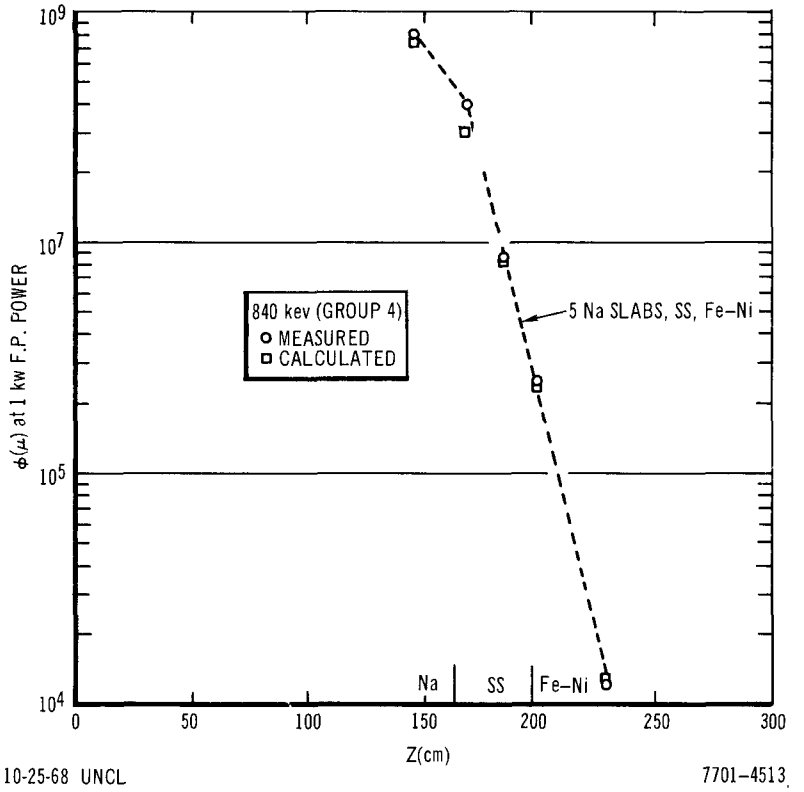

Figure 6.

Neutron Attenuation in Na, SS, and Fe-Ni

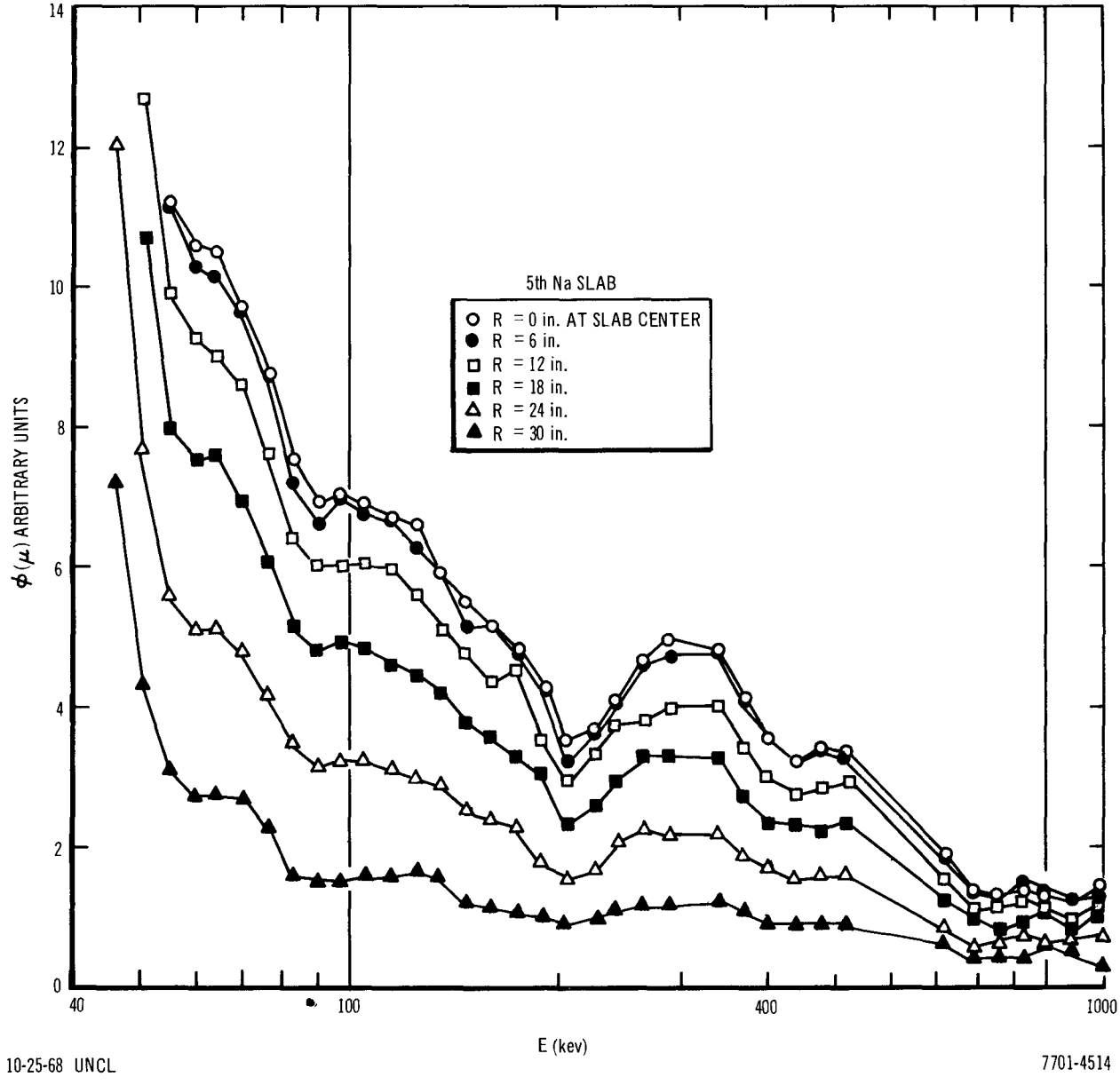

Figure 7. Neutron Spectra, Vertical Traverse

calculations, the slopes of the curves are quite similar. The worst divergence appears in the steel at 106 kev. It must be noted that measurements in the 5th Na slab followed by steel were much higher than when followed by more sodium. This is unexplainable at this point. Therefore, to provide continuity, all the data from the 5 Na slabs, SS, Fe-Ni were multiplied by 0.6 before plotting (Figures 3, 4, 5, and 6) and comparing with results from the sodium only measurements and calculations.

In the arrangement of 5 Na slabs, SS, Fe-Ni spectra were measured in the 5th Na slab from the center to the top at 6-in. intervals to determine the transverse distributions. This provided data for comparison with calculations on transverse leakage and a check on the wall scattered inleakage in the assembly. All the results are shown in Figure 7. Radial plots for 60 and 100 kev are shown in Figure 8. Since there is no significant upturn of the curves at R = 30-in. (top of the sodium slab), it appears that the shielding to eliminate room return neutrons is adequate, at least at these neutron energies.

A paper, "Neutron Spectra Measurements in Sodium and Stainless Steel," by R. K. Paschall was accepted for presentation at the 1968 Winter International Meeting of the American Nuclear Society in Washington, D.C.

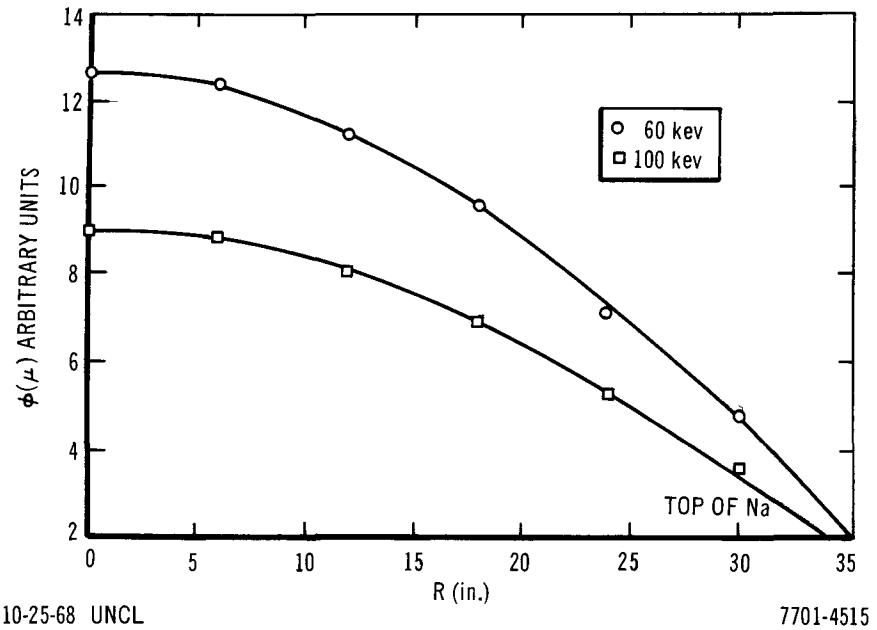

Figure 8. Neutron Spectra, Vertical Traverse

B. NEUTRON SPECTRA IN ECEL REACTOR CORE 17

Proton-recoil spectrometer measurements were completed in the ECEL reactor Core 17. Data analysis remains to be completed. Data were taken with 5 different detector gas fillings, 0.5 atm H_2; 1.0 atm H_2, 2.63 atm H_2 + 0.263 atm CH_4, 2.63 atm CH_4, and 8.1 atm CH_4. Those with more than 1 atm also had 5% N_2 included for calibration with the thermal neutron interaction, N(n, p)C. The reaction fragments ionize the gas and produce an ionization equivalent to that originated by a 615 kev neutron. These gas fillings allowed one-parameter data to be taken from approximately 30 to 2.25 Mev.

Additional measurements were made to determine the effect of lead around the detector. Also, the effect of positioning the detector off center was examined. Measurements made in the center with no lead were compared with measurements made 5-in. off center with lead around the detector; no difference was observed. Then, with lead around the detector, 5-in. off center, some fuel was removed from four adjacent drawers and additional lead pieces 1-in. thick, 2-in. wide, and 6-in. long were placed above, below, and on either side of the detector. A decrease of 8 to 10% was noted in the flux. This was probably caused by the removal of the fuel rather than by the Pb effect. The one-parameter spectra measured with this arrangement is shown in Figure 9 with the calculations (multiplied by 0.834) included for comparison.

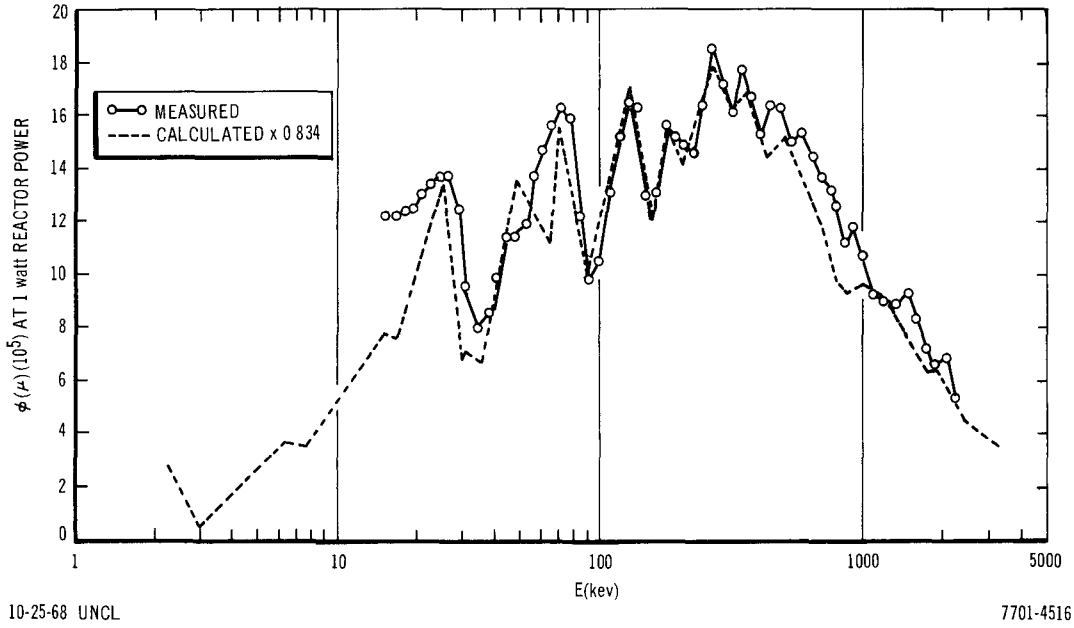

Figure 9. Neutron Spectra in ECEL Reactor

C. NEUTRON SPECTRA OUTSIDE OF THE ECEL REACTOR CORE 17

A proton-recoil detector was placed outside the ECEL reactor Core 17, surrounded with lead and paraffin except in the direction looking down an empty 2-in. square hole into the center of the core. Spectrum measurements were made with several arrangements of lead and paraffin. As much as a 13 to 1 ratio (foreground to background) was obtained at some energies. The background spectra (obtained by inserting 12-in. of paraffin in front of the detector in the 2-in. square hole) showed little similarity to the shape of the foreground. Some results are shown in Figure 10.

IV. EVALUATION OF EFFORT TO DATE

Analysis of the neutron spectrum measurements in sodium and in Na, SS, Fe-Ni assemblies was completed and comparisons were made between measurements and with calculations. Detectors with new gas fillings were used and a two-parameter analysis was employed to discriminate against gamma background. Data is shown from 1 kev to 1.2 Mev. Fair agreement in the slope of the attenuation at most energies was obtained between measurement and calculation. More work needs to be done to improve the agreement in magnitude and slope at some energies.

Spectrum measurements in the ECEL reactor Core 17 using newly filled detectors allowed data to be taken to 2.25 Mev. The effects of lead shielding seems to be negligible. Test region spectra measured outside the core show the same resonance structure as those measured in the core center.

V. NEXT REPORT PERIOD ACTIVITIES

Analysis of the spectrum data taken in the ECEL reactor Core 17 and in the beam outside of the core will be completed. A more complete study of the characteristics of the different detector fillings will be made.

A new series of spectrum studies will be performed in Core 18 which will be identical to Core 17 except that all of the cans containing Na and NaF will be removed and replaced by empty cans. In addition, the spectrum shift, if any, which occurs as a result of installing a small pin-type zone at the center of core will be investigated.

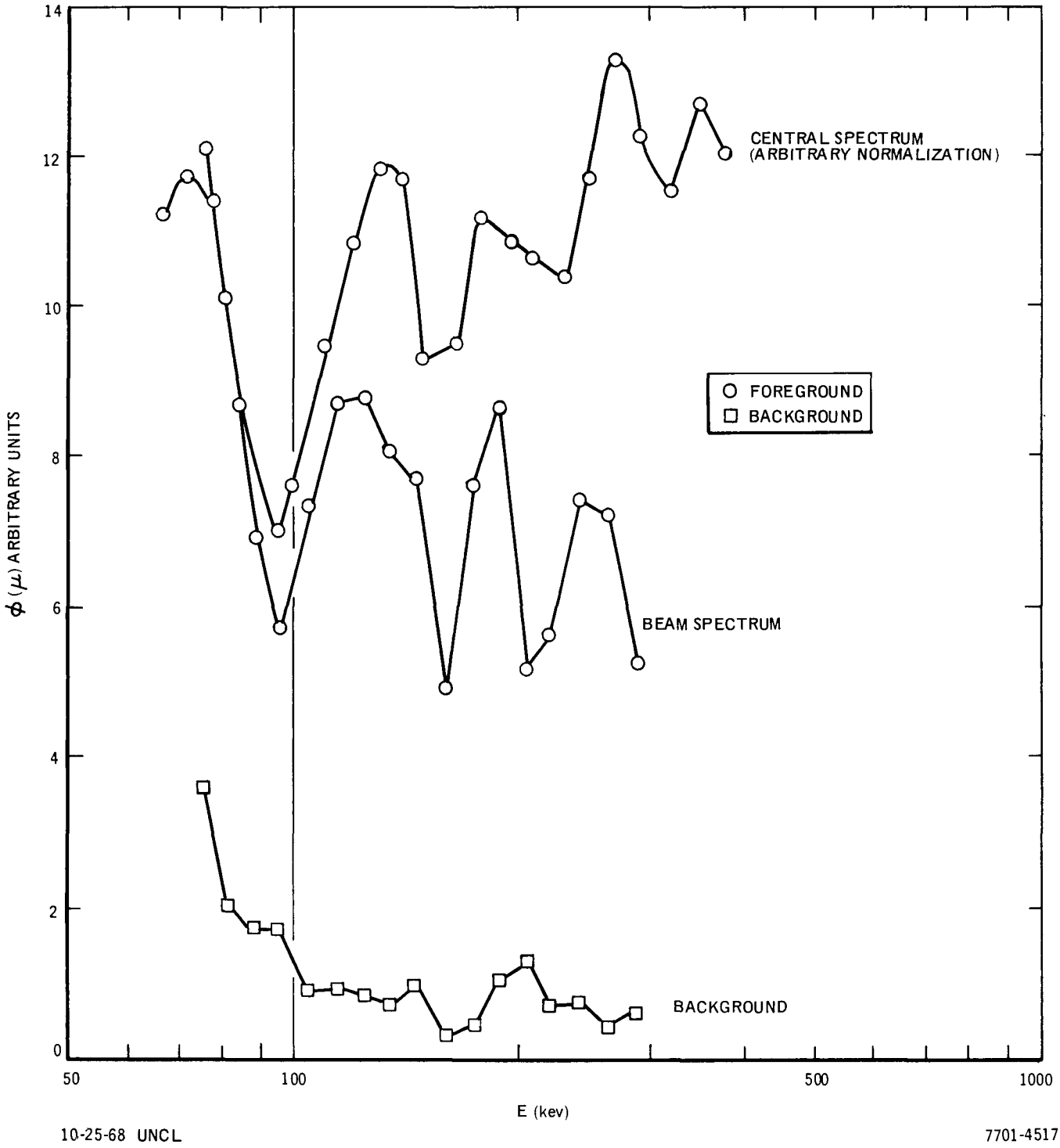

Figure 10. Neutron Spectra of ECEL With Detector Outside of Core

Program: Reactor Physics
AEC Task: 5-E, Fast Reactor Monte Carlo Methods
Project Manager: H. A. Morewitz
Reporting Period: July-September 1968
General Order: 7701 Subaccount: 14320 AEC Category: 04-01-61-02.1

Principal Scientist: L. B. Levitt, J. Spanier

I. PROJECT OBJECTIVES

The basic objective of this project is to advance the state of the art of Monte Carlo applications to the analysis of fast reactors and fast critical assemblies. This development is needed so that experimental programs as well as design studies may be optimized through the use of computer programs capable of describing complicated geometric configurations while calculating the effects of localized perturbations. These objectives will manifest themselves in the ultimate development of fast reactor criticality codes and specialized codes to treat perturbations due to changes in temperature, density, and material composition. The objectives of this project are related to Tasks 9-3.3 and 9-4.5 outlined in WASH-1109, LMFBR Program Plan, Volume 9, Physics.

II. MAJOR ACCOMPLISHMENTS IN FISCAL YEAR 1969

Not applicable.

III. PROGRESS DURING REPORT PERIOD

Progress was made in several areas related to the fast reactor Monte Carlo code VIM. The format in which the neutron cross section data will be utilized by the VIM code has been determined; a model for treating the inelastic scattering from discrete levels has been coded; a geometric description scheme for fast critical assemblies was developed; and coding of a scheme for geometry input has begun.

One of the problems facing a Monte Carlo criticality calculation is that the spatial distribution of fission neutrons is not known, except for a few special cases. This necessitates using a self-generating type of source selection procedure, so that in the limit of a large number of histories, the spatial

source coordinates chosen would be distributed very similarly to the distribution of neutrons in the actual physical case. A preliminary version of a self-generating type of source routine for use in VIM has been coded for fast critical assemblies.

A joint paper by Spanier and Levitt, which was prepared for journal publication, will formally describe the new adjoint techniques developed during last fiscal year and relate them to previously published work by Spanier and Gelbard. This paper shows specifically how the new work may be regarded as a generalization and extension of the earlier work to nonmultigroup nonthermal systems.

Material for a topical on the adjoint Monte Carlo work performed last fiscal year is now being prepared. It will encompass the descriptions presented to the ANS in Toronto and, in addition, will contain details of the Monte Carlo random walk generated in an adjoint simulation including specific tallying procedures, intercomparison of relative variances of alternative tallying procedures, and a detailed description of results obtained using the STRIFE code as well as a code description of STRIFE.

IV. EVALUATION OF EFFORT TO DATE

The work performed in this quarter on the VIM code has been basically the necessary structural setup of a major fast neutron Monte Carlo code. No major difficulties have been encountered.

The full criticality version of the VIM code will require a large present generation computer (an IBM 360-75 or a CDC 6600) since it has become clear that the computer core storage required will be in the neighborhood of 100,000 words. This does not preclude development of later versions of the code requiring less core storage as a result of compromises made possible by judicious selection of energies at which cross sections are to be tabulated. It is felt, however, that the first effort should be in obtaining a working direct Monte Carlo criticality code which can serve as a standard in evaluating fast critical assemblies. Given this decision, the coding of the cross section and reaction routines in the neutron history portion of the code has proceeded smoothly.

Resolution of formal difficulties in linking the adjoint Monte Carlo work developed under this contract and previous work developed primarily at Bettis by Spanier and Gelbard has lent considerable confidence and significance to these adjoint techniques. Incorporation of these techniques into the VIM code cannot take place until satisfactory procedures for handling ineleastic scattering in the adjoint mode have been developed. Since the initial effort is in developing a criticality estimator and since the primary utility of an adjoint calculation is in the area of estimating reaction rates in small physical regions, it is felt best to defer this work until the development of a fixed source version of VIM which will handle the latter type of problem.

V. NEXT REPORT PERIOD ACTIVITIES

The structural details of the neutron history portion of the code will be completed. Tallying and estimation procedures which will result in the maximum variance reduction possible in a relatively general code will be incorporated. The use of several simultaneous estimation procedures will be permitted so that an estimate based on a linear combination of estimators will be obtained.

This is advantageous since it is now accepted that such an estimate will have lower variance than any estimate making use of only a single type of estimation procedure.

The journal article will be completed and submitted for publication and the topical report on adjoint procedures will be written.

Program:	Reactor Development
AEC Task:	6-D&E, Nuclear Safety, Gaseous Effluents, Sodium Fires
Project Manager:	H. A. Morewitz
Reporting Period:	July-September 1968
General Order: 7702	Subaccount: 31111 AEC Category: 04-60-40-04.1

I. PROJECT OBJECTIVES

The general objective of this project is to develop experimental information and analytical methods which characterize the release and transport of effluents and energy generated during major LMFBR sodium accidents. The source of energy generation may be from the escaping coolant, by rapid thermal energy transfer, and/or by combustion of the sodium coolant. The effluents may be sodium (as Na 24) or its oxide, fuel materials, and fission products available as potentially serious dispersions of radioactivity. The information to be developed is required for the design and safeguards analysis of economical, sodium-cooled, fast reactors. The objectives of this project correspond to those of Task 10-2.6 and 2.7 of the LMFBR Program Plan, Section 10 Safety (WASH 1110). The results and technology obtained from this project are being applied for the safety analysis and engineered safeguards design for the FFTF.

II. MAJOR ACCOMPLISHMENTS DURING FISCAL YEAR 1969

Activation of the Phase II large fire modeling test chamber was completed and an initial sodium pool fire experiment was successfully conducted in the chamber.

Four papers were presented at the IAEA Symposium on Operation and Developmental Experience in the Treatment of Airborne Radioactive Wastes, being held in New York, August 26 through 30, 1968.

1. L. Baurmash, C. T. Nelson, and R. L. Koontz, "The Characterization of UO_2 Aerosols by Aerodynamic Parameters"
2. C. T. Nelson, R. L. Koontz, and M. Silberberg, "The Characterization of Sodium Spray Aerosols"

3. R. L. Koontz, C. T. Nelson, and L. Baurmash, "Model Characteristics of Aerosols Generated During LMFBR Accidents"
4. R. L. Koontz, D. F. Hausknecht, and H. A. Morewitz, "The Use of Agglomeration Modeling in Determining the Source Term for Reactor Siting Evaluations"

III. PROGRESS DURING REPORT PERIOD

A. FUNDAMENTAL EXPERIMENTS

1. Spray Fires

Two additional experiments have been performed in the Spray Test Vessel (STV), increasing the number of experiments to four. All tests, except the first, have been performed using the same spray nozzle. Test 3 was performed in a pure argon environment to provide a means of characterizing the liquid sodium spray. Thus, only liquid sodium remained airborne. Most of the liquid sodium fell out during the spray time (~7 sec). The concentration of sodium remaining airborne after the spray was only 1.2 μgm/cc although an equivalent 92.5 μgm/cc was released as liquid sodium. Following the spray period, the particle size distribution was measured with impactors. Particle growth was observed. The floor deposition half time was 15 min which is equivalent to an aerodynamic radius of 4.4μ. Since AER = $\sqrt{d} \cdot r_{50}$ and the density of sodium is near 0.9 gm/cc, the mean size of the particle which settles, by mass (r_{50}) is, is 4.6μ. It may be inferred from Test 3 that a large mass of hot liquid sodium sprayed into a closed volume with 0% O_2 rapidly falls so that the sodium concentration which remains airborne is negligible.

STV Test 4 produced the highest concentration of aerosol remaining airborne following the spray. The consumed O_2 was also increased to 1.8% and the measured pressure rise was 20 psig. Only a partial analysis of the data has been made but some of the results are available and are listed below.

1) The initial air concentration, 1/2 min after the spray, was 66 μgm/cc (if a uniform concentration is assumed). The average obtained from three different heights is ~40 μgm/cc.

2) Very rapid fallout occurred since the air concentration decreased with an initial half time of 1.5 to 2.5 min.

3) Released into the chamber, was 60 gm of sodium. If Na_2O_2 is produced, 24.5 gm of Na is oxidized per % O_2 consumed in the chamber. Since 1.8% O_2 was used, only 44.5 gm of the 60 gm would be oxidized. The computed ΔP is 16.5 psig vs 20 psig measured, if ~45 gm of sodium is oxidized to Na_2O_2. However, if the monoxide (Na_2O) is produced, 49 gm of Na is oxidized per % O_2; therefore, all of the sodium could have been oxidized (1.8 x 49 = 88.5 gm Na), there being only 60 gm of sodium available.

   Some mixture of the monoxide and peroxide probably was produced. No unoxidized sodium was found in the chamber after the test, therefore only an estimate of the amount of each compound could have been made.

4) By utilizing a high speed recorder, the rate of decrease of the oxygen percentage was observed during and after the spray period. In 2.7 sec, 50% of the oxygen was consumed, and the fractional rate of consumption decreased exponentially for about 10 sec, after 85% of the total consumed O_2 had been used up.

No exact estimate of the spray time has been made. This time is controlled by a timer which has been calibrated by using water as the spray fluid. The spray time for Test 4 was computed to be 7 sec, but the timer allowed the valves to remain open for 20 sec. The rate of decrease of the oxygen can be used to estimate the burning rate by the following logic. The time constant for oxygen decrease is

$$\frac{0.69}{\text{half time}} = \frac{0.693}{2.7 \text{ sec}} = K\left(\frac{\text{lb } O_2}{\text{hr - ft}^2 \text{ - \% } O_2}\right)\left[\frac{A(\text{ft}^2)}{3600 \frac{\text{sec}}{\text{hr}} \text{ x } 0.45 \frac{\text{lb } O_2}{\text{\% } O_2}}\right] \quad ; \quad \ldots(1)$$

therefore,

$$KA = 34.4 \text{ lb/hr of } O_2 \quad .$$

If the sodium is oxidized to Na_2O_2, this is equivalent to burning 100 lb of sodium per hour; if the sodium is oxidized to Na_2O, the rate is 200 lb/hr. The rate at which oxygen is consumed in a pool fire in a closed environment has been measured at 0.16 lb/hr-ft^2 - % O_2 when Na_2O formed; thus, 0.32 lb O_2/hr-ft^2 - % may be consumed when Na_2O_2 is formed. Therefore, the equivalent

pool surface area of the spray fire is 34.4/0.16 to 34.4/0.32 or 216 to 108 ft^2 depending on the oxide formed. If all of the sodium particles which are formed by the nozzle are of equal size, the size can be estimated from the mass of sodium which is assumed to be present.

$$Wt = d \cdot \frac{4}{3}\pi r^3 \cdot N \quad , \qquad \ldots(2)$$

and

$$SA = 4\pi r^2 N = \frac{4\pi r^2 \cdot Wt}{d\frac{4}{3}\pi r^3} = \frac{3Wt}{dr} \quad , \qquad \ldots(3)$$

where:

N = number of particles,

r = radius in cm,

SA = surface area in cm^2 (1×10^5 to 2×10^5 cm^2) ,

Wt = mass of sodium airborne, and

d = density of sodium 1 gm/cc.

If we assume Wt = 30 gm (1/2 of that introduced),

$$r = \frac{3 \times 30}{(1 - 2) \times 10^5} = (90 - 45) \times 10^{-5} \text{ cm} = 9 \text{ to } 4.5\,\mu \quad .$$

If 60 gm was present, the sizes would be larger by a factor of 2. If the particles had a log normal distribution, the average size would be increased by the factor $e^{1/2 \ln^2 \sigma}$; thus if $\sigma = 2$ (the geometrical standard deviation), the mean size, r_{50}, would be 1.75 x the values of r above, and 50% of the particles would be less than this size. These estimates of the sodium spray droplet size are much larger than those of the oxidized Na which were measured by impactors. The first measurement, made 1 min after the spray started, showed that the mean aerodynamic radius was 5 μ which gives a mass median radius for Na_2O_2 of 3 μ which is smaller than 9 μ or (9 x 1.75 = 15.7 μ if log normal). It was also determined, from cascade impactor data, that the AER_{50} increased from 5 to 11.54 μ at 8 min after the start of the spray, and then decreased to between 2 and 3 μ after 20 min.

2. Laboratory Test Chamber (LTC)

Several additional experiments involving the arc-vaporization of UO_2 in air have been performed in the LTC. Figure 1 shows how the air concentration of the total released material (tungsten, iron, and uranium oxides) decreases with time. The usual measurements of floor deposition rates were made, which allowed estimates of the floor deposition half time and the equivalent aerodynamic particle size (AER).

One additional experiment designed to study the behavior of uranium and sodium oxides released simultaneously into the chamber was performed. The fraction of uranium which was released was 0.5% of the total airborne. However, it was observed that the concentration of both the U_3O_8 and Na_2O as well as of the iron and tungsten oxide decreased together as one aggregate. Furthermore, the sodium (and all other) concentrations decreased at a faster rate than it would have if only the sodium oxide had been airborne. The wall plating half time was greater than it would have been if only sodium oxide had been airborne.

The new data points obtained from the somewhat higher released concentrations (ρ_R, μgm/cc) or uranium, iron, and tungsten oxides caused a shift in the relation between T_{50} the floor deposition half time, and ρ_R. Thus, the new relation between the released concentration ρ_R and the aerodynamic radius is such that

$$\sqrt{d} \cdot r_{50} = 2.1\ \rho_R^{0.3} \quad , \qquad \ldots(4)$$

where

d = density in gm/cc, and

r_{50} = the mass median radius in microns.

If d is 4 gm/cc, then $r_{50} = \rho_R^{0.3}$. It has previously been reported* that $r_{50} = \rho_R^{0.3}$ when the data is normalized with a density of ~3.2 gm/cc.

If the sodium oxide aerosol data is analyzed independently of the density, it could be described as $\sqrt{d} \cdot r_{50} = 1.57\ \rho_R^{0.4}$; and since the density, d, is 2.27 gm/cc, $r_{50} = \rho_R^{0.4}$.

*AI-AEC-12721, p 113

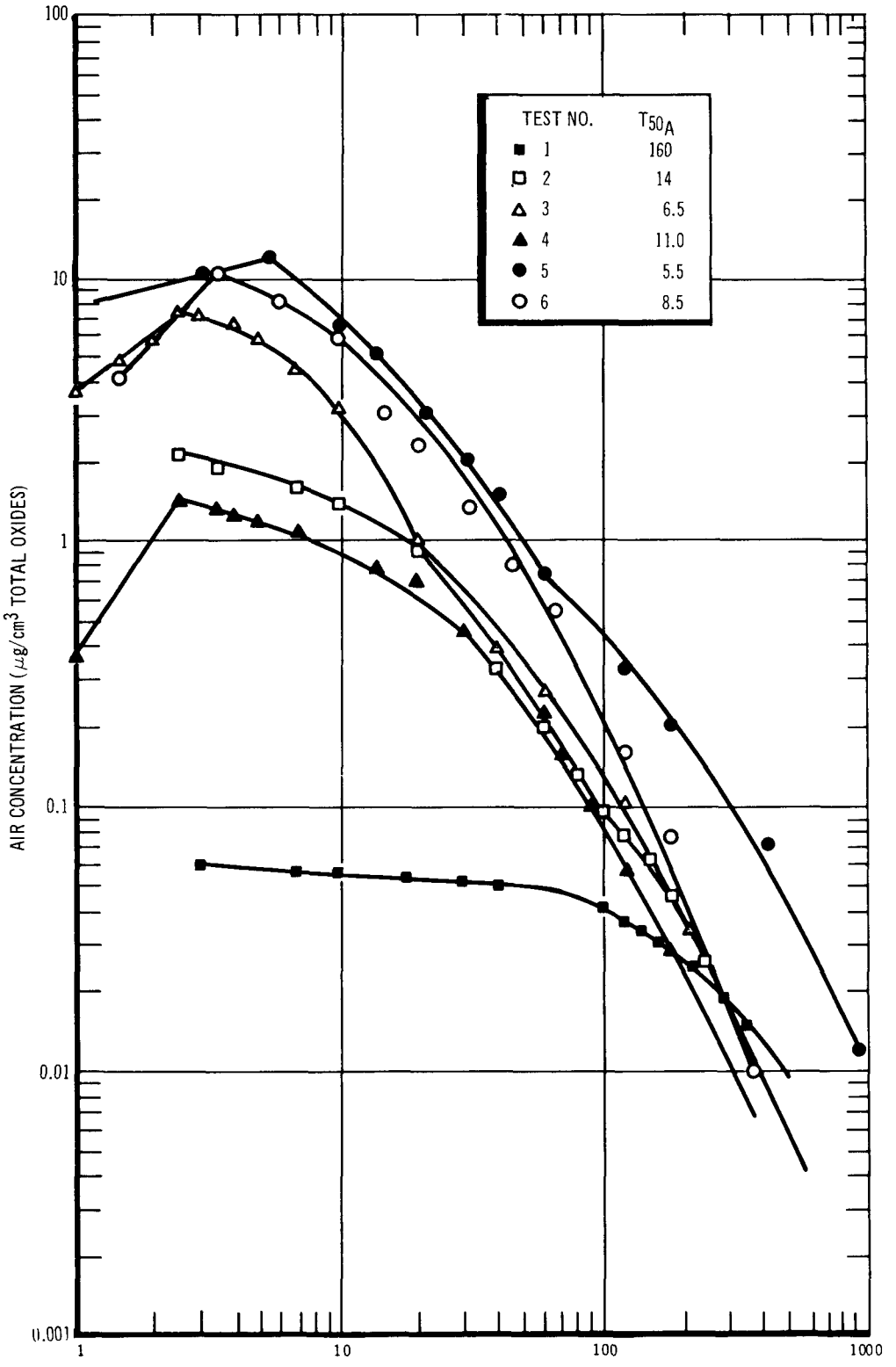

Figure 1. Airborne Concentration vs Time in Laboratory Test Chamber for Various Released Masses of Uranium Oxide (T_{50_A} = initial half time)

B. PHASE II LARGE MODELING FIRE EXPERIMENTS

During this report period, efforts were directed toward finalizing instrumentation, installation, assembly, and checkout of the Phase II test vessel in preparation for the initial test. Figure 2 is the interior of the test vessel prior to final assembly.

The initial large pool fire in the Phase II system was conducted in a highly successful manner. A schematic diagram of the Phase II system configuration for the initial test is shown in Figure 3. The initial conditions for the test are given in Table 1.

The test was initiated by introducing 25 lb of sodium from the auxiliary sodium preheat and transfer system into the rectangular burn pan with a spill time of approximately 20 sec. A 16-mm motion picture camera mounted near the lower view port of the cell was successfully used to visually document the sequence of events from the initial spillage of sodium into the pan through the initial several minutes of burning. Detailed evaluation of the film will be conducted in conjunction with the analysis of burning history from oxygen concentration measurements.

A preliminary evaluation only, of pressure, temperature, and oxygen concentration histories is available thus far, with the detailed reduction of all recorded data currently in progress. Preliminary results of gas pressure and sodium temperature vs time are shown in Figures 4 and 5, respectively. Preliminary oxygen concentration data indicated that almost all (~95%) of the sodium was consumed in about 25 to 30 min while the oxygen concentration decreased from 21 to ~17 vol %. The average sodium burning rate during this period of time was similar to those rates observed previously for air fires; however, the burning rate was apparently not constant as a function of time. Final results on burning rate history will be available on completion of detailed data reduction and analysis.

An initial comparison of the observed maximum pressure rise and average maximum sodium temperature with values predicted from SOFIRE-1 using the actual initial conditions of the test are given in Table 2.

10-23-68 UNCL 7702-4707

Figure 2. Test Vessel Prior to Final Assembly

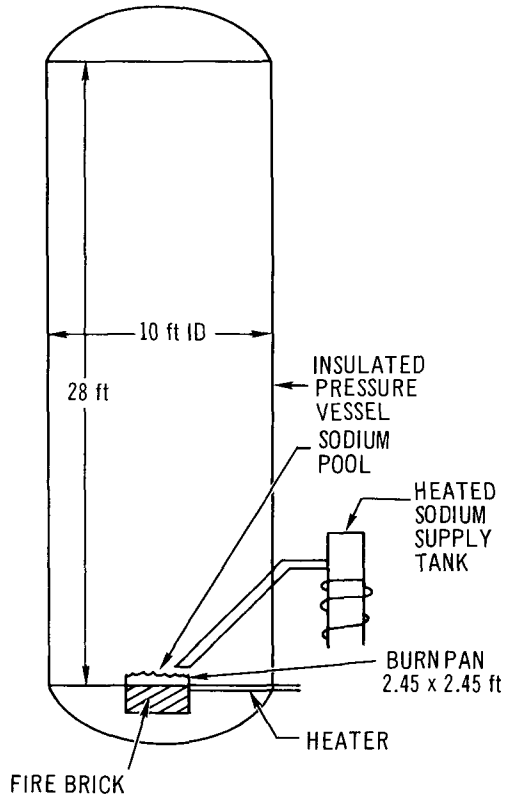

Figure 3. Initial Phase II Sodium Fire Test Setup

TABLE 1

INITIAL TEST CONDITIONS
(Phase II-1)

Parameter	Magnitude
Test Volume (ft^3)	2121
Oxygen Concentration (vol %)	21 (air)
Gas Temperature (°F)	200
Gas Pressure (psia)	18.7
Weight of Sodium Spilled (lb)	25
Sodium Temperature (°F)	955
Burn Pan Area (ft^2)	6
Burn Pan Temperature (°F)	950
Depth of Sodium (in.)	1

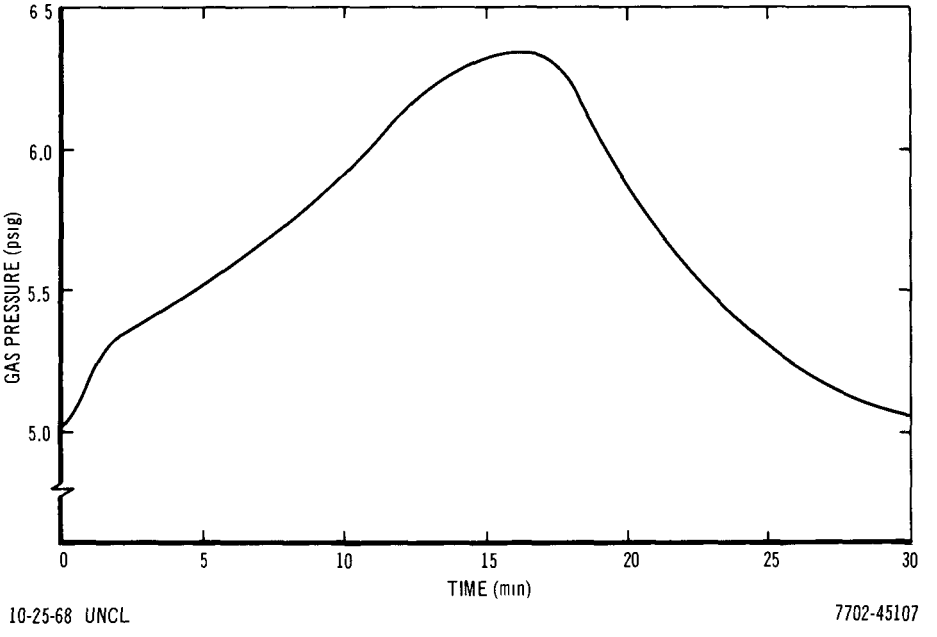

Figure 4. Phase II-1 Test Gas Pressure vs Time

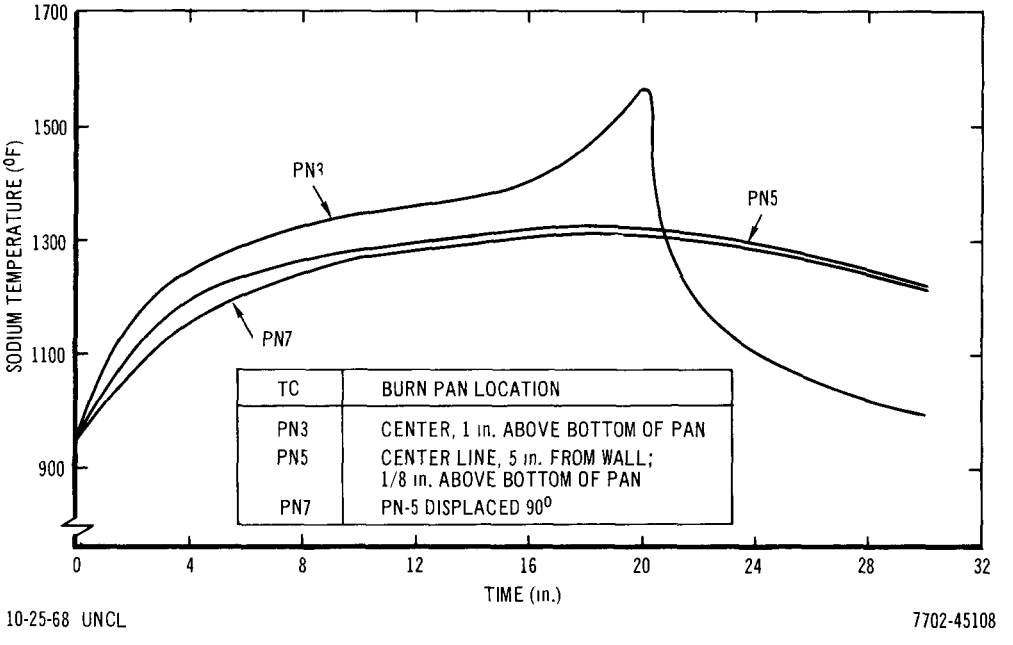

Figure 5. Phase II-1 Test Sodium Temperatures vs Time

TABLE 2

INITIAL DATA COMPARISON AT INITIAL TEST CONDITIONS

Data Source	Pressure		Temperature	
	Maximum Increase (psi)	Time to Reach Maximum (min)	Average Maximum Na Temperature (°F)	Time to Reach Maximum (min)
Experimental	1.34	16.5	1400	18-20
Calculated	2.15	5	1415	11

During the test, air concentration samples were taken about 12 ft above the fire pan. The highest measured concentration was 29 μgm/cc of sodium or 39 μgm/cc of Na_2O at 22 min after the start of the fire. The concentration decreased to 6.7×10^{-7} μgm/cc of Na_2O after 7 days. The initial half time of the air concentration was 10 to 11 min. Figure 6 shows the air concentration at this position during the experiment.

Visual observations made after the chamber had been opened revealed interesting features. The amount of material on the wall appeared to be very low (around 10% of the material released), and fallout samples collected at several heights had the same amount of material per unit area, indicating that the environment was stirred.

Because the release fraction of the oxidized sodium has not as yet been measured, it is somewhat difficult to evaluate the significance of the initial 10 min half time for the air concentration. In Section C-2, Figure 7, it is shown that an air concentration initial half time of 600 sec should be associated with a released concentration of 100 μgm/cc of Na_2O. If this concentration existed, ~40% of the oxidized sodium escaped from the pan. This is in contrast to 20% which escapes in the more quiescent LTC when a 6-in. diameter pot is used. The model described in Section C-2 has not been verified for Phase II studies; therefore, one should not assume that it is absolutely correct.

The cleanup of the Phase II test vessel interior is currently in progress.

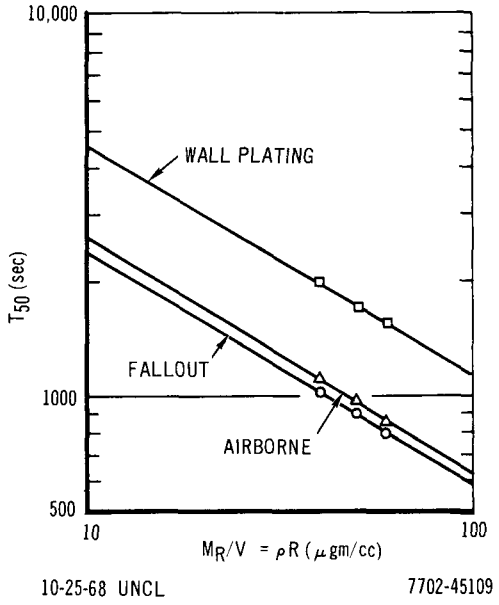

Figure 7.

Predicted Initial Half Times for Phase II and Geometry Using EMM-2 Code

Figure 6. Concentration of Sodium in Atmosphere vs Time

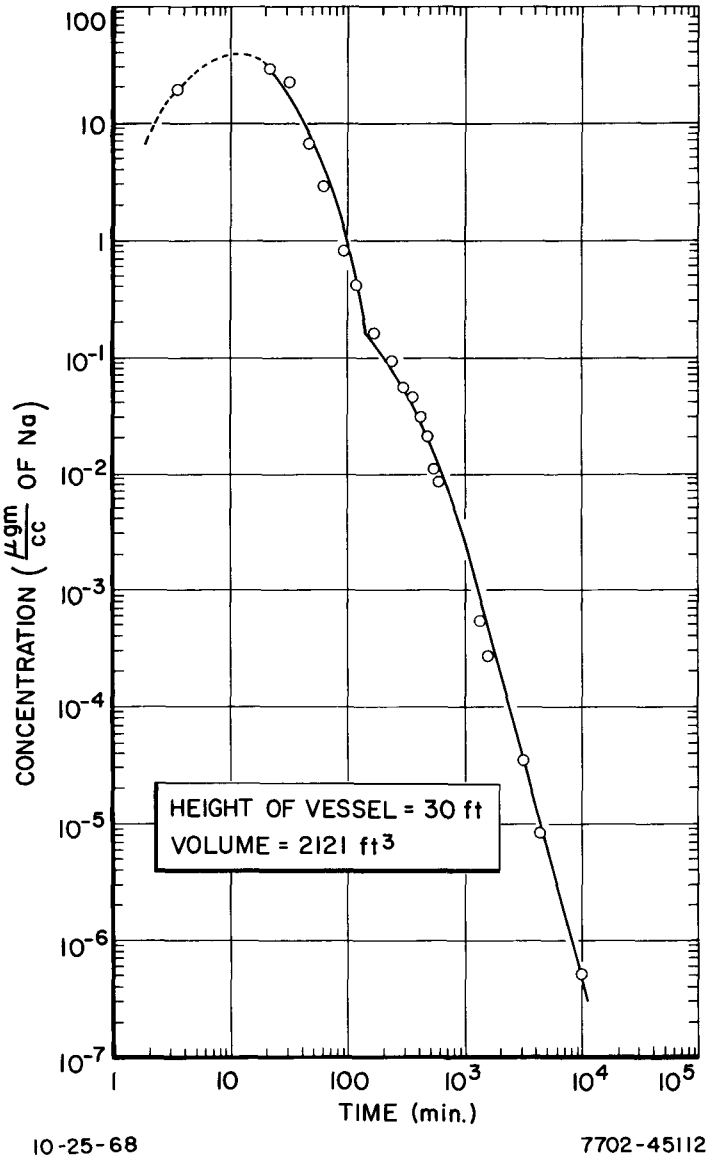

C. ANALYTICAL DEVELOPMENT

1. Recommendations for Improvement of Computer Evaluation of a Heterogeneous Aerosol Agglomeration Model

A review of earlier efforts to obtain an efficient computer evaluation of the aerosol agglomeration model has given rise to two recommendations which should lead to an improved program. Although the review included diverse alternatives; e.g., use of a logarithmic normal distribution to approximate $N(v,t)$, or use of a uniform v-grid for carrying out integrals, the recommended changes can be implemented as modifications of an already operational program. This program already incorporates a transformation which factors the solution into a rapidly- and a slowly-varying function of time, and a spline fitting technique for evaluation of integrals. Both of these methods will be maintained in the modified version.

The first modification recommended is to transform the dependent variable from the number distribution function $N(v,t)\,dv$ to the volume distribution function $\varphi(v,t)\,dv = vN(v,t)\,dv$. Besides being the distribution function of interest with respect to experimental comparisons, $\varphi(v,t)\,dv$ is a smoother function of v and a less rapidly changing function of t as compared with $N(v,t)\,dv$. The changes in the formulation of the model caused by going to $\varphi(v,t)$ can all be lumped with the kernel. The equation for $N(v,t)$ is

$$\frac{\partial N(v,t)}{\partial t} = \int_0^{v/2} N(v',t)N(v'',t)F_1(v',v'')\,dv' + S(v)$$

$$- N(v,t)\left[\int_0^{\infty} N(v',t)F_1(v',v'')\,dv' + R(v)\right] . \qquad \ldots(5)$$

where $v = v' + v''$ is required. For $\varphi(v,t)$, the equation becomes

$$\partial\varphi(v,t) = \int_0^{v/2} \varphi(v',t),\ \varphi(v'',t) \left[\frac{v}{v'v''} F_1(v',v'')\right] dv' + vS(v)$$

$$- \varphi(v,t) \left\{ \int_0^{\infty} \varphi(v',t) \left[\frac{1}{v'} F_1(v,v')\right] dv' + R_1(v) \right\} \quad . \qquad \ldots(6)$$

The terms in square brackets can readily be computed from the old kernels F_1, but it is apparent that the second term is no longer a symmetrical kernel. No computer related problem can be seen to arise from this difference.

The second modification is to remove the kernel from disk storage and place it in the computer core. This will accelerate computation due to speedier access of kernel data. In order for this to be possible with the system available at AI, a reduction in the number of v-grid points allowed is necessary. A reduction from 200 to 100 points will allow storage in the core and will not handicap evaluation of code performance. If future cases require more grid points, the program can readily be converted to operate on a different computer with sufficient storage capacity.

Although these modifications are substantial, their efficiency can be evaluated before all changes in the program are complete. In particular, the editing in the program must be entirely changed to agree with the new dependent variable (v, t) but most of this can be postponed until the value in the change is examined.

Several informal memorandums have been written which describe the operation of the code which is being modified.

2. Studies of Aerosol Behavior with a Complete Empirical Model

An empirical mass model (EMM) based extensively on experimental data have been programmed; (AI-AEC-12680) it is referred to as EMM II, and can be used to fit the experimental data which has been derived from sodium pool fires in the laboratory test chamber (LTC). The model derives from the relation of the initial floor and wall deposition half times which have been reported as:

$$T_{50\ (floor)} = \frac{70}{(\rho_R)^{0.8\ (min)}} \quad \text{and} \qquad \ldots(7)$$

$$T_{59\ (wall)} = \frac{77}{(\rho_R)^{0.6\ (min)}} \ , \qquad \ldots(8)$$

Both of these relations can be used to compute the deposition velocities as a function of ρ_R, the released mass concentration.

If the function v, and ρ are related throughout the life of the aerosol, and if room temperature is assumed; the equation which is programmed is

$$\frac{d\rho}{dt} = S_m - \frac{0.029\rho^{1.8}}{H} = 1.67 \times 10^{-3} \frac{A_w}{V} \rho^{1.6} \ , \qquad \ldots(9)$$

where:

H = height of container in cm = V/A_F,

ρ = concentration in $\mu gm/cm^3$,

A_w = wall surface area in cm^2,

A_F = floor surface area in cm^2,

V = volume of the container in cm^3, and

S_m = source term = ρ_R/V_t = released concentration/source time (sec) $\mu gm/cm^3$.

The coefficient 0.029 is the product of 0.012 times the density of sodium oxide. The coefficient 0.012 is obtained from Stokes Law and its value depends on the viscosity of the medium. The value of H and A_w/V for the LTC are 180 cm and 9.2×10^{-2}/cm. The coefficients are therefore 1.6×10^{-4} and 1.54×10^{-4} respectively. In order to fit the LTC results with EMM-II, it has been necessary to modify Equation 9 to the following:

$$\frac{d\rho}{dt} = S_m - 1.67 \times 10^{-4} \rho^{2.0} - 0.77 \times 10^{-4} \rho^{1.6} \ . \qquad \ldots(10)$$

Note that the exponent of the 2nd term has been changed from 1.8 to 2.0, and that the coefficient of the last term has been changed from 1.54×10^{-4} to 0.77×10^{-4} in order to obtain a better fit to the LTC results.

Some typical LTC results obtained by use of the EMM II code and the present input are given in Table 3.

TABLE 3

TYPICAL EMM II RESULTS FOR ADJUSTED LTC VALUES

ρ_R ($\mu g/cm^3$)	Time (sec)	Floor (%)	T_{50} Floor (sec)	T_{50}^* Floor (sec)	Floor* (%)
2	300	65.4	1833	2500	-
5	300	72.7	875	1200	70
10	300	77.5	510	680	-
20	300	81.6	308	400	85
50	300	86.0	173	185	-

*Experimental

By suitable adjustment of the exponents and coefficient, one can probably obtain an exact fit. The chief difficulty with the model is that it does not correctly account for growth and removal during the time that the aerosol is being produced.

Prior to the first test in the Phase II test cell, EMM II was used to predict the aerosol properties which could be compared to experimental values. By using the coefficients described in Equation 10 and correcting this equation for the different geometry of the Phase II container, the equation used was

$$\frac{d\rho}{dt} = S_m - 2.96 \times 10^{-5} \rho^2 - 1.08 \times 10^{-5} \rho^{1.6} \quad . \qquad \ldots(11)$$

Figure 7 shows the initial half time T_{50} values for the airborne concentration, the settled component on the floor, and the plated component on the wall, when the sodium is burned for a 20-min period.

3. Use of Agglomeration Modeling in Determining the Source Term for Reactor Siting Evaluations

At the time of a design basis accident, the released concentration is assumed to produce instantaneously a uniform concentration of aerosol with some known particle size. If the distribution is log normal, it can be characterized by two parameters, the mean size by mass r_{50} and the geometric standard deviation σ.

The equation which describes the log normal distribution of a particle size distribution has been programmed together with removal by leakage and fallout in various size vessels. This allows one to compute the fraction f, which leaks as a function of time. The actual equation which has been programmed is

$$f_t = \frac{\gamma H \int_0^{t/H} \exp - \gamma H \frac{t}{H} \, d\left(\frac{t}{H}\right) \, d \ln \frac{r}{r_g} \exp - v(r) \frac{t}{H} \, \frac{r^3 \exp\left(-\frac{\ln^2 (r/r_g)}{2 \ln^2 \sigma}\right)}{\sqrt{\pi} \ln \sigma}}{r_g^3 \exp \frac{9}{2} \ln^2 \sigma} \quad \ldots (12)$$

where:

$$v(r) = 1.2 \times 10^{-2} \, dr^2 \left[1 + \frac{1}{r}(0.083 + 0.0264 \exp(-16.7r)\right],$$

v = in cm/sec,

r = particle radius in μ,

d = particle density gm/cc = 1 gm/cc,

$$\ln \frac{r_v}{r_g} = 3 \ln^2 \sigma,$$

r_v = mass mean radius in μ,

r_{50} = mass mean radius in μ,

r_g = median radius by number in μ,

γ = fractional rate of leakage in sec^{-1},

t = time in sec,

H = building height in cm, and

σ = the geometrical standard deviation.

The leaked fraction f at t = ∞ is the reduction factor afforded by fallout; since, if the released mass did not settle, all of it would eventually leak out. By computing f for a number of values for r_g, σ, γ, and H, a final equation derived was

$$f(\infty) = \frac{\text{Mass leaked}}{\text{Mass released}} = \frac{2.4 \times 10^{-2} H \sigma^{0.85} \gamma}{d r_{50}^2} \quad . \qquad \ldots(13)$$

If $r_{50}^2 = \rho_R^{0.8}$ as has been reported from work performed at Atomics International, one can see that the leaked fraction depends directly on the leak rate and the height of the enclosure, and inversely to the material density and concentration (mean particle size) of the released mass.

4. Data Reduction Codes

Compilation of the Phase II heat balance code HTBAL = II has been completed and a computer run made by use of sample data. Analysis of the computer run and geometry refinements required for the initial Phase II test identified several modifications which were needed for proper operation. These modifications were made, and the code is now being used for reduction of the data from the Phase II-1 test.

5. Sodium Pool Fire Model

Several modifications were made to the transient sodium burning code (now referred to as SOFIRE II) which calculates the temperature, pressure, burning rate, and heat flow parameters during a sodium pool fire. The code is capable of calculating these parameters for fires in either an open or closed cell geometry. To date, calculations have been performed for both open and closed cell configurations by using selected values for the initial conditions. The experimental results from the Phase II-1 test conducted in a closed cell are now being compared to the analytical predictions of the code. Differences will be resolved

by making changes to the code and by improving the initial condition input. Heat and mass flow balances will be performed to determine the areas that are in disagreement.

IV. EVALUATION OF EFFORT TO DATE

The initial test conducted in the Phase II system was highly successful with respect to the operational performance requirements of the installation. Although detailed reduction, analysis, and evaluation of recorded thermal data and aerosol sampling devices are still in progress, overall results available thus far indicate that the Phase II test installation will enable attainment of program goals with respect to large scale model testing of release and transport of energy and effluents from sodium fires. A preliminary comparison of the observed history of sodium temperature during the Phase II-1 test with the SOFIRE-1 predicted behavior for this parameter shows rather good agreement. The results for gas pressure rise vs time in the test and the pressure history computed with SOFIRE-1 indicate limited agreement with respect to peak pressure, but rather poor agreement for the time of the pressure peak. The differences between observed and computed pressure history may in part lie in the burning rate model used in SOFIRE-1. This model computes the maximum value for sodium burning in air (~10 lb/hr-ft^2) at zero time (sodium pool has formed) and then provides for reduction in the burning rate proportional to the oxygen concentration as the oxygen is consumed. However, if the actual initial burning rate is lower; e.g., factor of ~2, but increases in time to a maximum value (as observed in Phase I-H air test), the pressure history from SOFIRE-1 would tend to peak somewhat higher and considerably earlier than that found in the experiment. This area will be explored in more detail as the analysis of Phase II-1 progresses. These preliminary results suggest that the SOFIRE-1 code may be somewhat conservative when used for accident analysis.

Preliminary data on the first Phase II fire shows a peak airborne concentration of 39 μgm/cc sodium oxide at the end of the fire which decreased to 6.5×10^{-7} μgm/cc in seven days. The Phase II vessel and the experiments conducted in it are designed for modeling purposes. The 30-ft high vessel is equivalent to the design height of many primary containment systems for liquid

metal fast breeder reactors. Two very important experimental observables which were predictable from small scale tests are the short initial half time (600 sec) for a released concentration near 100 μgm/cc and the near total fallout of the released concentrations in times of much less than 30 days.

The codes which are presently being used in order to determine the effects of agglomeration or fallout show that a considerable reduction of the leaked mass occurs when these factors are considered. By using this model, the Phase II test results show that an initial half time of 600 sec would be produced by a particle distribution with a mass mean radius (r_{50}) of 6 μ and a geometric standard deviation, σ, of 1 to 2. When the concentration decreased by a factor of 10^{-3} and 10^{-4}, the model shows that the effective σ is near 1.5 for the same r_{50} of 6 μ. This model assumes that the 10-min half time is contributable only to floor deposition and thus can only serve to demonstrate the adequacy of these assumptions.

Comparison of the settling rates of the aerosols produced by spraying liquid sodium into 0 or 21% oxygen environments indicates that large droplets (mean radius of 5 to 10 μ) are produced by the spray nozzle. The effect of oxidation on these droplets is to reduce the size of the aerosol with a resultant increase in the concentration which remains airborne.

Vaporization experiments with UO_2 in which the concentration of uranium was increased to 10 to 15 μgm/cc did not change the previous empirical relationships of concentration and settling half time by a significant amount.

A mixed sodium- uranium-oxide experiment, at a high sodium concentration and a large sodium-to-uranium oxide ratio, was performed. An increase in the settling velocity of the mixed aerosol over that for pure sodium was observed as in a previous test.

V. NEXT REPORT PERIOD ACTIVITIES

Detailed analysis and evaluation of Phase II-1 test data will continue. Comparisons will be made of test results and models for sodium fires, with respect to burning, energy transport, and aerosol transport.

A major effort will be devoted to additional experiments on the characterization of burning rates, energy and mass release rates, and aerosol behavior in the Phase II test installation.

The spray test vessel will be operated for the continued evaluation of the same parameters mentioned above.

LTC experiments with high uranium to sodium-oxide concentration ratios will be continued.

Possible improvements to the analytical models for aerosol behavior will be made, and all models will be studied for their agreement with the experimental aerosol removal time constants.

Topical report preparation activity will be initiated.

Program:	Fast Reactor Development		
AEC Task:	6-G, Nuclear Safety (Kinetics), Boiling Studies for Sodium Reactor Safety		
Project Manager:	H. A. Morewitz		
Reporting Period:	July-September 1968		
General Order:	7702	Subaccount: 13410	AEC Category: 04-60-01-09.1

Principal Investigators: D. Logan, J. Landoni, and C. Baroczy

I. PROJECT OBJECTIVES

The general objective of this project is to develop basic information on two-phase flow and boiling required in the safety evaluation of LMFBR designs. This information is important because of the key role that sodium boiling plays in reactor dynamics, in fuel meltdown accidents, and in the ultimate shutdown mechanism of the reactor. Specific objectives of the experimental program include the development of reliable high-flux heaters, and the measurements of boiling heat transfer characteristics, two-phase pressure drop, void fraction, liquid superheating, transient voiding rates and pressures in single channels, and hydrodynamic instabilities. Specific objectives of the theoretical study, in addition to any analyses required to support the experimental work, are: the development of digital computer codes which will predict transient void fraction, flowrate, and heat transfer for single and multichannel sodium flow; and the incorporation of these codes into a general reactor kinetics code.

II. MAJOR ACCOMPLISHMENTS IN FISCAL YEAR 1969

One hundred sodium liquid superheating transients have been run at 5 and 15 psia with a highly polished heater surface (heater surface was polished with 23 micron abrasive). The liquid superheating exhibited the usually random scatter; however, the maximum obtained superheat was greater by approximately 50°F at 5 psia, and 80°F at 15 psia, than values obtained previously with a surface polished with 600 grit abrasive.

A new condenser and surge tank have been fabricated and are being installed in the loop. This modification should greatly reduce the probability of gas entrainment.

III. PROGRESS DURING REPORT PERIOD

A. SODIUM-LIQUID SUPERHEATING

1. Experimental

Sodium-liquid superheat tests are being run to determine the extent of liquid superheating required to initiate boiling in a single LMFBR, coolant channel as influenced by parameters such as velocity, heat flux, subcooling, coolant purity, pressure, heater surface finish, etc.

Thirty five runs were made with the KA resurface, 20 at 15 psia and 15 at 5 psia. Forty runs were made with the KB resurface and twenty five with the KC resurface; all at 5 psia. These 100 experimental runs, see Table 1, were made by gradually increasing the heater heat-flux while all other parameters were held constant. The pressure for the twenty 15 psia runs was obtained by throttling against the pump pressure head. The pressure for the 5 psia runs was established by the cover gas pressure in the condenser.

2. Data Analysis

This group of experimental runs KA1 through KC25 shown in Table 1 were made with a highly polished surface. The initial surface was prepared by successive sanding with 600-grit abrasive and then with 23-micron abrasive. Figure 1 is a stereophotograph of a surface replica of a typical surface after the polishing preparation. Figure 2 has stereophotographs of surface replicas made after the KC series of runs. It can be seen by the difference in Figures 1 and 2 that during the 25 KC superheat runs, the surface of the heater was greatly altered.

The three groups of experimental runs each of which started with highly polished heater surfaces (KA, KB, and KC) had maximum superheats that were much higher than previously obtained in the apparatus with an as-received heater surface or a heater surface refinished only with 600 grit abrasive. These maximum superheats with the polished surface are approximately 50°F higher at 5 psia, and 80°F higher at 15 psia, than those obtained with rougher surfaces.

An analysis has been made of bubble radius at departure in forced convection boiling liquid sodium and compared to similar data obtained in ambient water. The liquid sodium bubble radius at departure was derived from maximum

Run No.	Condenser (psia)	Test Sect (psia)	Inlet Temp (°F)	Heat Flux (Btu/hr-ft^2)	Flow (ft/sec)	Bulk Superheat (°F)
KA-1	8.0	14.96*	1422	0.563×10^6	3.20	56
KA-2	8.0	14.85	1424	0.521×10^6	3.22	44
KA-3	8.0	15.00	1430	0.563×10^6	3.26	73
KA-4	8.0	14.69*	1424	0.586×10^6	3.20	125
KA-5	8.0	14.80	1427	0.533×10^6	3.20	88
KA-6	8.0	14.79	1425	0.461×10^6	3.18	34
KA-7	8.0	14.38	1427	0.476×10^6	3.20	26
KA-8	8.0	14.90	1428	0.400×10^6	3.22	-1
KA-9	8.0	14.75	1429	0.413×10^6	3.22	-3
KA-10	8.0	15.07	1427	0.464×10^6	3.24	15
KA-11	8.0	14.61	1429	0.531×10^6	3.24	86
KA-12	8.0	14.67	1427	0.489×10^6	3.24	56
KA-13	8.0	14.75	1428	0.471×10^6	3.24	40
KA-14	8.0	14.93	1428	0.452×10^6	3.24	17
KA-15	8.0	15.07	1430	0.510×10^6	3.24	56
KA-16	8.0	14.88	1430	0.432×10^6	3.24	17
KA-17	8.0	15.26	1430	0.486×10^6	3.24	46
KA-18	8.0	14.62	1430	0.484×10^6	3.26	51
KA-19	8.0	14.91	1431	0.461×10^6	3.22	40
KA-20	8.0	15.12	1431	0.492×10^6	3.26	46
KA-21	5.0	5.02†	1131	0.651×10^6	3.28	38
KA-22	5.0	4.95	1130	0.600×10^6	3.24	-20
KA-23	5.0	4.95	1131	0.599×10^6	3.22	-21
KA-24	5.0	4.92	1134	0.698×10^6	3.26	42
KA-25	5.0	4.94	1135	0.733×10^6	3.24	59
KA-26	5.0	4.92	1138	0.730×10^6	3.24	68
KA-27	5.0	4.98	1139	0.746×10^6	3.24	53
KA-28	5.0	5.00	1137	0.575×10^6	3.28	-26
KA-29	5.0	5.03	1137	0.734×10^6	3.24	57
KA-30	5.0	5.00	1137	0.634×10^6	3.26	-3
KA-31	5.0	5.03	1135	0.825×10^6	3.26	98
KA-32	5.0	5.00	1132	0.577×10^6	3.30	-54
KA-33	5.0	5.06	1132	0.736×10^6	3.26	31
KA-34	5.0	5.02	1129	0.661×10^6	3.26	-1
KA-35	5.0	5.04	1129	0.599×10^6	3.26	-53
KB-1	5.0	4.98†	1238	0.399×10^6	3.17	-9
KB-2	5.0	5.00	1237	0.470×10^6	3.26	17
KB-3	5.0	5.01	1237	0.460×10^6	3.26	13
KB-4	5.0	5.02	1239	0.536×10^6	3.15	60
KB-5	5.0	5.02	1240	0.453×10^6	3.11	10
KB-6	5.0	5.01	1241	0.533×10^6	3.22	54
KB-7	5.0	5.02	1239	0.590×10^6	3.24	84
KB-8	5.0	5.01	1238	0.470×10^6	3.26	24
KB-9	5.0	5.03	1238	0.500×10^6	3.22	35
KB-10	5.0	5.02	1237	0.435×10^6	3.22	-2
KB-11	5.0	5.02	1238	0.543×10^6	3.20	58
KB-12	5.0	5.03	1239	0.600×10^6	3.28	96
KB-13	5.0	5.03	1239	0.596×10^6	3.15	85
KB-14	5.0	5.04	1238	0.759×10^6	3.26	161
KB-15	5.0	5.01	1237	0.536×10^6	3.28	55
KB-16	5.0	5.12	1237	0.547×10^6	3.26	63
KB-17	5.0	5.06	1237	0.627×10^6	3.20	95
KB-18	5.0	5.02	1238	0.557×10^6	3.26	73
KB-19	5.0	5.02	1238	0.410×10^6	3.26	-1
KB-20	5.0	5.03	1239	0.539×10^6	3.26	62
KB-21	5.0	5.01§	1333	0.287×10^6	3.20	18
KB-22	5.0	5.19	1334	0.350×10^6	3.20	1
KB-23	5.0	4.93	1335	0.240×10^6	3.17	3
KB-24	5.0	5.40	1333	0.358×10^6	3.20	-1
KB-25	5.0	4.98	1334	0.306×10^6	3.17	50
KB-26	5.0	4.98	1332	0.490×10^6	3.22	146
KB-27	5.0	5.02	1333	0.266×10^6	3.24	21
KB-28	5.0	5.00	1334	0.238×10^6	3.22	7
KB-29	5.0	5.01	1335	0.282×10^6	3.24	29
KB-30	5.0	5.04	1335	0.389×10^6	3.26	95
KB-31	5.0	5.03	1337	0.490×10^6	3.24	129
KB-32	5.0	5.04	1337	0.349×10^6	3.22	66
KB-33	5.0	5.03	1336	0.410×10^6	3.26	105
KB-34	5.0	5.04	1336	0.588×10^6	3.32	143
KB-35	5.0	5.07	1334	0.365×10^6	3.20	77
KB-36	5.0	4.95	1333	0.327×10^6	3.22	59
KB-37	5.0	4.96	1333	0.393×10^6	3.22	100
KB-38	5.0	4.96	1331	0.262×10^6	3.26	11
KB-39	5.0	4.97	1332	0.279×10^6	3.20	28
KB-40	5.0	5.00	1330	0.252×10^6	3.22	13
KC-1	5.0	5.10*	1408	0.132×10^6	3.17	18
KC-2	5.0	5.01	1406	0.090×10^6	3.26	-2
KC-3	5.0	5.01	1405	0.140×10^6	3.26	24
KC-4	5.0	5.00	1404	0.139×10^6	3.26	13
KC-5	5.0	4.97	1405	0.191×10^6	3.24	43
KC-6	5.0	5.01	1404	0.235×10^6	3.26	60
KC-7	5.0	5.10	1406	0.203×10^6	3.28	50
KC-8	5.0	5.03	1406	0.173×10^6	3.22	45
KC-9	5.0	5.00	1407	0.183×10^6	3.26	42
KC-10	5.0	5.03	1408	0.093×10^6	3.26	-2
KC-11	5.0	5.05	1408	0.183×10^6	3.28	39
KC-12	5.0	5.01	1408	0.219×10^6	3.30	66
KC-13	5.0	5.10	1407	0.249×10^6	3.22	65
KC-14	5.0	5.03	1406	0.176×10^6	3.22	40
KC-15	5.0	5.03	1405	0.154×10^6	3.26	36
KC-16	5.0	5.00	1406	0.169×10^6	3.26	42
KC-17	5.0	4.98	1406	0.170×10^6	3.28	43
KC-18	5.0	5.00	1406	0.171×10^6	3.30	39
KC-19	5.0	5.01	1406	0.112×10^6	3.26	8
KC-20	5.0	5.03	1408	0.143×10^6	3.26	18
KC-21	5.0	5.03	1406	0.196×10^6	3.24	50
KC-22	5.0	5.16	1407	0.230×10^6	3.26	65
KC-23	5.0	5.07	1407	0.164×10^6	3.30	30
KC-24	5.0	5.07	1408	0.219×10^6	3.28	51
KC-25	5.0	5.02	1407	0.203×10^6	3.28	45

*Max press = 15 psia, held for 24 hr
†Max press = 15 psia, held for 1 hr
§Max press = 18 psia, held for 1 hr

Table 1. Sodium-Liquid Superheat Tests

superheat data at 5 psia by using the Laplace formula for spherical bubbles. The boiling water data of Koumoutsos* was obtained by direct photographic measurements. In both cases, the radius at departure decreases with increasing velocity; however, a comparison of the bouyant, surface, and drag forces, shows that in the sodium case, the bouyant forces are negligible in comparison to the surface tension, unlike the case of ambient water, where the drag force is small compared to the buoyant and surface forces.

An examination of the sodium data shows that the thickness of the laminar sublayer is on the order of 1 mil. This layer is sufficiently thick to contain the departing bubble, but too thin to have any significant temperature gradient across it (because of the high thermal conductivity of the sodium). Under these conditions, the saturated vapor contained in the departing bubble is at the wall temperature and Hsu's criterion† cannot be applied to the initiation of boiling in the forced flow of liquid sodium. A topical report on the single pin superheating program is presently under preparation.

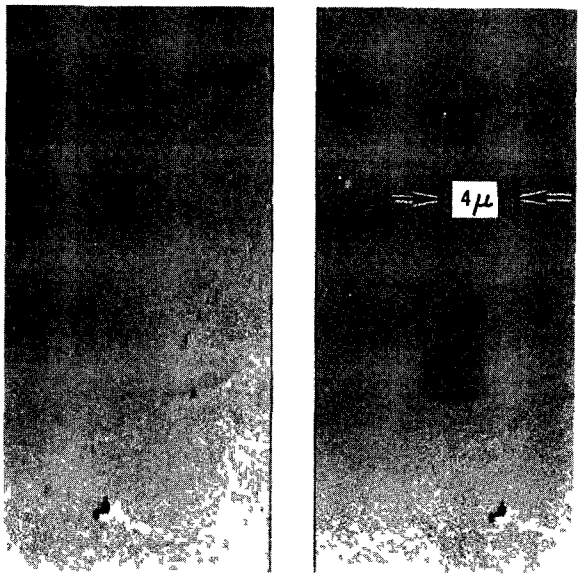

7702-45110

Figure 1. Stereophotomicrograph Showing a Typical View of the Polished Surface of the K High Heat Flux Heater

*N. Koumoutsos, et al., "A Study of Bubble Departure in Forced Convection Boiling," Trans. ASME, Journal of Heat Transfer, 90, 223 (1968)

†Y. Y. Hsu, "On the Size Range of Active Nucleation Cavities on a Heating Surface," Trans. ASME, Journal of Heat Transfer, 84, 207 (1962)

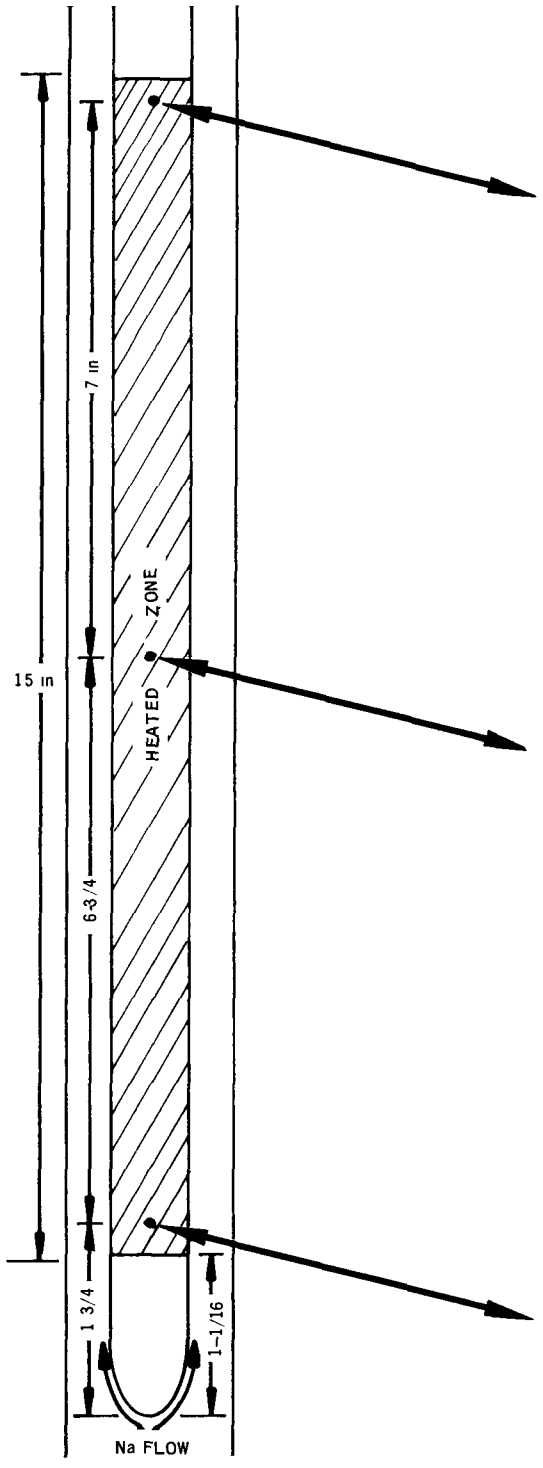

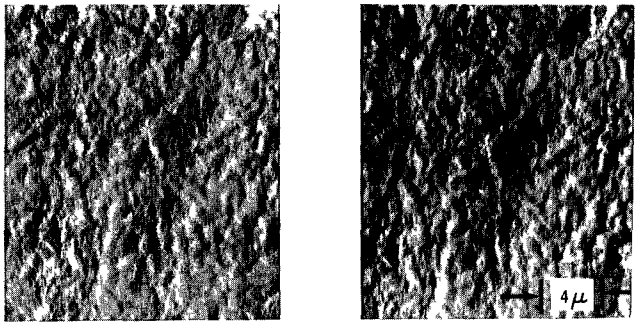

2c

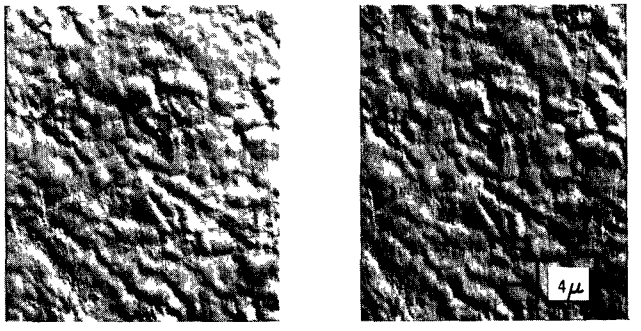

2b

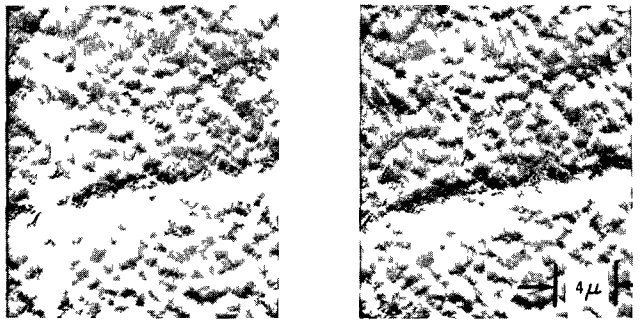

2a

10 25-68 UNCL

7702 4 5110

Figure 2. Stereophotomicrographs of Three Points on the Surface of the K High Heat Flux Heater After the KC Series of Test Runs

B. HEATER DEVELOPMENT

There was no developmental effort on the high heat flux heater this quarter.

C. LOOP MODIFICATION

The loop is presently being modified to reduce the possibility of gas entrainment. The sodium flow from the test section is now released below the free sodium liquid surface level in the new condenser. A surge tank has been fabricated and will be installed so that the free sodium liquid level in the condenser can be maintained to within ±4 in.

D. THEORY: TRANSFUGUE IIa DEVELOPMENT

No effort has been expended on the TRANSFUGUE IIa development this quarter.

E. THEORY: CONVERSION OF TWO-PHASE STEAM CODES TO USE WITH SODIUM

The transient, multichannel, boiling sodium code, TRANSODIFAZE, was transmitted to BNWL, for use in FFTF core safety studies.

A topical report on the multichannel, boiling sodium code, SODIFAZE, has been started.

IV. EVALUATION OF EFFORT TO DATE

Progress is considered satisfactory. Liquid superheat testing has progressed substantially with 100 tests having been performed for studying the effect of heater surface on sodium liquid superheat at 5 and 15 psia. Topical reports have been started on the single pin superheating studies and on the multichannel, boiling sodium code, SODIFAZE. The new components designed to reduce possible gas entrainment have been fabricated and are being installed in the loop.

V. NEXT REPORT PERIOD ACTIVITIES

Additional liquid superheat testing will be performed with a single pin. Emphasis will be on studying velocities greater than 4 ft/sec as soon as the loop modifications to reduce the possibility of gas entrainment are complete.

The topical reports on the single pin superheating studies and on the multi-channel, boiling sodium code, SODIFAZE will be completed.

The loop modifications to reduce the possibility of entrainment will be completed.

Component fabrication will be started and materials ordered for conversion of the loop for use with a three-channel test section.

Development of a shaped flux heater will be continued.

Program:	Fuel Cladding and Structural Materials			
AEC Task:	10A, Materials Management			
Project Manager:	J. L. Ballif/J. J. Gill			
Reporting Period:	July-September 1968			
General Order:	7706	Subaccount:	29511-2	AEC Category: 04-01-61-01.5

Principal Investigators: E. W. Murbach - D. F. Atkins

I. PROJECT OBJECTIVES

Project objectives are to: (1) to manage a source of stock "systems quality" sodium for the program, (2) to monitor the compositions of sodium and of gas atmospheres in use on all the subtasks in the program and provide a management system for insuring the use of proper procedures in sampling, transferring and analyzing of sodium, and (3) to procure, characterize, and manage a supply of cladding materials for the program.

II. MAJOR ACCOMPLISHMENTS DURING FISCAL YEAR 1969

A new oxygen meter electrode was tested in the supply loop and found to be responsive to oxygen injections.

Negotiations were initiated for the procurement of an additional 500 ft of Type 316 stainless steel tubing for use in mechanical property tests. This tubing will be fabricated from the highly characterized heat which is used for all phases of the program.

III. PROGRESS DURING REPORT PERIOD

The experiment to test a new oxygen meter electrode was completed. Three injections of oxygen were made to the cover gas of the surge tank. The first two injections were calculated to add 25 ppm of oxygen to the sodium and the third to add 50 ppm additional. The behavior of the electrode since its installation in May is shown in Figure 1. As can be seen, the electrode is responsive to oxygen; however, the gettering action of the stainless steel in the loop can also be plainly seen. Plugging temperatures during the experiment are also shown in Figure 1. After a few days of cold trapping, the plugging temperature decreased to the freezing point of sodium which is normal for the loop.

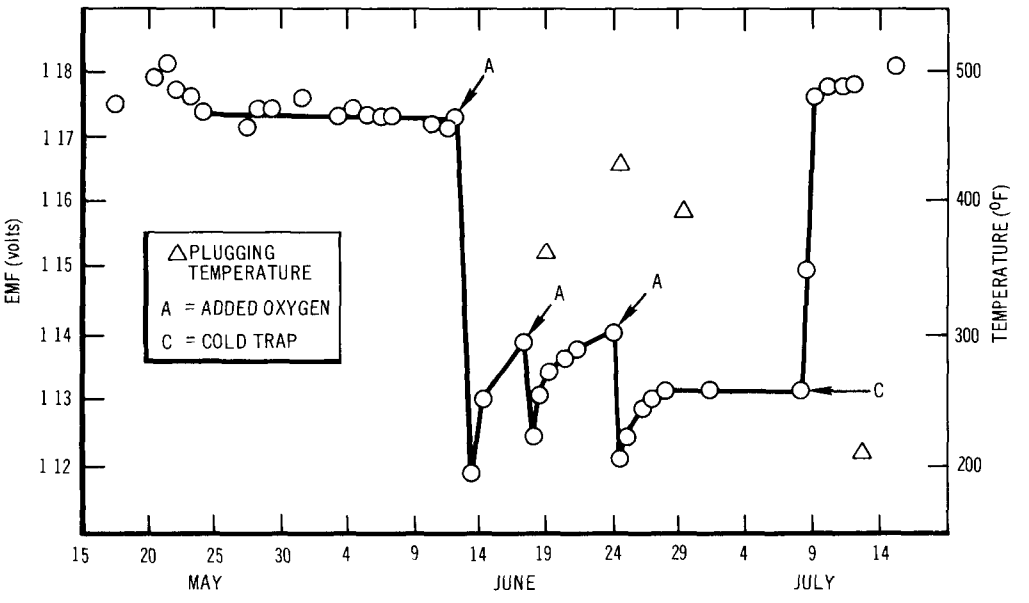

7706-4755

Figure 1. Oxygen Meter Results

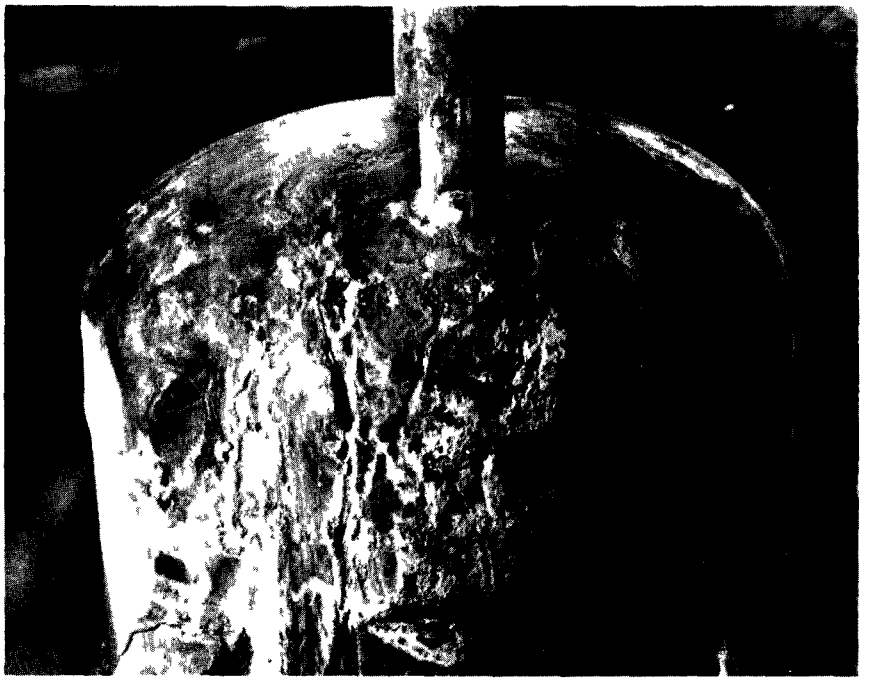

7706-4756

Figure 2. Top of Failed Hot Trap from the Sodium Supply Loop

It was planned to carry out additional experiments to measure the temperature coefficient of the electrode; however, some difficulties were encountered with the hot trap so that the test temperatures could not be attained.

Two of the hot trap heaters became inoperative. The hot trap was shut down and cooled for heater replacement. On removal of the insulation, it was found that a sodium leak had developed. The reaction product of the sodium with the atmosphere had corroded the heaters, causing failure. The trap was cut out of the loop and removed. A photograph of the head is shown in Figure 2. It is thought that the leak occurred in one of the pipe stub welds; however, an attempt to check the welds with dye penetrant was inconclusive. The trap has been turned over to LMEC for further study.

The loop temperature was reduced to 300°F during removal of the hot trap and then increased to the normal 500°F operating level. Nine retorts were loaded for Task 10-C during the report period, three following removal of the hot trap. Two containers were also loaded for the Sodium Chemistry project, (Task 12).

During a recent experiment with the Task 10-D loop, two sodium samples were taken. Five retorts were also sampled during the report period. Higher oxygen contents than normally found for samples removed from the loop and retorts tested in a similar manner were measured in some cases. An investigation disclosed that the inert atmosphere in the analytical glove box was contaminated with oil vapor. The purification train is being overhauled and cleaned.

Arrangements were finalized with the tubing mill for drawing 500 ft of 0.275-in. I.D. by 0.010-in. wall seamless tubing from reference heat No. 65808 of Type 316 stainless steel. This tubing will be purchased to replenish the present supply which is being used by other subtasks of the program. The tubing will be fabricated to specification STO160NB0017.

IV. EVALUATION OF EFFORT TO DATE

The failure of the hot trap is not a problem at present. There are no carbon sources in the loop, so the present low carbon level should be stable. However, the sodium in the drain tank has not been hot-trapped; therefore, if this sodium is transferred into the main loop, hot-trapping will be required.

Although oxygen analysis results have been somewhat erratic, the tests are being carried out in specification grade sodium as verified by the electrochemical oxygen meter emf's.

V. NEXT REPORT PERIOD ACTIVITIES

Routine activities of dispensing and sampling sodium will be continued. A decision will be reached concerning installation of another hot trap in the sodium supply loop.

Routine control, release, and inventory of characterized tubing and sheet stock will be conducted as needed. The 500 ft order of 316 stainless steel tubing will be received, and characterization of the material will be started.

E

Program:	Fuel Cladding and Structural Materials	
AEC Task:	10-B, Helium Effects and Failure Mechanisms	
Project Manager:	J. L. Ballif/J. J. Gill	
Reporting Period:	July-September 1968	
General Order: 7706	Subaccount: 29620	AEC Category: 04-40-02-01.1

Principal Investigator: D. Kramer

I. PROJECT OBJECTIVES

Project objectives are to: (a) obtain a detailed understanding of the motion, agglomeration, and trapping of helium atoms and bubbles in fast reactor cladding and structural materials, including the effects of initial distribution of helium atoms and the ultimate distribution of these trapped product atoms, (b) investigate the basic nature and form of the mechanical property changes induced by fast reactor transmutation damage, and (c) assist in the translation of these data into interpretation of environmental behavior of cladding alloys and the selection, heat treatment, and design of fast reactor materials.

II. MAJOR ACCOMPLISHMENTS DURING FISCAL YEAR 1969

Tensile tests of 304L SS with helium have shown that this alloy is embrittled by helium to the same degree as 304 SS.

Heat-to-heat variations in composition of Incoloy 800 do not have a significant effect on helium embrittlement.

III. PROGRESS DURING REPORT PERIOD

A. TYPE 304L STAINLESS STEEL

Tensile testing of 304L SS obtained from ANL was completed. The composition of this alloy and the tensile data are given in Tables 1 and 2.

TABLE 1

COMPOSITION OF 304L SS IN wt %

C	Cr	Fe	Ni	Mn	Si
0.02	18.5	bal	9.0	1.3	1.0

TABLE 2

TENSILE DATA OF 304L SS
(Prior to helium injection the samples were annealed 24 hr at 760°C)

Atom Fraction Helium ($x10^{-6}$)	Test Temperature (°C)	Yield Strength (kpsi)	Tensile Strength (kpsi)	Elongation (%)	
				Uniform	Total
0	400	20.3	59.5	30	31
31	400	22.8	59.4	28	29
0	500	17.2	53.0	25	29
31	500	18.4	55.1	25	28
0	600	15.8	45.9	32	39
1.5	600	16.0	44.4	28	30
31	600	18.0	44.9	23	24
0	700	15.0	29.9	21	48
1.5	700	14.6	29.1	17	23
31	700	15.6	27.8	12	14
0	800	12.2	16.5	12	33
1.5	800	12.2	15.6	9	17
31	800	12.5	15.1	6	8

The drop in total elongation with increasing temperature is the same as that previously observed for 304 SS. The uniform elongation is affected to a greater degree by helium in 304L SS than in 304 SS. Metallography of 304L SS is in progress.

B. TYPE 304 STAINLESS STEEL

Stress-rupture testing of 304 SS at 760°C (1400°F) was completed, and the data are plotted in Figure 1. The observations previously made in the annual progress report (AI-AEC-12721) are valid for the two additional data points shown.

The bubble density in the sample containing 3×10^{-5} atom fraction helium that failed after 325 hr is significantly higher than that found in its tensile tested counterpart. Figure 2 shows these bubbles in the matrix and on grain boundaries. Bubbles were also observed in the sample with 1×10^{-6} atom fraction helium which failed after 419 hr. Previous attempts to detect bubbles at this low concentration in tensile samples were fruitless.

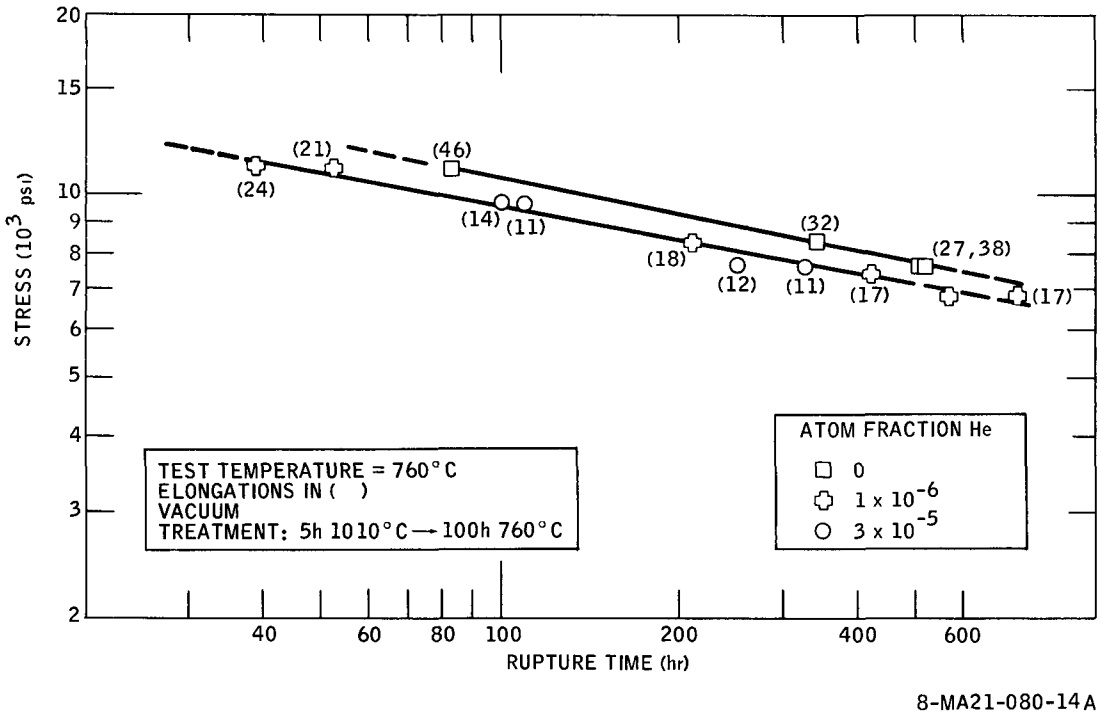

Figure 1. Stress-Rupture of Type 304 Stainless Steel

UNCL

7706-4757

Figure 2. Helium Bubbles in Stress-Rupture Tested 304 Stainless Steel at 700°C
(Helium concentration = 3 x 10^{-5} atom fraction; rupture life = 325 hr)

C. TYPE 316 STAINLESS STEEL

Stress-rupture testing of samples without helium is in progress. The results to date are given in Table 3.

TABLE 3
STRESS-RUPTURE DATA FOR 316 SS

Treatment	Test Temperature (°C)	Stress (kpsi)	Rupture Time (hr)	Total Elongation (%)
6*	700	20.8	28.2	52
13†	700	25.0	66.4	13
6*	700	14.1	345	41
13†	700	14.1	in progress	-
6*	700	12.1	in progress	-

*CR → 1 hr 982°C → 8 hr 760°C.
†CR → 24 hr 482°C → 144 hr 704°C.

D. INCOLOY 800

A second heat of Incoloy 800, having higher Al and Ti contents than the first heat, was tensile tested at 700°C (1292°F) with 4.0×10^{-5} atom fraction helium and without helium. The compositions of the two heats are given in Table 4.

Table 4
COMPOSITION OF TWO INCOLOY 800 HEATS IN wt %

Heat	C	Cu	Cr	Ti	Al	Ni	Fe
HH 7531A	0.03	0.16	19.3	0.20	0.10	32.4	bal
HH 4617A	0.04	0.21	21.0	0.40	0.50	31.0	bal

The tensile results for both heats are given in Table 5. A comparison of data is meaningful because embrittlement is not very sensitive to the small difference in helium contents of the two heats. In the absence of helium, the second heat showed greater elongations; but with helium, the percent loss in ductility was about the same as that of the first heat.

TABLE 5

TENSILE RESULTS AT 700°C FOR TWO HEATS
INCOLOY 800

Heat No.	Treatment	Atom Fraction Helium	Yield Strength (kpsi)	Tensile Strength (kpsi)	Elongation (%)	
					Uniform	Total
HH 7531A	4*	0	14.2	30.6	13	39
	4*	4.0×10^{-5}	15.8	30.3	11	14
	11†	0	14.2	27.0	12	46
	11†	4.0×10^{-5}	14.8	26.0	6	7
HH 4617A	4*	0	21.8	39.7	15	55
	4*	3.1×10^{-5}	23.0	40.4	14	20
	11†	0	26.0	38.0	13	57
	11†	3.1×10^{-5}	26.2	36.9	9	11

*CR → 1 hr 1010°C → 100 hr 760°C.
†CR → 100 hr 760°C.

E. TYPE 405 STAINLESS STEEL

The tensile data of 405 SS previously reported in the annual progress report (AI-AEC-12721) are plotted with the data of 316 SS in Figure 3 to compare their performance. At 650°C (1202°F), only a small drop in total elongation is evident for 405 SS whereas a large decrease has occurred for 316 SS due to helium. Total elongation at 750°C (1382°F) has decreased significantly for 405 SS.

Metallographic examination of a sample of 405 SS with 4×10^{-5} atom fraction helium tested at 750°C showed the failure to be intergranular and revealed many large grain-boundary cracks in the failure zone. These are seen in Figures 4 and 5. Fractographs confirmed the mode of failure to be intergranular as shown in Figure 6.

Replica electron micrographs of the tensile sample facilitated detection of voids or incipient cracks on the grain boundaries adjacent to carbide particles. Such a void is seen in Figure 7 in the center of the photograph. Intergranular failure begins by the formation of these voids which grow and link together to form large cracks.

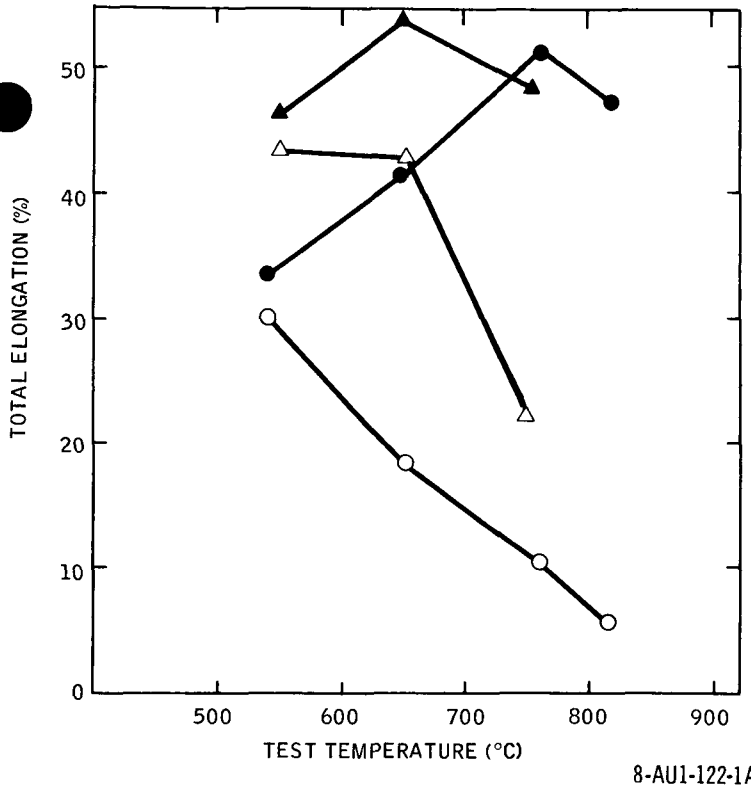

ALLOY	ATOM FRACTION HELIUM	TREATMENT
▲405	0	24 hr, 760°C
△405	4×10^{-5}	
● 316	0	1 hr, 980°C → 8 hr, 760°C
○ 316	4×10^{-5}	

Figure 3. Total Elongation vs Test Temperature for 405 and 316 Stainless Steel

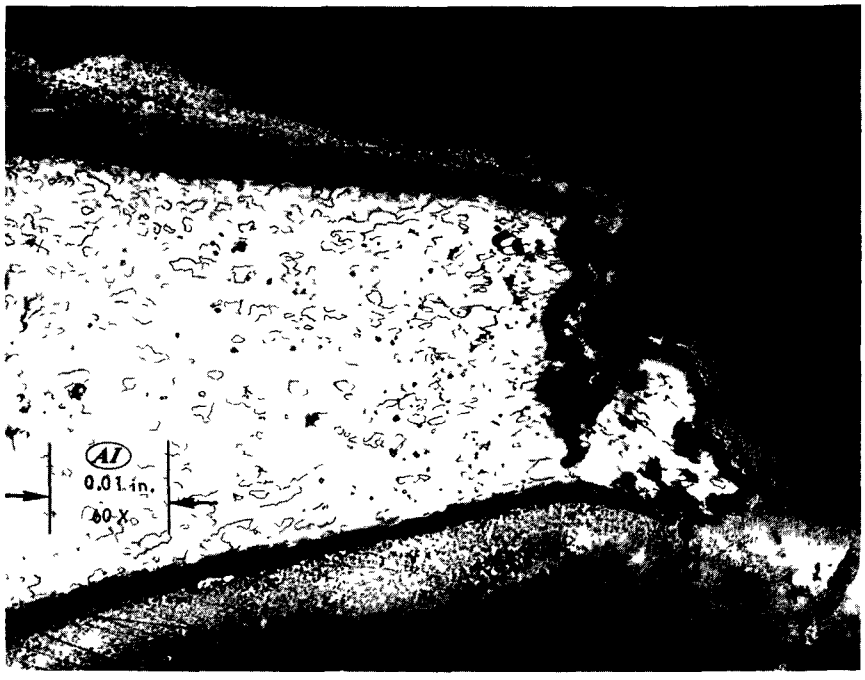

10-25-68 UNCL 7706-4758

Figure 4. Failure Zone in 405 Stainless Steel With 4×10^{-5} Atom Fraction Helium, Tested at 750°C

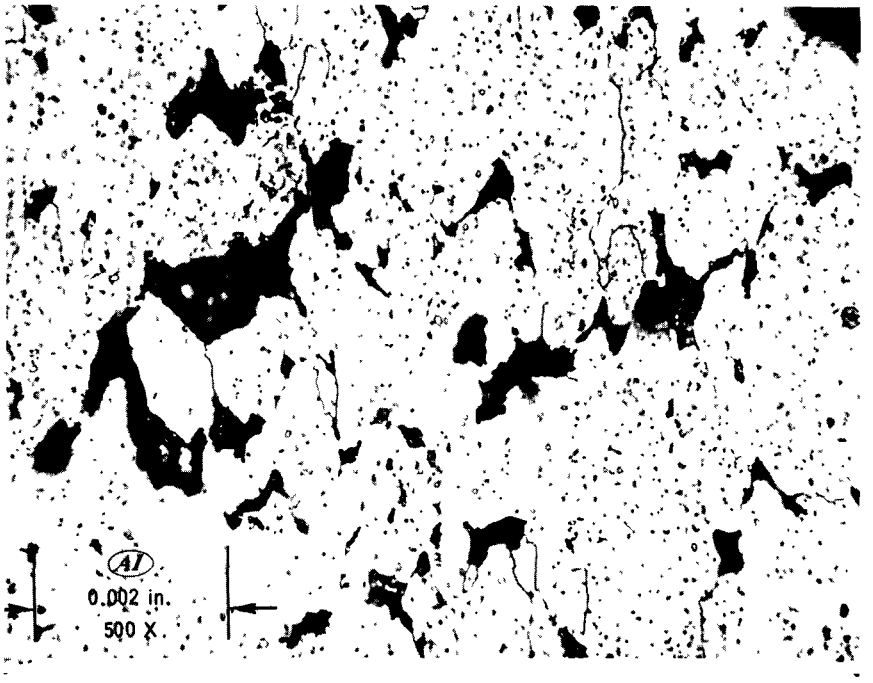

500X

10-25-68 UNCL 7706-4759

Figure 5. Large Grain Boundary Cracks in 405 Stainless Steel With 4 x 10^{-5} Atom Fraction Helium, Tested at 750°C

Transmission electron micrographs show large helium bubbles on grain boundaries, Figure 8, and on carbide particles located on grain boundaries, Figure 9. Helium bubbles on these grain-boundary carbide particles are nucleation sites for cracks which readily form during high-temperature strain due to grain-boundary sliding.

F. 19-9DL

Tensile testing of 19-9DL is in progress. The composition of this alloy is given in Table 6 and the tensile data appears in Table 7. Ductility losses due to helium are a considerable improvement over the stainless steel when the alloy is given Treatment 16.

UNCL

7706-7766

Figure 6. Intergranular Failure in 405 Stainless Steel With 4 x 10^{-5} Atom Fraction Helium, Tested at 750°C (Electron Fractograph)

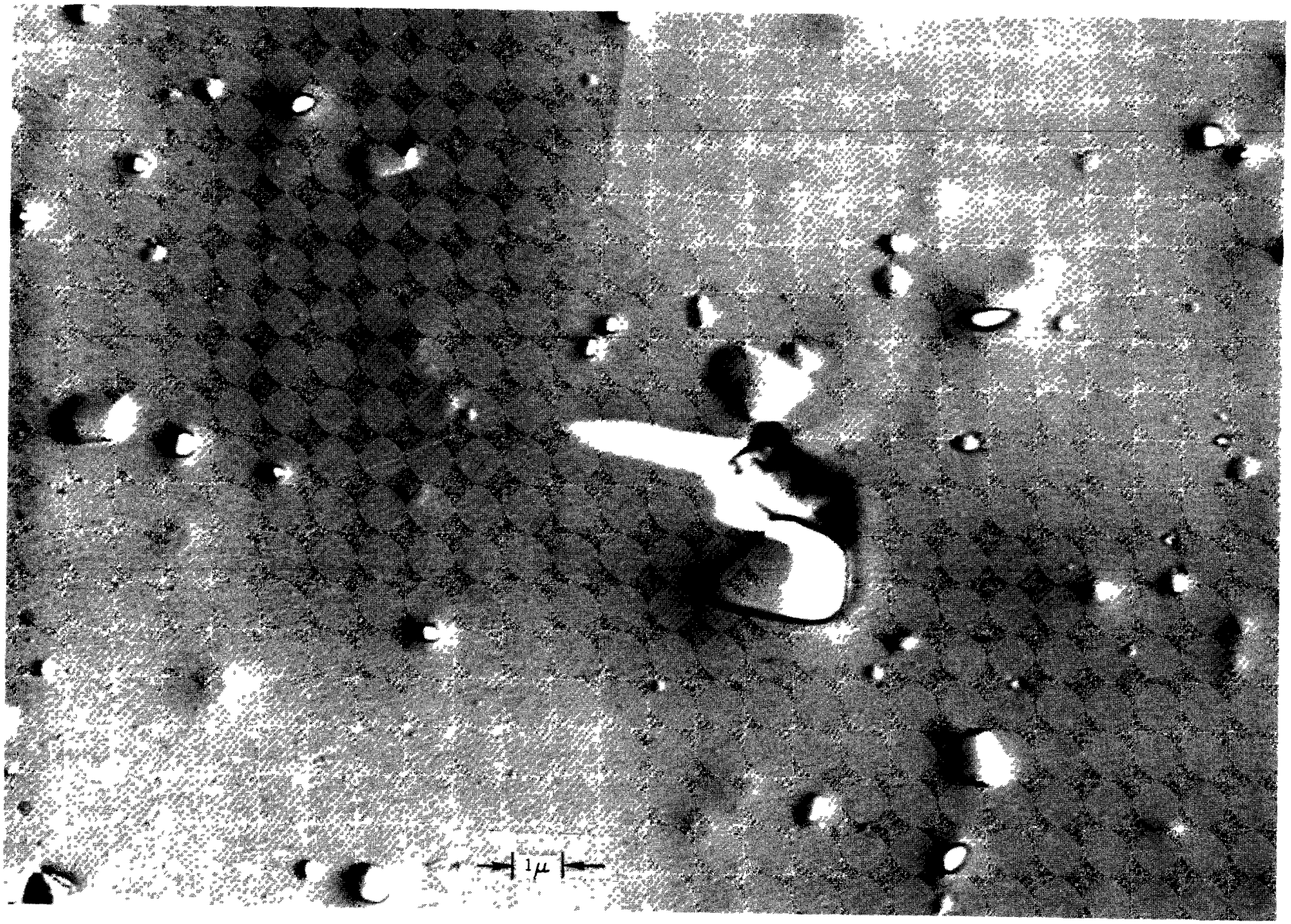

UNCL

7706-7767

Figure 7. Void Adjacent to a Carbide Particle in 405 Stainless Steel With 4 x 10^{-5} Atom Fraction Helium, Tested at 750°C (Replica Electron Micrograph)

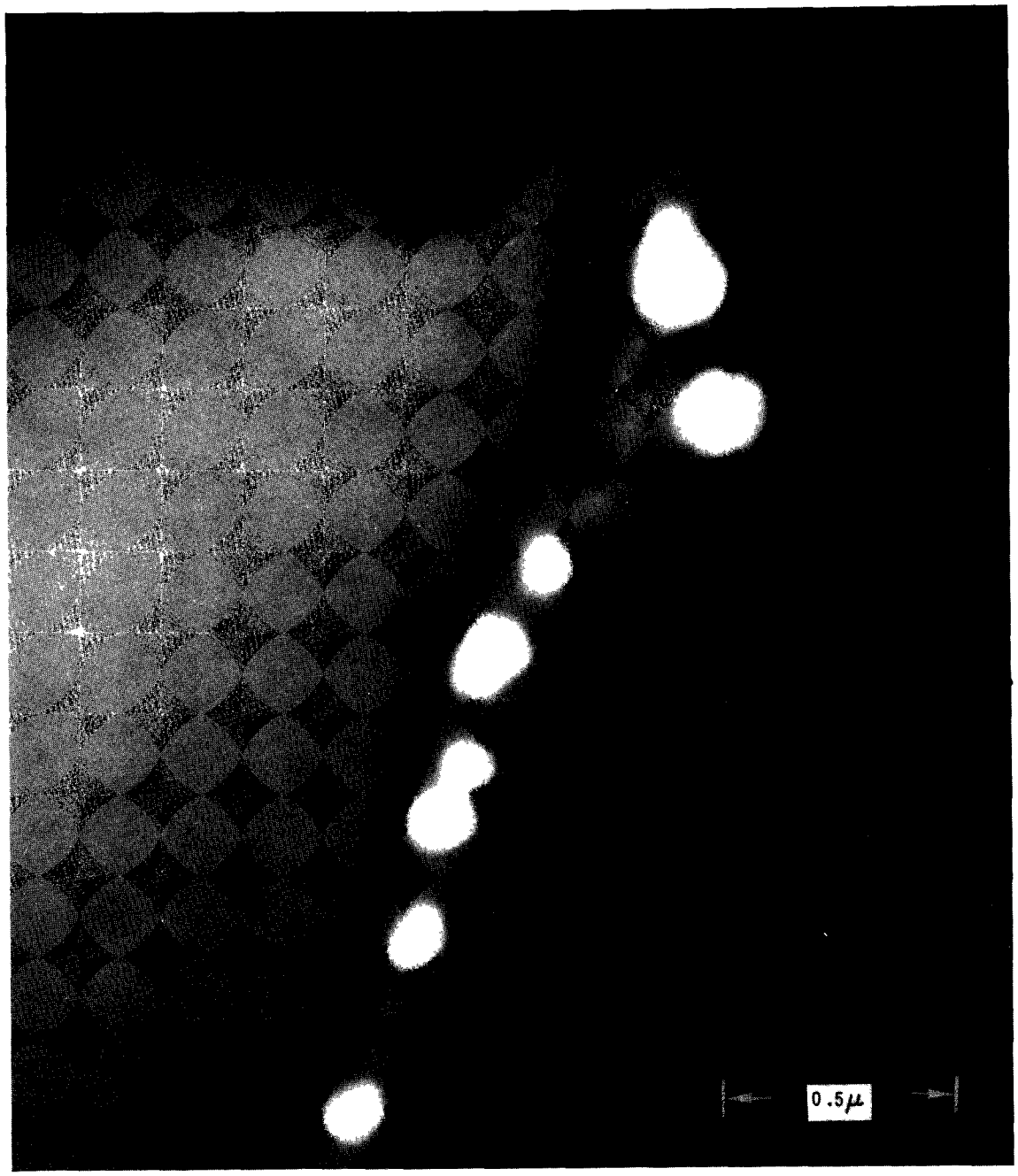

UNCL 7706-7768

Figure 8. Helium Bubbles on a Grain Boundary of 405 Stainless Steel With 4 x 10^{-5} Atom Fraction Helium, Tested at 750°C (Transmission Electron Micrograph)

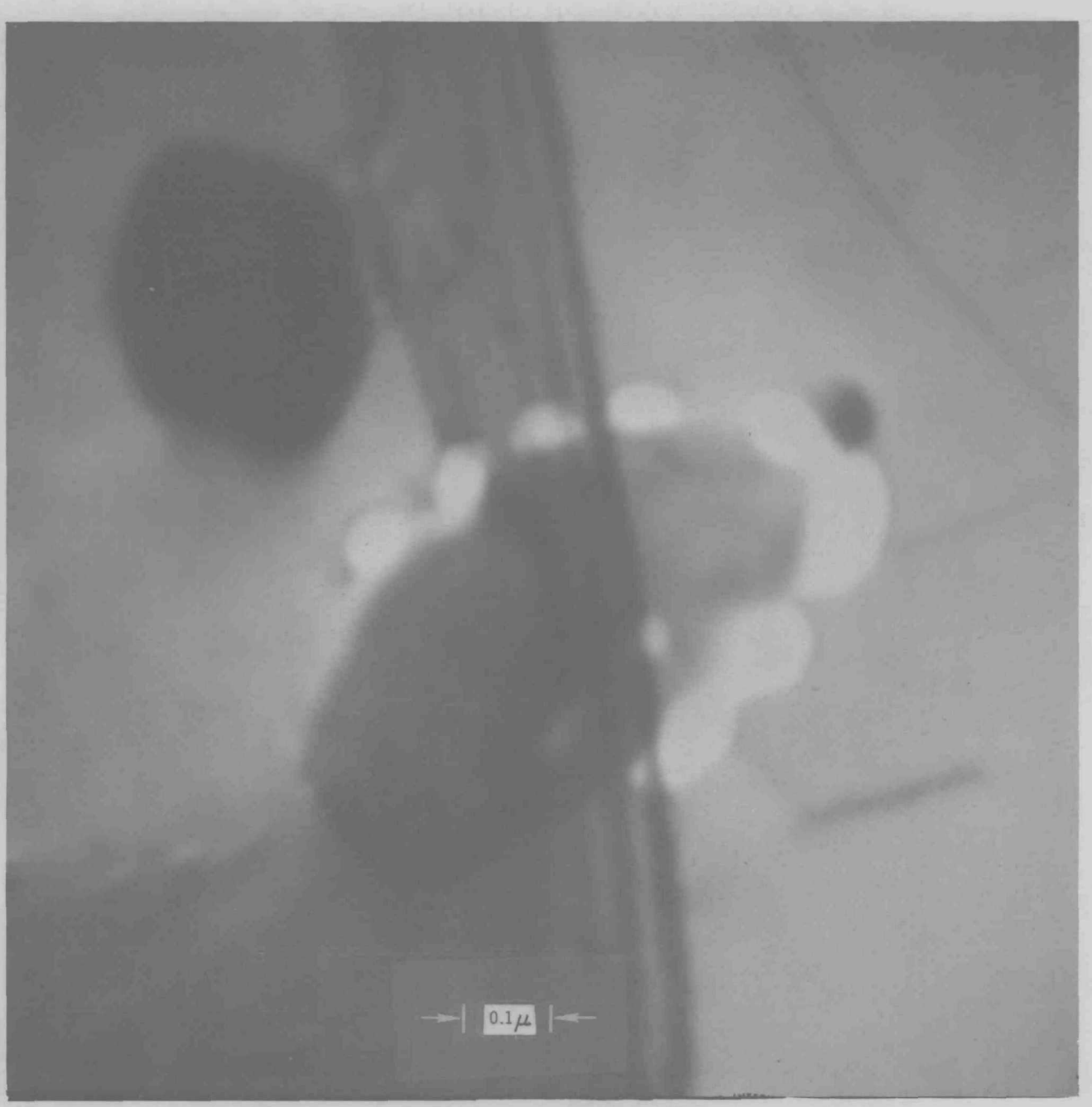

UNCL 7706-7769

Figure 9. Helium Bubbles on a Grain-Boundary Carbide in 405 Stainless Steel With 4 x 10^{-5} Atom Fraction Helium, Tested at 750°C (Transmission Electron Micrograph)

TABLE 6

COMPOSITION OF 19-9DL IN wt %

C	Cu	Cr	Mo	Ta/Nb	W	Ti	Ni	Fe
0.32	0.12	18.9	1.44	0.38	1.12	0.32	8.8	bal

TABLE 7

TENSILE DATA OF 19-9DL

Treatment	Atom Fraction Helium	Test Temperature (°C)	Yield Strength (kpsi)	Tensile Strength (kpsi)	Elongation (%)	
					Uniform	Total
16*	0	800	18.5	25.3	8.8	58.9
	3×10^{-5}	800	19.7	26.8	8.8	26.4
	0	700	23.6	42.6	15.8	43.4
	3×10^{-5}	700	22.4	39.2	14.6	30.1
	0	600	26.1	60.4	25.0	28.2
	3×10^{-5}	600	24.2	57.4	21.7	24.1
18†	0	800	24.6	28.7	3.1	39.0
	3×10^{-5}	800	23.4	30.2	2.6	10.3
	0	700	44.7	51.1	4.6	32.1
	3×10^{-5}	700	41.5	50.6	3.8	10.9
	0	600	58.5	75.4	7.6	10.7
	3×10^{-5}	600	58.4	73.8	7.5	9.5

*CR → 1 hr 1100°C → 100 hr 700°C.
†CR → 100 hr 700°C.

G. MASS SPECTROMETRY

Five capsules each containing seven subcapsules filled with elements and compounds have been sent to Pacific Northwest Laboratories for inclusion in an experimental irradiation in EBR-II. The capsules, which are expected to receive a 10-day irradiation late in September, contain 650 pieces of 30 pure elements and 23 crystalline compounds each wrapped in gold foil and sealed under vacuum. Each of the milligram-size pieces was etched, weighed, and photographed for later identification. Later analyses of the helium content of each piece by high sensitivity gas mass spectrometer, when correlated with the neutron flux spectral measurements that are simultaneously being made by PNL at the five core positions will lead to estimates of the differential (n,α) cross sections for the 47 elements involved.

IV. EVALUATION OF EFFORT TO DATE

With the completion of tensile testing of 304L SS, only 316L remains to be done of the four austenitic alloys of prime interest (304, 304L, 316, and 316L). It is apparent that austenitic alloys with simple microstructures will all suffer helium embrittlement to about the same degree.

The stress-rupture data for 304 SS is valuable but interpretation is hampered because strain measurements cannot be made during testing. In the second pair of stress-rupture machines being built, strain will be measured during testing. In this way, the duration of the different stages of creep will be known.

V. NEXT REPORT PERIOD ACTIVITIES

Tensile testing of 19-9DL will continue.

Metallography of 405 SS and 304L SS will continue.

Stress-rupture testing of 316 SS will continue.

Construction of the second pair of stress-rupture machines will continue.

Tensile testing of some Ni-base alloys will begin.

Program:	Fuel Cladding and Structural Materials				
AEC Task:	10-C, Mechanical Properties, Static Sodium				
Project Manager:	J. L. Ballif/J. J. Gill				
Reporting Period:	July-September 1968				
General Order:	7706	Subaccount:	29530	AEC Category:	04-01-61-01.5

Principal Investigator: D. F. Atkins

I. PROJECT OBJECTIVES

The project objective is to determine the individual and combined effects of environment (sodium and helium), strain rate (10^{-7} to 10^{-3}/hr), and stress condition (uniaxial and biaxial) on the creep and stress-rupture characteristics of Type 304 stainless steel and Type 316 stainless steel cladding alloys.

II. MAJOR ACCOMPLISHMENTS DURING FISCAL YEAR 1969

Two 12-specimen sodium retorts were assembled and placed on test under a 1/2:1 biaxial stress mode. These tests, together with others already underway or planned, will provide long term design information at 1200 and 1000°F for 304 and 316 stainless steels.

The design of the 1:1 biaxial test specimen was finalized following an evaluation of three different design alternatives. Six specimens were placed on test in 1200°F sodium, and some preliminary conclusions have been made regarding effects of state-of-stress on rupture strength and ductility.

III. PROGRESS DURING REPORT PERIOD

Mechanical testing in high purity static sodium was continued on tubular material (0.010-in wall) from the characterized reference heats of Type 304 and 316 stainless steel. Two new biaxial 12-specimen retorts were placed on test and three retorts completed tests during this period. The status of all 12-specimen sodium retort is summarized in Table 1. In addition to the 12-specimen biaxial retorts which impose a 1/2:1 stress ratio on the specimens, single specimen sodium retorts are being used to study the effect of a 1:1 biaxial stress on creep and stress-rupture behavior. The status of these tests is given in Table 2.

TABLE 1

LMFBR CLADDING PROGRAM BIAXIAL STRESS RUPTURE TESTS

Retort No.	Test Temp. (°F)	SS Alloy	Clad Cond. *	Environ	Life Span (hr)	Status		Remarks	Date Start/Completed
						Test	Exam.		
1	1300	304	AR	Na+Zr	100-700	Comp.	Comp.	Scoping test	2-11-67/3-13-67
2	1400	304	AR	Na+Zr	100-400	Comp.	Comp.	Scoping test	2-6-67/2-22-67
3	1400	304	AR	He	100-800	Comp.	Comp.	Effect of sodium	3-18-67/4-21-67
4	1200	304	AR	Na+Zr	100-2600	Comp.	Comp.	Scoping test	3-27-67/7-14-67
5	950	304	AR	Na+Cu	100-3000	Comp.	Comp.	Effect of copper	4-21-67/9-18-67
6	1400	304	AR	Na	100-900	Comp.	Comp.	Scoping test	6-2-67/7-7-67
7	1100	304	AR	Na	100-3000	Comp.	Comp.	Scoping test	6-9-67/10-30-67
8	1400	304	Ann	Na	100-2000	Comp.	Comp.	Effect of cold work	6-15-67/9-12-67
9	1000	304	AR	Na	100-700	Comp.	Comp.	Scoping test	8-12-67/9-11-67
10	1400	304	AR	Na	1000-3000	Comp.	Comp.	Extension of data	8-10-67/12-18-67
11	1200	304	AR	Na	100-4000	Comp.	Comp.	Extension of data	8-12-67/1-10-68
12	1100	304	AR	Na+Cu	100-700	Comp.	Comp.	Effect of copper	8-18-67/9-18-67
13	1200	304	AR	He	100-5000	Comp.	Comp.	Effect of sodium	10-20-67/6-11-68
14	1200	304	AR+Aged	Na	100-1000	Comp.	Comp.	Effect of thermal aging	11-2-67/3-6-68
15	1200	304	AR	Na	5000-6100	Comp.	-	Extension of data	11-9-67/7-25-68
16	1000	304	AR	Na	100-3000	Comp.	Comp.	Extension of data	11-22-67/3-31-68
17	1200	304	Ann	Na	5000-10,000	1/4 Comp.	-	Extension of data	2-22-68
18	1200	304	Ann	Na	100-5000	Comp.	-	Effect of cold work	1-25-68/8-18-68
19	1000	304	AR	Na	5000-10,000	In Prog.	-	Extension of data	4-2-68
20	900	304	AR+Ann	Na	100-7100	Comp.	-	Scoping test	12-1-67/9-22-68
21	1000	304	Ann	Na	100-2300	Comp.	Comp.	Effect of cold work	2-15-68/5-20-68
22	1000	304	Ann	Na	5000-10,000	1/4 Comp.	-	Extension of data	2-29-68
23	1200	304	Ar+Na Exp.	Na	100-5000	1/4 Comp.	-	Effect of flowing sodium	8-22-68
24	1300	304	AR	Na+Cu	100-1000	Comp.	Comp.	Effect of copper	3-26-68/5-15-68
101	1400	316	AR	Na	100-1000	Comp.	Comp.	Scoping test	8-10-67/9-21-67
102	1200	316	AR	Na	100-7100	Comp.	Comp.	Extension of data	8-12-67/6-6-68
103	1000	316	AR	Na	100-4000	Comp.	Comp.	Scoping test	9-14-67/3-5-68
104	1400	316	AR	He	100-1600	Comp.	Comp.	Effect of sodium	8-31-67/11-15-67
105	1400	316	Ann	Na	100-800	Comp.	Comp.	Effect of cold work	10-19-67/11-27-67
106	1200	316	Ann	Na	100-2000	Comp.	Comp.	Effect of cold work	10-24-67/1-18-68
107	1000	316	Ann	Na	100-600	Comp.	Comp.	Effect of cold work	12-6-67/1-8-68
108	1000	316	AR	He	100-2000	Comp.	Comp.	Effect of sodium	1-12-68/4-9-68
109	1200	316	AR	Na	100-2000	Comp.	Comp.	Scoping test	2-9-68/4-25-68
110	1000	316	AR	Na	1000-10,000	In Prog.	-	Extension of data	4-23-68
111	1000	316	Ann	Na	100-10,000	Comp.	-	Extension of data	5-10-68/6-4-68
112	900	316	Ann	Na	100-5000	3/4 Comp.	-	Extension of data	6-20-68
113	900	316	AR	Na	100-5000	In Prog.	-	Extension of data	8-16-68

*AR = As-received tubing containg 10 to 15% cold work
Ann = Annealed tubing

TABLE 2

1:1 BIAXIAL STRESS RUPTURE TESTS

Test. No.	Test Temp. (°F)	SS Alloy	Clad Cond. *	Environ	Stress (psi)	Rupture Time (hr)	Date Start/Complete
424B	1200	304	Ann	He	28,000	221	4-29-68/5-9-68
425B	1200	304	AR	He	30,000	460	5-14-68/6-2-68
426B	1200	304	Ann	Na	28,000	161	7-8-68/7-15-68
427B	1200	304	Ann	Na	24,000	373	7-26-68/8-10-68
428B	1200	304	AR	Na	30,000	413	7-31-68/8-16-68
430B	1200	304	Ann	Na	21,000	-	9-12-68/
601B	1200	316	Ann	Na	22,000	-	9-17-68/
602B	1200	316	Ann	Na	22,000	-	9-24-68/

*AR = As-received tubing containing 10 to 15% cold work
Ann = Annealed tubing

Twelve 304 stainless steel stress rupture specimens which were exposed without stress to 1200°F flowing sodium for 2000 hr were assembled into a 12-specimen static sodium retort. The retort is currently on test at 1200°F. The specimens were exposed in the MSA Research clean sodium loop ($\Delta T \sim 150°F$, sodium flow velocity <0.05 ft/sec) in an attempt to produce a significant ferritic surface layer on the O. D. of the tubular specimens. However, metallographic studies on one of the specimens revealed only about a 0.0002-in. layer on the O. D. of the tubing. This layer can be detected in the photomicrograph in Figure 1. Profilometer measurements on the O. D., before and after exposure to the loop, revealed that there was no detectable surface loss as a result of the flowing sodium. The specimens under stress-rupture test are biaxially stressed (1/2:1) to produce rupture data within the range 500 to 5000 hr. The data obtained to date are too limited to permit any comment on the effect of the flowing sodium exposure on the stress-rupture behavior of 304 stainless steel.

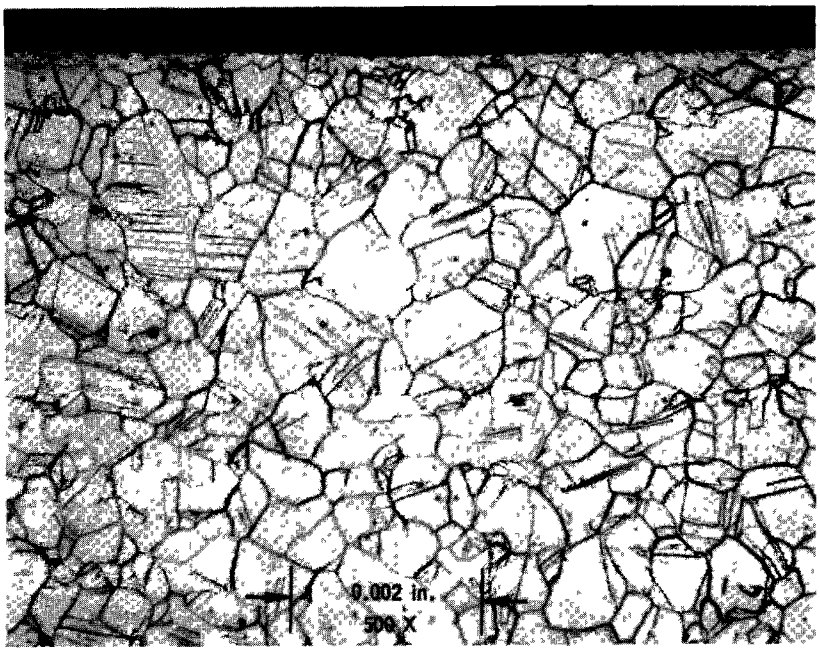

7706-4760

Figure 1. Thin Surface Layer, Probably Ferrite, on 304 Stainless Steel After Exposure to 1200°F Flowing Sodium; Cross Section (Transverse); Marble's Etch; 8361-10-1

Metallographic studies were performed on 304 and 316 stainless steel specimens from several biaxial stress-rupture retorts tested in 1000 and 1200°F sodium. As has been observed previously, ruptures which develop in the tubing wall as small longitudinal cracks or pin-holes, are entirely intergranular. However, the rather large explosive-type ruptures were found to contain a combination of both intergranular and transgranular fracture. Evidence indicates that the fractures initiated as intergranular fissures and cracks, and that transgranular cracking occurred as a crack propagated at high velocity. In the 316 stainless steel containing 10 to 15% cold work, carbide precipitation on grain boundaries and slip bands was found to be considerably heavier at 1200 than at 1000°F. Carbide decoration of slip bands was not observed on annealed material, indicating that the banding observed in the 10 to 15% cold worked alloy results from cold work during tubing fabrication and not from strain during testing.

Diametral strain measurements were made on tubular specimens from five 12-specimen stress rupture retorts tested at 1000 and 1200°F. The data are tabulated in Tables 3 through 7. These data, together with data generated on previous tests, have defined the strain rate behavior of the two alloys in the cold worked condition.

Figure 2 presents the strain-rate behavior curves for 304 stainless steel tubing containing 10 to 15% cold work. Included on the 1200°F curve, are data obtained in a helium environment and in sodium. The 304 stainless steel shows essentially the same strain-rate behavior in either environment. For 316 stainless steel, the strain-rate behavior at 1000 and 1200°F is shown in Figure 3. The data again have very little scatter. The strain-rate values on annealed 304 and 316 stainless steel are not in sufficient quantity to justify the presentation

TABLE 3

STRESS RUPTURE PROPERTIES OF 304 STAINLESS STEEL WITH 10 TO 15% COLD WORK IN 1200°F SODIUM (RETORT NO. 15)

Specimen Number	Hoop Stress (psi)	Rupture Time (hr)	Diametral Strain (%)	Ave Strain Rate (%/hr)
4-164	16,000	6208	2.49	4.01×10^{-4}
4-165	16,000	5927	3.03	5.11×10^{-4}
4-166	16,000	6102	2.75	4.51×10^{-4}
4-167	17,000	5473	2.12	3.87×10^{-4}
4-168	17,000	5271	2.59	4.91×10^{-4}
4-169	17,000	5487	2.66	4.85×10^{-4}
4-170	18,000	4431	1.98	4.47×10^{-4}
4-171	18,000	4953	3.13	6.32×10^{-4}
4-172	18,000	4560	2.52	5.53×10^{-4}
4-173	20,000	3397	1.98	5.83×10^{-4}
4-174	20,000	3296	2.25	6.83×10^{-4}
4-175	20,000	3121	1.95	6.25×10^{-4}

TABLE 4

STRESS RUPTURE PROPERTIES OF 304 STAINLESS STEEL WITH 10 TO 15% COLD WORK IN 1200°F HELIUM (RETORT NO. 13)

Specimen Number	Hoop Stress (psi)	Rupture Time (hr)	Diametral Strain (%)	Ave Strain Rate (%/hr)
4-140	17,000	4964	2.90	5.84×10^{-4}
4-141	17,000	5012	3.09	6.16×10^{-4}
4-142	17,000	5598	3.52	6.29×10^{-4}
4-143	22,000	2937	3.12	1.06×10^{-3}
4-144	22,000	2783	2.79	1.00×10^{-3}
4-145	22,000	2751	2.45	0.89×10^{-3}
4-150	28,000	1233	2.18	1.77×10^{-3}
4-151	28,000	1257	2.80	2.23×10^{-3}
4-147	35,000	372	2.18	5.86×10^{-3}

TABLE 5

STRESS RUPTURE PROPERTIES OF ANNEALED 304 STAINLESS STEEL IN 1200°F SODIUM (RETORT NO. 18)

Sample No.	Stress (psi)	Rupture Time (hr)	Strain (%)	Strain Rate (%/hr)
A4-13	19,000	4097	6.42	1.57×10^{-3}
A4-14	19,000	4561	8.61	1.89×10^{-3}
A4-15	19,000	4949	7.56	1.53×10^{-3}
A4-16	25,000	875	10.72	1.22×10^{-2}
A4-17	25,000	850	9.34	1.10×10^{-2}
A4-19	30,000	228	Burst	-
A4-20	30,000	228	Burst	-
A4-21	30,000	228	Burst	-
A4-22	35,000	37	8.77	2.37×10^{-1}
A4-23	35,000	58	9.28	1.60×10^{-1}
A4-24	35,000	58	9.48	1.63×10^{-1}

TABLE 6

STRESS RUPTURE PROPERTIES OF ANNEALED 304 STAINLESS STEEL IN 1000°F SODIUM (RETORT NO. 21)

Sample No.	Hoop Stress (psi)	Rupture Time (hr)	Diametral Strain (%)	Ave Strain Rate (%/hr)
A4-31	45,000	2000	9.82	4.91×10^{-3}
A4-32	45,000	2280	Explosive Rupt.	-
A4-33	45,000	2024	Explosive Rupt.	-
A4-34	47,000	1089	9.85	9.04×10^{-3}
A4-35	47,000	1236	9.85	7.97×10^{-3}
A4-36	47,000	1105	Explosive Rupt.	-
A4-37	50,000	370	Explosive Rupt.	-
A4-38	50,000	598	Explosive Rupt.	-
A4-39	50,000	300	Explosive Rupt.	-
A4-40	55,000	85	Explosive Rupt.	-
A4-41	55,000	89	Explosive Rupt.	-
A4-42	55,000	89	Explosive Rupt.	-

TABLE 7

STRESS-RUPTURE PROPERTIES OF 10 TO 15% COLD-WORK 316 SS IN 1200°F Na (RETORT NO. 102)

Sample No.	Hoop Stress (psi)	Rupture Time (hr)	Diametral Strain (%)	Ave Strain Rate (%/hr)
6-13	22,000	6770	4.26	6.29×10^{-4}
6-14	22,000	7152	5.77	8.07×10^{-4}
6-15	22,000	7046	4.76	6.76×10^{-4}
6-16	25,000	3412	6.67	1.96×10^{-3}
6-17	25,000	3623	9.82	2.71×10^{-3}
6-18	25,000	3396	5.10	1.50×10^{-3}
6-19	30,000	752	6.94	9.23×10^{-3}
6-20	30,000	790	6.34	8.03×10^{-3}
6-21	30,000	764	Explosive Rupt.	-
6-22	35,000	129	Explosive Rupt.	-
6-23	35,000	129	Explosive Rupt.	-
6-24	35,000	105	5.50	5.24×10^{-2}

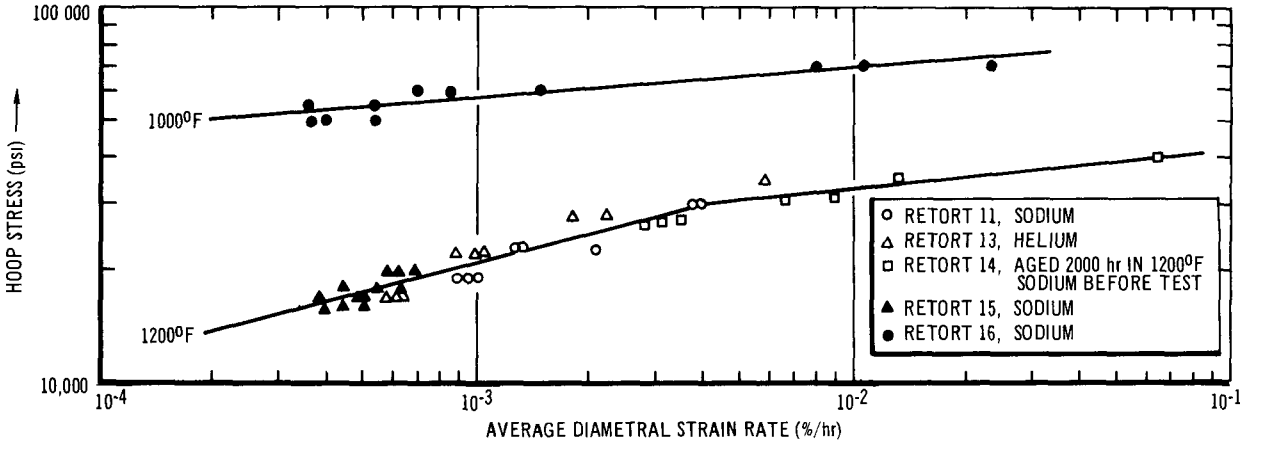

7706-4761

Figure 2. Strain Rate Behavior of 10-15% Cold Worked Type 304 Stainless Steel

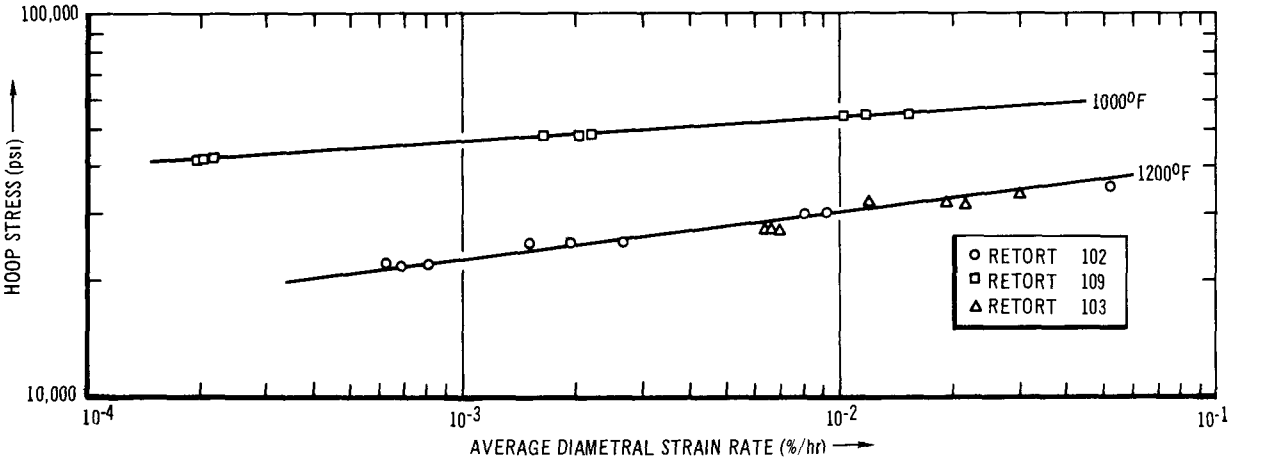

7706-4762

Figure 3. Strain Rate Behavior of 10-15% Cold Worked Type 316 Stainless Steel in a High Purity Static Sodium Environment

of strain-rate curves at this time. Tests which are presently in progress will provide additional data on the annealed alloys.

The retort with twelve 10 to 15% cold-worked Type 304 stainless steel specimens exposed to 1300°F copper-saturated sodium was disassembled. Diametral strain measurements were taken on the specimens and are listed in Table 8. From the results, it is obvious that neither copper-plating nor the

TABLE 8

STRESS RUPTURE PROPERTIES OF 10 TO 15% COLD WORKED 304 STAINLESS STEEL IN 1300°F Cu-CONTAMINATED SODIUM

Specimen Number	Cu-Thickness (in.)	Hoop Stress (psi)	Rupture Time (hr)	Max Dia Strain (%)	Strain Rate (%/hr)
4-211	0	12,000	1186	3.93	3.31×10^{-3}
4-212	0	12,000	1186	4.20	3.54×10^{-3}
4-206	0.0002	12,000	1175	4.30	3.66×10^{-3}
4-213	0	15,000	715	4.04	5.65×10^{-3}
4-214	0	15,000	705	3.60	5.11×10^{-3}
4-207	0.0002	15,000	681	3.76	5.52×10^{-3}
4-215	0	20,000	298	4.27	1.43×10^{-2}
4-216	0	20,000	280	3.87	1.38×10^{-2}
4-208	0.0006	20,000	280	4.20	1.50×10^{-2}
4-217	0	25,000	106	4.87	4.59×10^{-2}
4-218	0	25,000	121	3.50	2.89×10^{-2}
4-209	0.0006	25,000	121	4.30	3.55×10^{-2}

1300°F copper-saturated sodium had any adverse effect on the ductility (diametral strain) or the average strain rate of the 10 to 15% cold-worked Type 304 stainless steel tubing. The diametral strain was found to be insensitive to rupture time up to 1200 hr. All specimens exhibited about 4% rupture strain. This strain insensitivity is attributed to the delicate balance of strain-rate effect and recovery processes occurring at 1300°F. This behavior has been observed in the 10 to 15% cold-worked Type 304 stainless steel tubing tested at 1100, 1200, and 1400°F,* and in the British M-316 alloy containing about 20% cold work.† The strain-rate behavior of 10 to 15% cold-worked Type 304 stainless steel in 1300°F copper-saturated sodium is shown in Figure 4. The data obtained from tests conducted at 950 and 1100°F are included for comparison purposes.

*W. T. Lee, "Biaxial Stress-Rupture Properties of Austenitic Stainless Steels in Static Sodium," AI-AEC-12694 (June 30, 1968)

†H. K. Richardson and R. McDowell, "Elevated Temperature Stress Rupture Properties of M316, FV548, and Niomonic PE16 PFR-Type Tube," TRG Report 1482 (C) (1967)

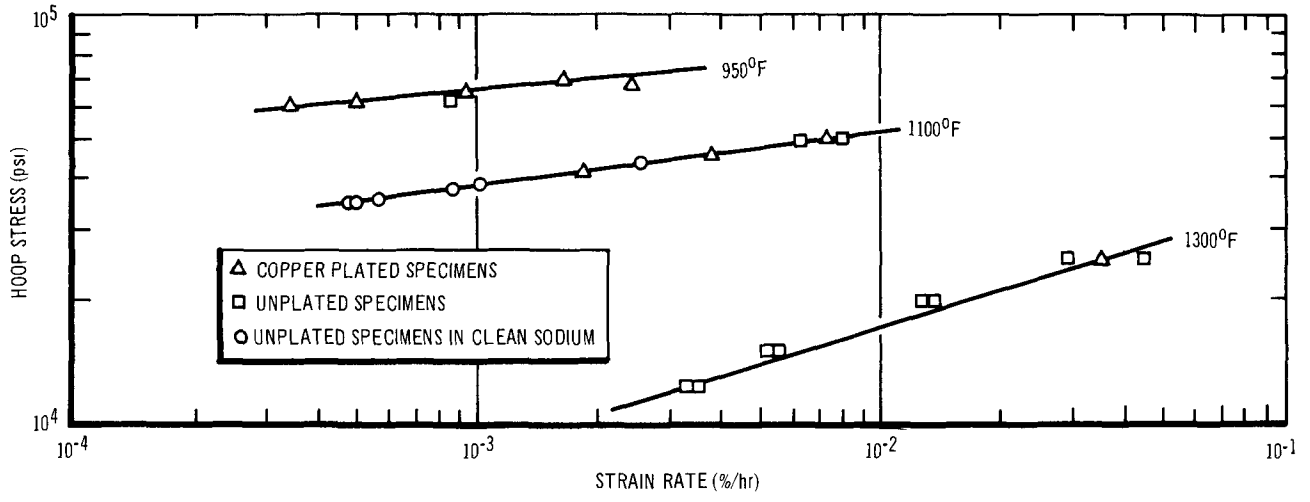

7706-4763

Figure 4. Strain Rate Behavior of 10-15% Cold Worked 304 Stainless Steel in Copper Contaminated Sodium

Metallographic examination of the specimens ruptured in 1300°F copper-saturated sodium revealed normal intergranular fracture and grain boundary fissures. No abnormal microstructure was detected in the copper-plated or nonplated specimens exposed to the copper-contaminated sodium. The structure contained normal carbide precipitation on slip bands, twin boundaries, and on grain boundaries. A minute amount of sigma phase was also found randomly on grain boundaries. These metallographic observations further substantiate the conclusion that 1300°F copper-saturated sodium has no adverse effect on the stress-rupture properties of Type 304 stainless steel tubing under the test conditions imposed. Similar conclusions were reported previously for tests conducted at 950 and 1100°F. Four Charpy impact specimens which were in the 1300°F copper-saturated sodium for 1200 hr were submitted (through the AEC) to the Naval Research Laboratory for impact testing. To protect the sensitized specimens from atmospheric corrosion, special packaging procedures were used for shipment.

Specimens of 316 stainless steel tubing containing 10 to 15% cold work were assembled into a static sodium, 12-specimen retort and placed on test at 900°F. Four biaxial (1/2:1) stress levels were applied to the specimens to obtain data over the range 1000 to 5000 hr.

Three stress rupture tests, whereby tubular 304 stainless steel specimens were subjected to a 1:1 biaxial stress state, were completed in 1200°F sodium. In these tests, the specimen were stressed equally in both the tangential and axial directions. The first specimen, annealed 304 stainless steel, was stressed to 28,000 psi and failed after 161 hr. The axial strain was 8.4% while the maximum diametral strain was 8.7%. The second specimen, also annealed 304 stainless steel, was stressed at 24,000 psi. The specimen ruptured after 372 hr, which is about the same rupture life as observed in pure uniaxial tension for the same stress level. The axial strain was 7.7% while the maximum diametral strain was 7.9%. The third 304 stainless steel specimen contained 10 to 15% cold work and was stressed to 30,000 psi. Failure occurred after 413 hr with 2.5% axial strain and 1.9% tangential strain. A previous test, under identical conditions, except that the environment was helium, failed in 460 hr. This is within acceptable scatter. However, the strain on the helium test was 6.2% axial and 8.7% tangential. Additional testing will be required before the differences in strain between these specimens can be resolved. It should be noted that in the numerous 1/2:1 biaxial tests, no difference in rupture strength or strain-rate behavior were observed between the helium and sodium environments.

Three additional 1:1 biaxial retorts were assembled and are currently under test in 1200°F sodium. Two of these tests are on annealed 316 stainless steel. Details of the tests are given in Table 2.

A uniaxial stress rupture test on 304 stainless steel sheet stock was initiated in a helium environment. All previous uniaxial tests were conducted in high purity sodium. The results of the present test in helium is compared to those of an identical test in sodium in Figure 5. Although the helium test is not complete, it does demonstrate that the secondary or steady-state creep rate is the same in both test environments.

A supply of 316 stainless steel tubing, 0.275-in. I.D. by 0.010-in wall, to meet the currently foreseen requirements, was annealed for 1/2 hr in dry hydrogen at 1950°F. This material will be used on creep/stress-rupture tests to provide long term test data and to evaluate cold work effects.

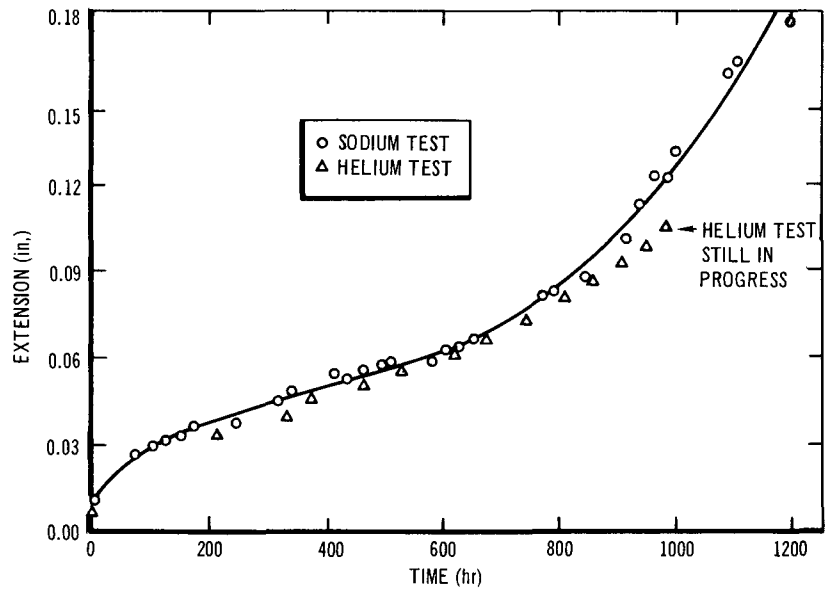

Figure 5. Comparison of Stress Rupture Characteristics of Annealed Sheet 304 Stainless Steel in High Purity Sodium to Those When in Helium

IV. EVALUATION OF EFFORT TO DATE

The biaxial (1/2:1) testing program on 304 stainless steel and 316 stainless steel will now be concentrated mainly on the generation of long term test data. This will provide needed design information under the biaxial state of stress. Although the effects of cold working have been well defined in the shorter term stress rupture studies at 1200°F and above, there is still some uncertainty as to cold work behavior at lower temperatures under long term low-stress conditions. The current testing program has been designed to provide this information.

The 1:1 biaxial testing studies which are just beginning have yielded some preliminary data on the effect of stress state on 304 stainless steel. The stress rupture strength of annealed 304 stainless steel under the 1:1 biaxial stress state seems to be the same as that found for uniaxial (0:1) stress. As shown in Figure 6, the three 1:1 biaxial points are on the stress-rupture curve generated from the uniaxial test data. This behavior would be predicted from the

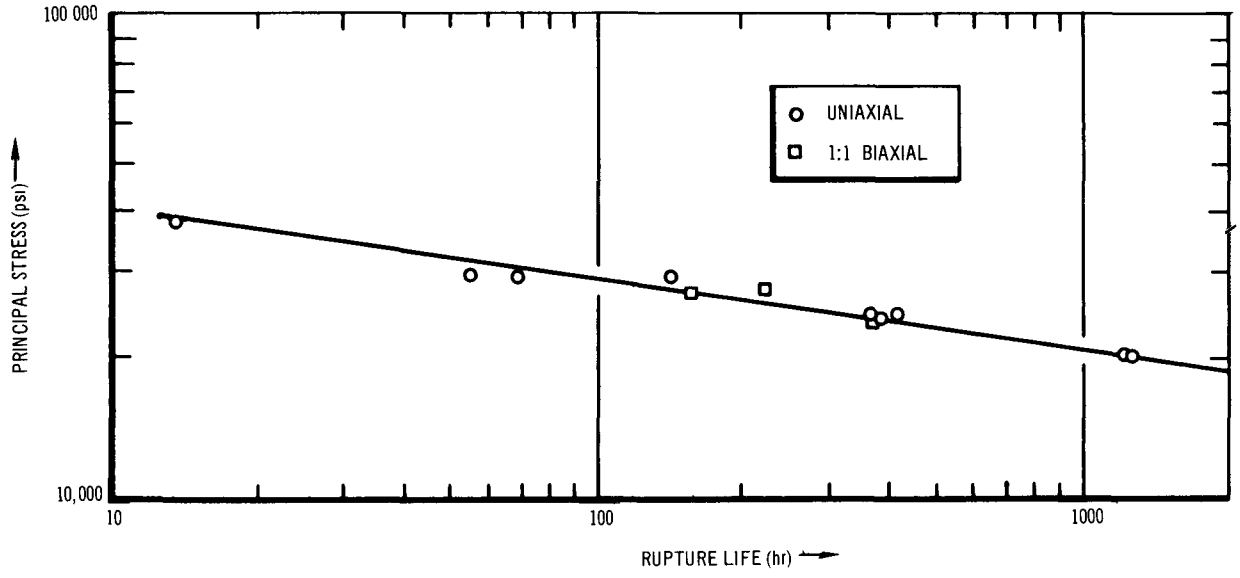

7706-4765

Figure 6. Comparison of Stress Rupture Strength of Uniaxial to 1:1 Biaxial Specimens in 1200°F Sodium

Von Mises' distortion energy yield criterion. While the rupture life in the 1:1 stress mode seems to be essentially the same as for the uniaxial condition, the strain at rupture was found to be markedly different. The 1:1 biaxial stress mode produces a much lower rupture strain. For example, at an equivalent stress level of 28,000 psi, the total uniaxial strain at rupture was observed to be about 40%; whereas, in the 1:1 biaxial case, the strain is only about 8% in both the axial and tangential directions. It should be emphasized that these observations are very preliminary. The additional 1:1 biaxial tests which are scheduled should provide a high confidence level and permit an accurate analysis of the 1:1 biaxial stress state.

V. NEXT REPORT PERIOD ACTIVITIES

Biaxial stress rupture testing (1/2:1) will be continued on the long term (to 10,000 hr) tests on both 304 and 316 stainless steel. Four new 12-specimen retorts will be assembled and placed on test.

Tests under a 1:1 biaxial stress mode will be conducted in single specimen sodium retorts. It is anticipated that 10 to 12 specimens will be placed on test with major emphasis on 316 stainless steel in both the cold-worked and annealed conditions.

Microstructural studies will be conducted as tests are completed. These studies will provide further insight into cold work behavior, stress induced reactions, and fracture mechanisms.

Program:	Fuel Cladding and Structural Materials		
AEC Task:	10-D, Dynamic Sodium Testing		
Project Manager:	J. L. Ballif/J. J. Gill		
Reporting Period:	July-September 1968		
General Order: 7706	Subaccount: 29541-4	AEC Category: 04-01-61-01.5	

Principal Investigator: J. H. Shively

I. PROJECT OBJECTIVES

Project objectives are to: (1) provide the design basis for the combined effects of mass transfer, temperature, heat flux, biaxial stresses, and load cycling on the creep and stress rupture behavior of fuel cladding in flowing sodium, (2) develop and test an engineering approach to definition of mass transfer phenomena in cladding materials under fast reactor conditions, and (3) improve and extend the present concept of a high flux heater assembly with cladding for use at high linear power ratings (heat flux) and longer life (greater than 1000 hours).

II. MAJOR ACCOMPLISHMENTS DURING FISCAL YEAR 1969

Four high flux heater assemblies with internally pressurized cladding (Model C) were built and tested. The tests were made to obtain additional information on mass transfer phenomena and mechanical properties in dynamic sodium and to contribute to a better understanding of heater performance. Four additional heater assemblies with nonpressurized cladding (Model B) were assembled and inserted into the sodium loop for testing.

Two compatibility experiments were performed in support of the heater improvement phase of the subtask. These were performed to optimize the materials and fabrication processes for the electrode system, particularly for the upper diffusion barrier.

Biaxial stress-rupture of helium injected tubes showed that helium reduced the life and ductility of both Type 304 and 316 stainless steel. Comparison of the strain at failure of these tubes to a creep curve for noninjected tubes revealed that helium reduced the amount of nonuniform strain.

III. PROGRESS DURING REPORT PERIOD

A. SUMMARY

The test conditions and results for the four heater assemblies with pressurized cladding (Model C) are displayed in Table 1. The stress-rupture life under a steady state heat flux conforms to previous findings for the same conditions, and correlates with a predicted life based on stress-rupture data obtained in static sodium. The predicted life is obtained by interpolation of the static sodium test results for the stress and peak longitudinal temperature at the tubing midwall. Cycling the heat flux produced increased strain at failure and reduced life under stress, by a ratcheting mechanism. Comparison to other tests under cyclic internal heating revealed little effect on stress-rupture life when the cyclic heat flux is reduced from 1×10^6 to 0.8×10^6 Btu/ft^2-hr.

TABLE 1
SUMMARY OF TEST CONDITIONS

Exp No.	Heater No.	Heat Flux (Btu/ft^2-hr)	Mode	Internal Pressure (psi)	Sodium Velocity (ft/sec)	Sodium Temp (°F)	Time to Fail (hr)	Strain at Failure (%)	Purpose of Test
M-304-2	53	1.0×10^6	Steady-state	1220	20	1200	391.8	2.5	Mechanical properties
M-304-3	54	0.8×10^6	Steady-state	150	20	1200	387.1	-	Mass transfer
M-304-6	55	0.8×10^6	12-min cycle	1600	20	1200	109.8	3.3	Mechanical properties
M-304-6	56	0.8×10^6	12-min cycle	1600	20	1200	112.2	3.3	Mechanical properties

*Cladding did not fail.

Four heater assemblies with nonpressurized cladding were built and inserted into the sodium loop for testing. These tests are combined mass transfer and heater improvement studies. The heater assemblies contain several design modifications made to extend heater performance: (1) a reduced sheath thickness to improve heat transfer to the flowing sodium, (2) new upper diffusion barrier materials selected to reduce the extent and rate of carbide formation, and (3) a hollow graphite electrode with end plugs to reduce the temperature at the interface between the graphite and the molybdenum electrodes. Another

innovation is that cladding is attached to the Model B heater assemblies for mass transfer studies. Previously, this model was used for heater development work only and did not have cladding. The cladding is not internally pressurized and sodium surrounds the cladding. The sodium, however, is stagnant in the annulus between the heater sheath and the cladding and serves only to transfer heat while the sodium external to the tube is flowing at a high rate.

Two compatibility experiments were performed in support of the heater improvement phase of the task. In the first experiment, several candidate diffusion barrier materials were studied to determine the extent of reaction with graphite and boron nitride. Rhenium and tungsten exhibited the least effect of interaction with graphite. The second test was designed to study other potential diffusion barrier materials and braze alloys for metallurgically joining the diffusion barrier to the graphite. The latter effort may help to reduce the autocatalytic nature of the carbide formation during cyclic heater operation. The results of this test were negative insofar as neither the diffusion barrier materials nor the braze alloys tested exhibited desirable chemical compatibilities.

Activation analysis of the cladding exposed to 387 hr of flowing sodium under a steady state heat flux of 800,000 Btu/ft^2-hr is almost complete. Preliminary results point to the merits of this technique in the study of mass transfer in liquid sodium. Loss of activity was limited to the region of heating, which is consistent with theory. In addition, the rate of loss of iron corresponds to a corrosion rate of 1.43 mils/year. This agrees with a surface layer recession rate of 1.10 mils/year from surface indentation analysis.

Stress-rupture testing of helium-injected tubes of annealed Type 304 and 316 stainless steel were completed. As expected, helium injection substantially reduced the life under internal pressure and reduced the total strain at failure for Type 304 stainless steel. A composite biaxial creep curve was obtained in the same test retort on noninjected tubes. The strain at failure of the injected tubes lay on the creep curve of the noninjected tubes at the beginning of third stage creep. Helium analyses revealed that the greatest concentration of helium was present at the surface.

B. ENGINEERING APPLICATION

The recent stress-rupture test under a steady state heat flux of 1×10^6 Btu/ft^2-hr (23 kw/ft) demonstrates that, for design purposes, it may be possible to predict creep of cladding under a known force from fuel swelling or fission gas pressure by using conventional isothermal biaxial stress-rupture data. The peak temperature and stress at the cladding midwall must be known to make the prediction. The isothermal data are then interpolated for these conditions. The approach demands that the force on the cladding from fuel swelling be known, either through experiment or analysis. One uncertainty in the approach is how radiation and helium effects respond to thermal gradients. For example, helium redistribution under a temperature gradient may force the use of some position other than the midwall for definition of conditions. In addition, the largest fuel swelling force on the cladding (maximum burnup) in a fuel element generally does not occur at the peak temperature position, so that the largest strain may occur somewhere between the peak cladding surface temperature and the region of maximum burnup.

The recent tests of cladding under a cyclic heat flux reaffirms the view that cyclic heating enhances the rate of deformation and reduces the total life at temperature by almost a factor of four. Although it is true that the test conditions do not duplicate those anticipated as a result of reactor load variations, the phenomena believed to be responsible for the reduced life and increased average strain rate are not expected to be different in actual application. Stress relaxation by primary and/or secondary creep has been suggested as being responsible for the stress-rupture behavior under cyclic heating.* This action may occur for a reactor fuel pin where variation in power demands on the reactor lead to time varying thermal stresses from heat extraction and internal pressure stresses from the fuel. In order to make a reasonable prediction of the life under enhancement of creep due to reactor load variations, stress relaxation from primary and secondary creep under biaxial stress and at high temperatures must be calculated. In addition, a set of failure criteria are needed to make predictions of the effect of cycling on life.

---

*Shively, J. H., "Thermal Gradient Effects on Stress-Rupture Behavior in Thin-Walled Tubing," AI-AEC-12695 (June 25, 1968), Blackburn, W. S., Journ. Strain Anal., 3, 176 (1968), and Bree, J., Journ. Strain Anal., 3, 122 (1968)

The absence of a large influence of heat flux, particularly when the decreased surface temperature is factored into the analysis, seems to indicate that it is stress relaxation during the off portion of the heat cycle that determines the strain and the life under internal stress; i.e., the strain per cycle.

The question of failure criteria for fuel element design under thermal cycling conditions is difficult to resolve because the strain at failure is a function of strain rate (i.e., the strain at failure decreases with decreasing strain rate). Accelerated creep by ratcheting may therefore increase the average strain rate and increase the strain at failure. Assuming this to be the case, the same set of ductility criteria applied to steady state condition can be applied to the cyclic condition when the average accelerated strain rate is employed. In order to calculate the effect of cycling on strain rate, primary and secondary creep data are needed for the stresses and temperatures at the high- and low-load conditions.

The preliminary results obtained in the recent mass transfer experiment showed a corrosion rate of 1.43 mils/yr when it is assumed that iron going into solution represents a surface recession. The absence of corrosion just upstream of the heated section implies that the inlet sodium is saturated with respect to the corroding species examined (viz., iron, chromium, and cobalt). The corrosion rate under internal heating with a heat flux of 800,000 Btu/ft^2-hr, which produces a ΔT in the sodium of $\sim$20°F and a ΔT bulk to cladding surface of $\sim$40°F is comparable in magnitude to that observed with unheated specimens in a loop with a 400°F ΔT.

The recently completed tests of helium injected tubes of annealed Type 304 stainless steel have some significance to fuel pin designers. Perhaps most significant is the observation that helium proportionately reduced rupture strain by far less under biaxial stress (6 to 4%) than under uniaxial stress (40 to 10%). In addition, the strain at failure for stress rupture life of the helium injected tube fell on the unirradiated creep curve at the beginning of third stage creep. This indicates that helium has its greatest influence on the nonuniform strain during creep and short time tensile tests. Since the biaxial stress condition produces much less nonuniform strain in stress-rupture than the uniaxial, the

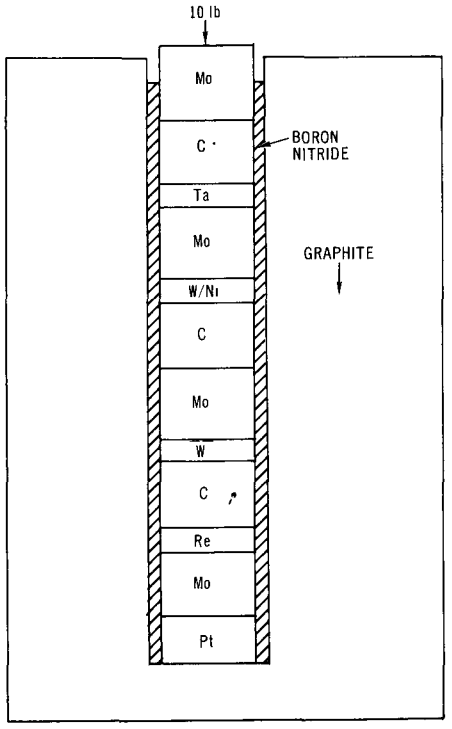

Figure 1. Configuration for the First Compatibility Test

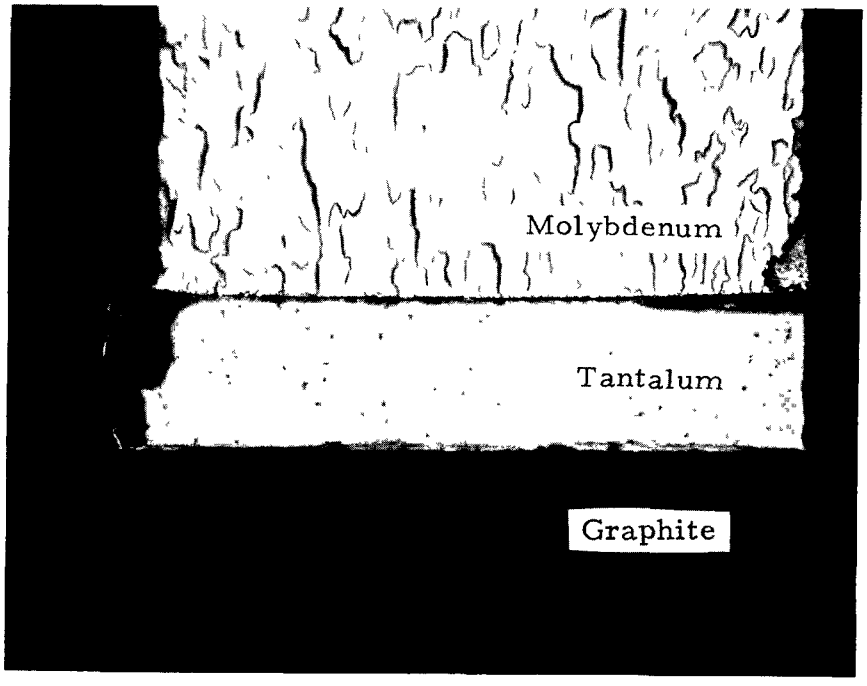

10-16-68 UNCL 7706-4076

Figure 2. Cross Section of a Tantalum Diffusion Barrier (Miarkami's Etch) 30X

effects of helium on ductility are understandable. Uniform strain is more important than total rupture strain since the strain after mechanical instability (necking on third stage creep) is not really useful for design purposes. Mechanical instability marks virtual failure. On the other hand, helium may help to initiate instability at an earlier time. It would then reduce uniform strain and the time spent in second stage creep. In order to resolve this important question, more information is needed about the effects of helium on uniform strain, secondary creep rate, and crack initiation.

C. TECHNICAL PROGRESS

1. Heater Improvement

a. Compatibility Tests

A compatibility test was conducted at 2500°F in vacuum on materials for potential use as the upper diffusion barrier in the high flux heaters with cladding. The purpose of this test was to determine the extent of interaction between graphite and rhenium, tungsten, and tantalum. The disc specimens were sandwiched between rods of molybdenum and graphite, loaded in a boron nitride sleeve, and compressed under a weight. This is represented by the sketch shown in Figure 1. The results of the test are displayed in the photomicrographs of the sectioned specimens; see Figures 2 through 4.

The extent of interaction between tantalum and graphite is shown by the thin yellow layer on the tantalum in Figure 2. This is indicative of formation of tantalum carbide. Since it is currently believed that carbide formation in the upper diffusion barrier is a limiting factor in the life of heaters under steady and cyclic operation, tantalum does not appear to be a good candidate for the upper diffusion barrier.

The tungsten interaction was small on both the nickel coated and uncoated discs; see Figure 3. The presence of a nickel coating improved the bonding between the molybdenum and the tungsten, but also created a somewhat larger carbon interaction zone. Although it is not evident in the photographs, the interaction zone was less than that with tantalum.

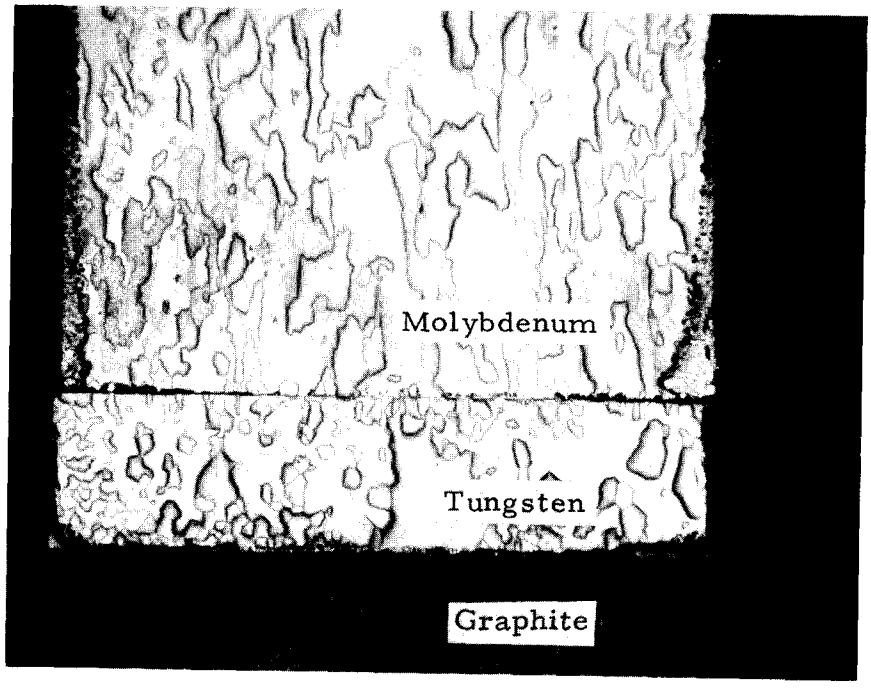

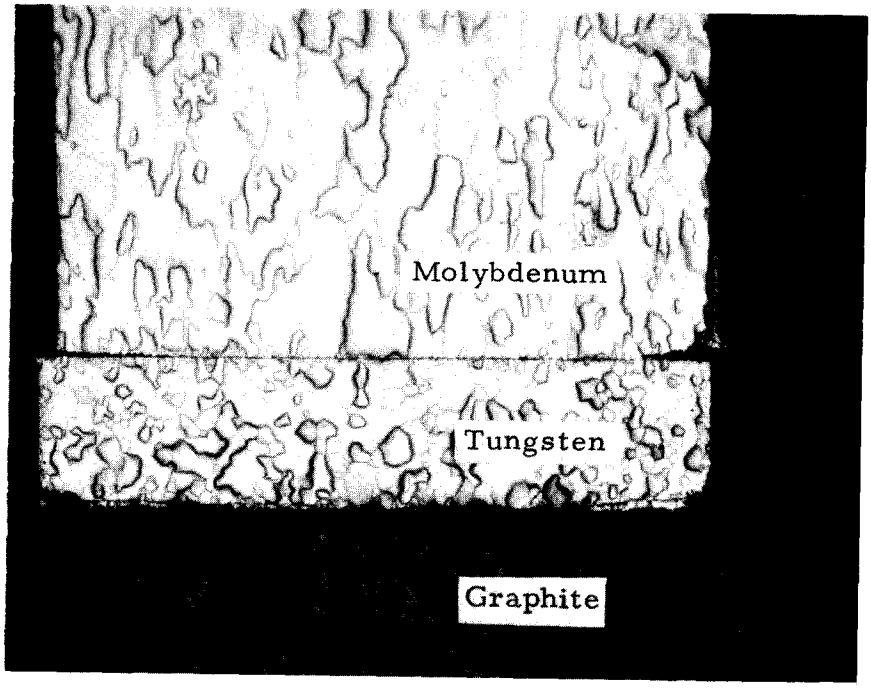

10-16-68 UNCL 7706-4077

Figure 3. Tungsten Diffusion Barriers (top) With and (bottom) Without a Thin Coating of Nickel (Mirakami's Etch) Each at 30X

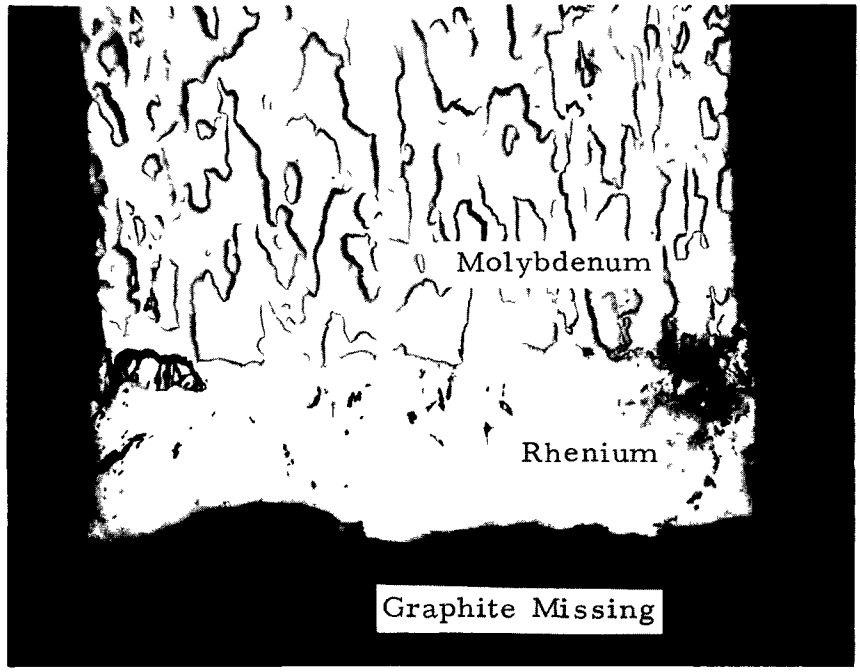

10-16-68 UNCL 7706-4078

Figure 4. Rhenium Diffusion Barrier (Mirakami's Etch) 30X

The rhenium disc did not interact with graphite at all. This is evidenced by the cross-section in Figure 4 and by the lack of bonding between graphite and rhenium. In all other cases, the graphite adhered tightly to the disc, presumably as a result of chemical interactions. The loading of the weight produced a small amount of deformation in the rhenium which possibly indicates that rhenium does not possess the strength properties of tungsten and molybdenum at 2500°F. While this may be a problem for very long-term heater operation, the near term is still plagued by the carbide formation problem, and rhenium offers considerable promise in this area. The problem of deformation can be resolved through weight reduction, should this become necessary.

A second compatibility test was run in vacuum at 3000°F for more than 200 hr. This test was aimed at studying the high temperature behavior of several braze alloys which were used to join graphite to refractory metals. A test of the chemical compatibility of tungsten carbide with graphite, molybdenum, and boron nitride was included. The test configuration and materials tested are displayed in Figure 5. After testing, the specimens were sectioned and polished for metallographic examination.

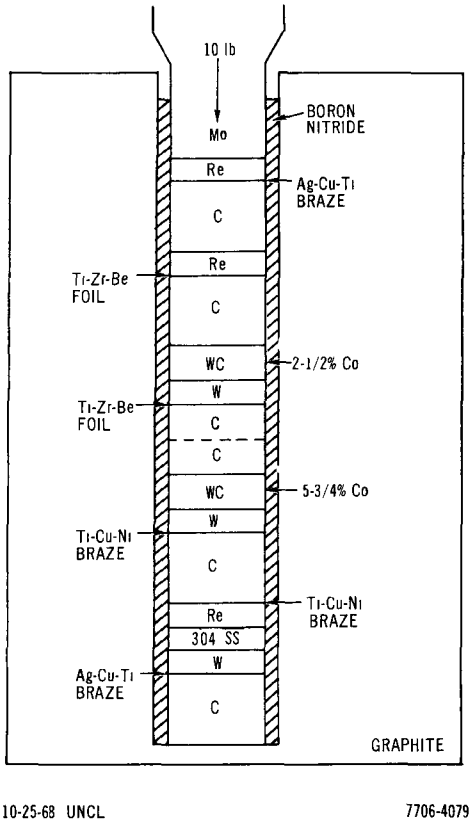

Figure 5. Configuration for the Second Compatibility Test

The braze alloys tested were not satisfactory because they melted, would not bond properly to rhenium, and showed evidence of a chemical interaction with the boron nitride. The tungsten carbide (both types) also interacted with the boron nitride. The rhenium exhibited no evidence of interaction with the graphite, the molybdenum, or with the braze alloys. The stainless steel melted as expected; and, unfortunately, the molten steel obscured the results with tungsten and rhenium at the bottom. Some evidence of bonding was found for tungsten-to-graphite.

b. Post-Mortem Examinations of Heaters

Post-mortem studies on two heaters which operated on a 6-min-on, 6-min-off cycle were made. When these results are compared with the behavior under steady state operation, it is evident that cyclic operation is deleterious to the life of a heater; see Figure 6. The relationship of carbide formation to the number of cycles during operation is clearly evident. The effect was attributed to interfacial heating when the power is cycled. It is hoped that the development of new concepts with regard to the diffusion barrier material, joining, and heater element design will alleviate the problem.

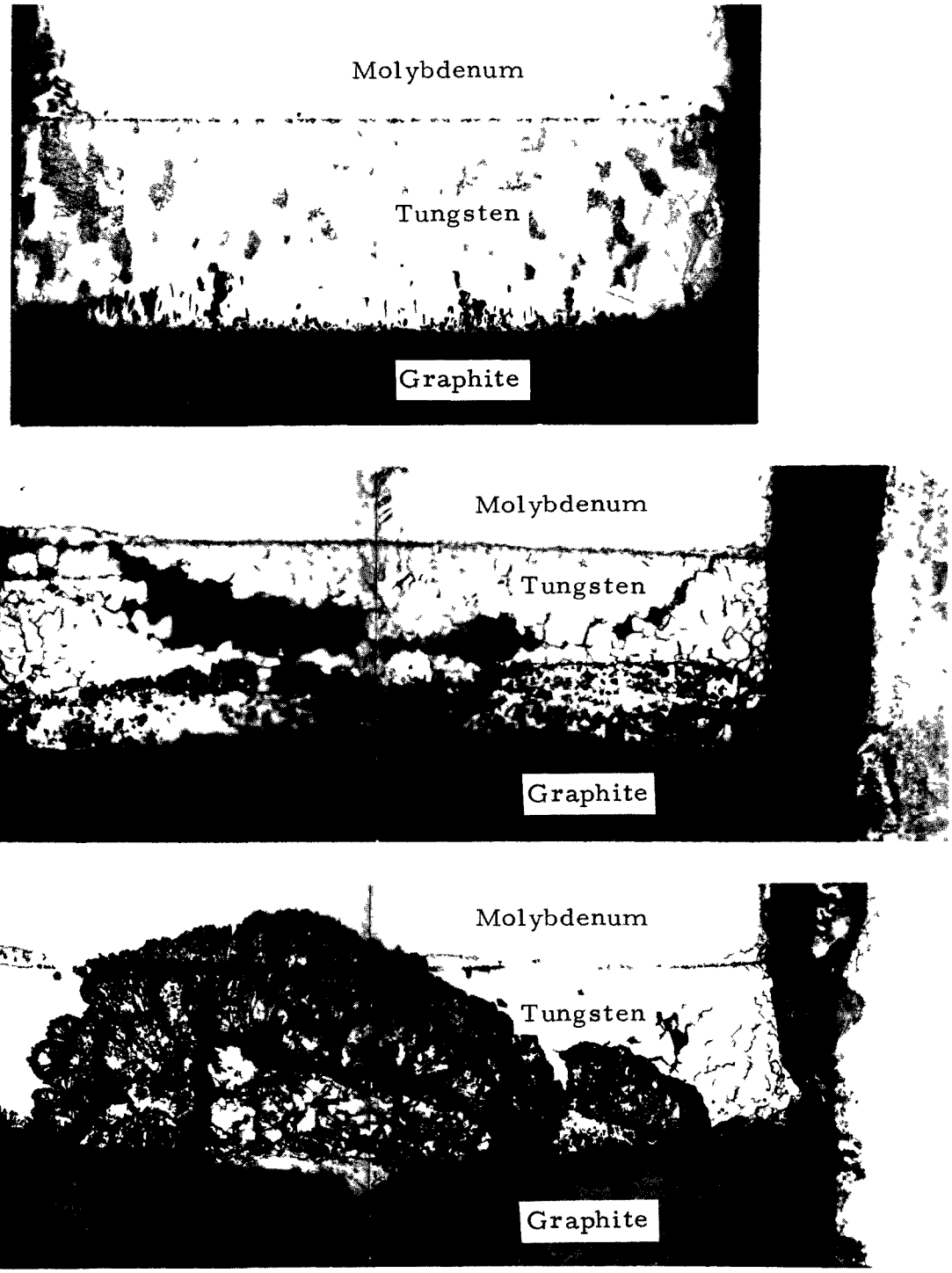

10-16-68 UNCL 7706-4080

Figure 6. Effect of Cyclic Operation on the Rate of Carbide Formation in the Diffusion Barrier (Top, 558 hr, Steady State, Htr 36; Center, 585 hr, 865 Cycles, Htr 40; and Bottom, 446 hr, 3728 Cycles, Htr 48) 33, 40, and 40X respectively

Cyclic operation of heaters appears to enhance the rate at which carbides form in the diffusion barrier because of the higher temperatures. Therefore a program was started to develop a braze between graphite and the candidate materials for the diffusion barrier, to reduce contact resistance. A titanium-nickel-copper braze alloy which has been successfully used in the aerospace industry for joining refractory metals to graphite was selected. Initial tests demonstrated that it is possible to join these materials, but that the time and temperature conditions required for sound joints must be determined. Unfortunately, tests of the braze joint at temperatures present in high flux heaters showed it to be unsatisfactory.

The operating and design conditions of the last group of Model C heater assemblies tested are displayed in Table 2. X-ray radiography revealed that the nickel coating did not help to reduce the rate of carbide formation at the tungsten-carbon interface. Replacement of the disc concept diffusion barrier with a rod of tungsten also behaved as observed previously with cyclic heaters. It would therefore seem that if the molybdenum-tungsten interface contributed to the carbide formation problem, the rate of carbide formation would be less; however, this was not the case. The graphite interface interaction must therefore be reduced by reducing the temperature, interfacial resistance, and material carbide stability. The rhenium disc performed well under cyclic operation and will be retested with the next group of heaters.

TABLE 2

CONDITIONS AND DESIGN PARAMETERS IN MODEL C HEATERS

Heater No.	Heat Flux ($Btu/ft^2/hr$)	Mode	Sodium Temp (°F)	Diffusion Barrier Material
53	1×10^6	Steady-State	1210	Ni on W disc
54	0.8×10^6	Steady-State	1210	Ni on W disc
55	0.8×10^6	Cyclic	1210	W rod
56	0.8×10^6	Cyclic	1210	Re disc

c. Electrode Assembly Tests

A new series of experimental tests is currently in progress to improve the electrode system for cyclic operation of long duration. In these tests, a full size electrode system including the graphite, diffusion barriers, and molybdenum are constructed and operated without a sheath in a bell jar at the rated surface temperatures of the graphite. Under these conditions, visual and radiometric observations can be made on the electrode assembly; see Figure 7.

10-16-68 7706-4081

Figure 7. Electrode Assembly Test Apparatus

One important conclusion reached as a result of the heater electrode tests is that the upper temperature limit for boron-nitride-and-graphite system is 4200°F. Above this temperature, B_4C forms rapidly. Under heater operation in flowing sodium, this would cause a short circuit to develop. Since the rate of reaction is undoubtedly influenced by impurities in the boron nitride insulation, at lower surface temperatures the purity of the insulator material becomes important to the performance and longevity of a high flux heater. This, in part, may explain the premature failures of two heaters tested last year when the source of the failure was traced to the selection of lower quality boron nitride actually specified as an H. P. grade.

The distribution of temperatures calculated for a cored graphite heater element were confirmed by the mockup experiment of the electrode assembly. With a hollow inside and plugs at each end, the temperatures at the ends of the heating element are reduced. The temperature at the center of the ends of the hollow element is several hundred °F lower than the reference solid heating element at an equal power rating.

Two potential diffusion barrier materials, tungsten carbide and pyrolytic graphite, were examined in the same apparatus as described above. The tungsten carbide dropped the surface temperature at the interface between the carbides and the molybdenum electrode. It also maintained strength at operating conditions and, therefore, is a candidate for use as a diffusion barrier, subject to the requirements of compatibility with graphite and molybdenum. With the cored graphite, the temperature at the interface is less without a diffusion barrier because of the lower resistance of molybdenum than that of tungsten or rhenium.

d. Heater Improvement Tests

The hollow graphite element shows considerable promise as a means of reducing the graphite end temperatures. Because of this, platinum becomes a potential candidate for the upper diffusion barrier. It has performed well as the lower barrier between the graphite and the stainless steel sheath where the temperature is lower. The hollow carbon heating element may be sufficiently cool that no barrier is required.

Four new heaters were constructed, and will be operated under the conditions shown in Table 3. The operating conditions are not identical because the heater improvement work is combined with mass transfer experiments. Nevertheless, the operation of these heaters should reveal whether the design modifications extend the life of a heater. Besides the above modifications, the graphite grade was changed to one of high purity and with a fine grain, and the sheath was reduced in thickness to improve heat transfer. Hopefully, these modifications will result in heater life in excess of 1000 hr.

TABLE 3

CONDITIONS AND CONSTRUCTION OF MODEL B HEATERS

Heater No.	Heat Flux (Btu/ft^2-hr)	Mode	Cladding	Graphite	Diffusion Barrier Material	Sodium Velocity (ft/sec)
56A	1×10^6	Steady-State	None	Solid	Re	1
201	1×10^6	Steady-State	316 SS	Solid	Re	20
211	1×10^6	Steady-State	316 SS	Hollow	Re	20
212	8×10^5	Steady-State	316 SS	Hollow	Pt	20
213	7.5×10^5	Steady-State	316 SS	Hollow	None	10

2. Mechanical Properties

a. Loop

Three high flux heater tests with cladding were completed. The conditions of the tests are displayed in Table 1. Both cyclic and steady-state tests were performed.

The stress-rupture life in tests at 1×10^6 Btu/ft^2-hr in 1200°F flowing sodium is displayed in Figure 8. The stress-rupture life agrees with that obtained in a previous test at the same condition within expected experimental scatter. More important, the stress-rupture life correlates with that behavior expected on the basis of isothermal tests in static sodium for the peak midwall temperature and stress in the test under heating. As explained previously (AI-AEC-12695), the peak temperature is selected because the creep rates increase with increasing temperature. The midwall position was selected because thermal stress relaxation compensates for the thermal gradient effects on creep to produce a uniform strain rate across the wall.

The average strain rate sensitivity to stress also conforms to that from isothermal tests performed in static sodium; see Figure 9. The average strain rate is defined as the strain at failure divided by the time to failure. As before, the best correlation exists for the position of the peak temperature and the stress

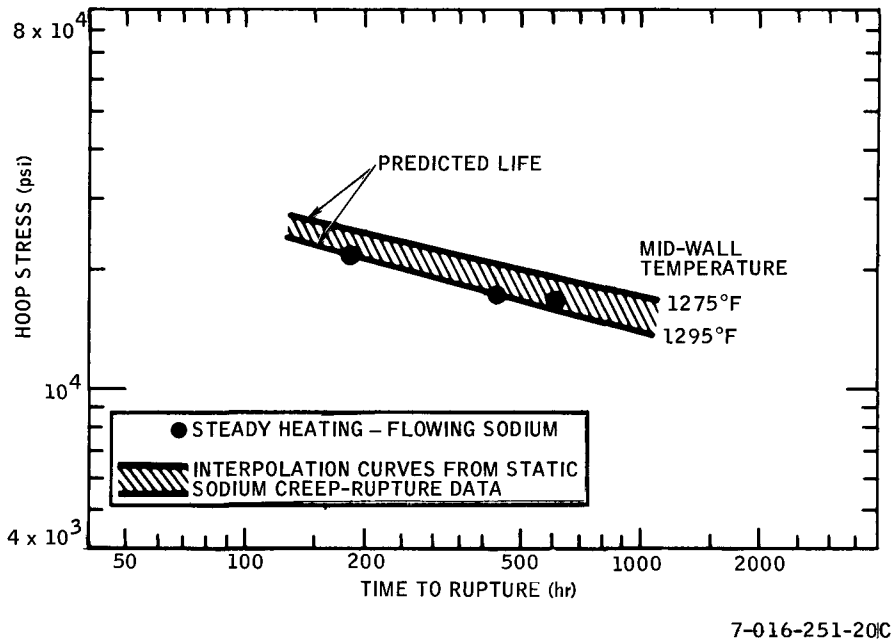

Figure 8. Predicted vs Actual Life of Tubes Under Steady-State Heat and Pressure

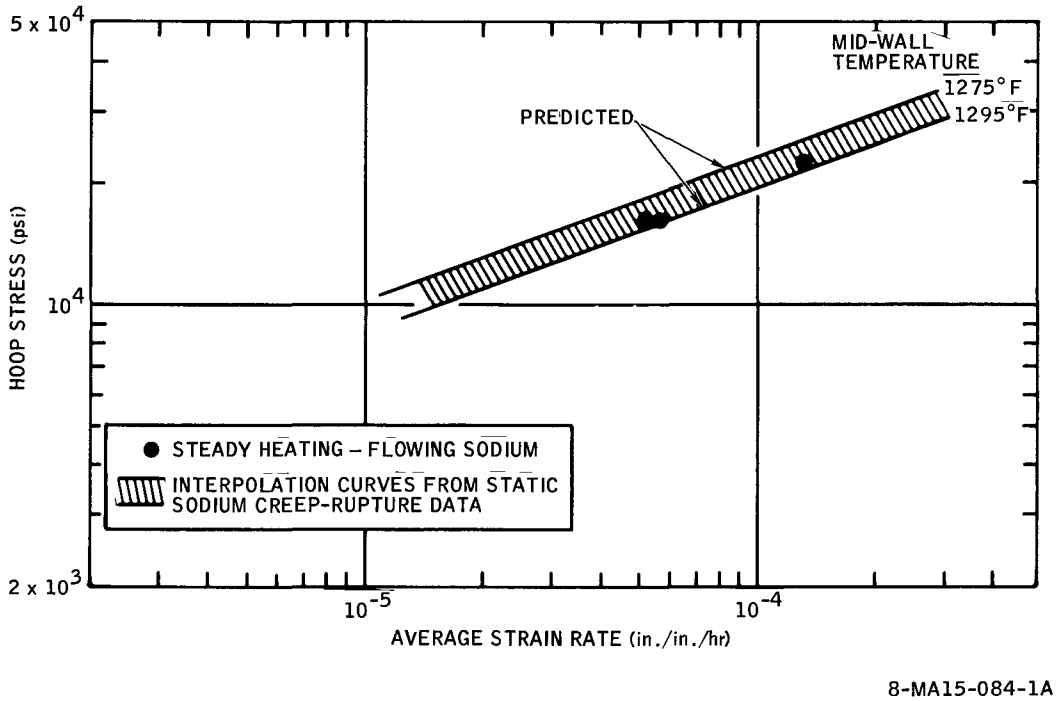

Figure 9. Effect of Stress on the Average Strain Rate

at the midwall. The strain at failure agrees with that observed in a previous test under the same test conditions. The failure occurred at the point of highest temperature in the cladding, which is expected.

The tests under cyclic heating, in which the heater is turned off and on every 6 minutes, was performed at a lower heat flux (8×10^5 Btu/ft^2-hr). This choice was based on the design prediction that the FTR will have a linear power rating of 18 kw/ft; while the previous tests using a cyclic heat flux of 1×10^6 Btu/ft^2-hr corresponds to a linear power rating of 23 kw/ft over the 2 in. heat zone. In addition, it is important to obtain some knowledge of the effects of heat flux on the stress-rupture behavior under cyclic heating.

The stress-rupture life under the lower heat flux condition, compared to that at the higher condition, is displayed in Figure 10. A preliminary thermal analysis at the lower heat flux indicates that the surface temperature is reduced only slightly while the temperature gradient is reduced by about 20%. Based on previous analysis, the stress-rupture life comparison should be made for the average stress and surface temperature. The average temperature is the average between the surface temperature with and without the heater flux. This

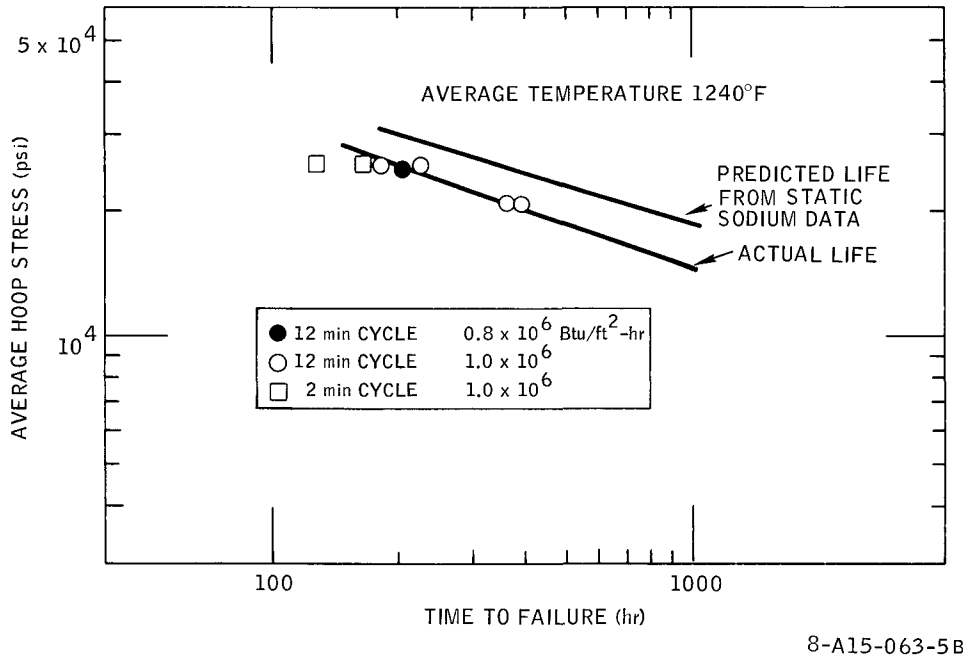

Figure 10. Predicted vs Actual Life of Tubes Under Cyclic Heat and Static Pressure

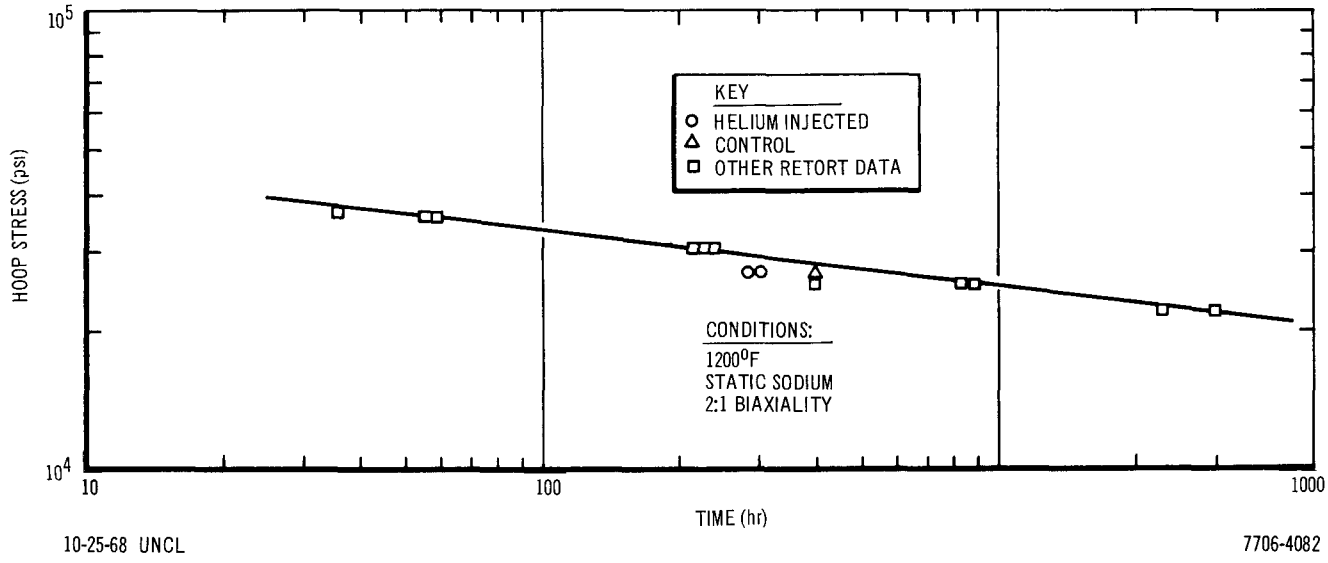

Figure 11. Effect of Helium on the Stress-Rupture Life of Annealed Type 304 Stainless Steel in Static Sodium

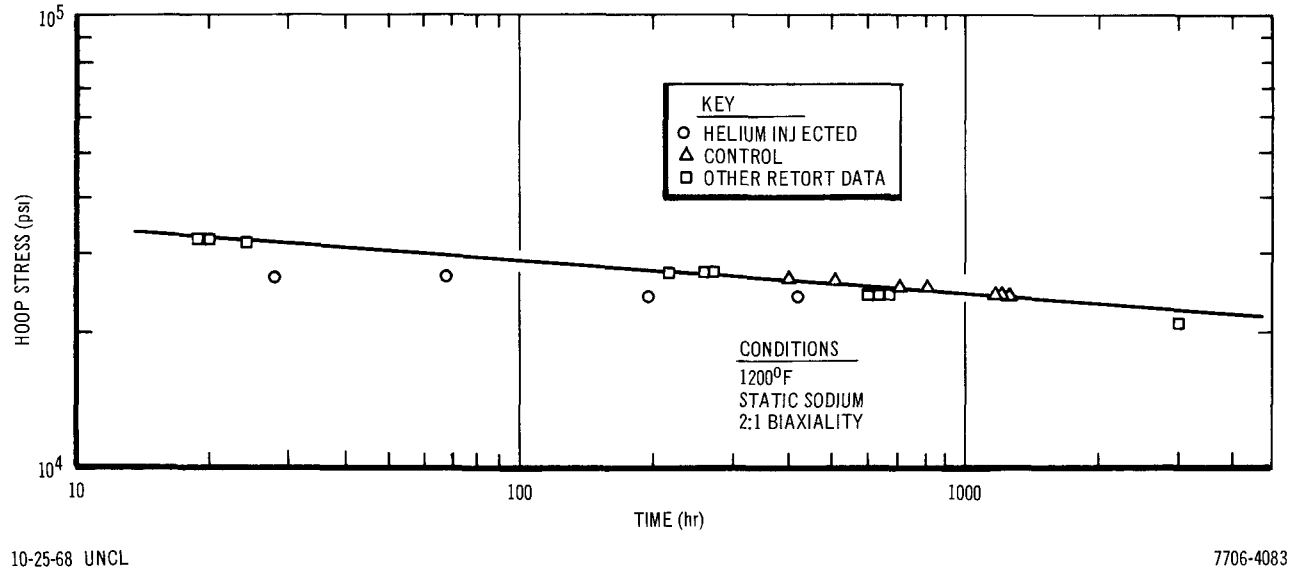

Figure 12. Effect of Helium on the Stress-Rupture Life of Annealed Type 316 Stainless Steel in Static Sodium

temperature is between 1230 and 1250°F at 8×10^5 Btu/ft^2-hr. The average stress is the hoop stress plus 1/2 the thermal stress. For the lower heat flux, the combined stress is 24,000 psi. If this analysis is correct, the behavior at a lower heat flux is essentially that expected as a result of the lower thermal stress caused by the 20% reduction in the thermal gradient. Since the reduction in stress was small, the life of the cladding at a lower heat flux is not significantly different from that at a heat flux of 1×10^6.

The strain profiles were similar to those obtained on previous runs at a higher heat flux. The largest diametral strain took place at the highest temperature point along the cladding, which also corresponds to the location of the failure in the cladding. The peak diametral strain was 3.3% at a heat flux of 8×10^5 Btu/ft^2-hr. This value is slightly lower than the 3.6% obtained at 1×10^6 Btu/ft^2-hr. However, isothermal stress-rupture tests frequently exhibit comparable experimental scatter in the rupture strain; the small reduction in rupture strain with lower heat flux may be a reflection of this scatter.

The surface of the internally heated specimens exhibited a polished zone which may be linked to corrosion. This will be examined when the specimens are sectioned.

b. Biaxial Stress-Rupture of Helium Injected Tubes

The testing of helium injected tubes in static sodium and under internal pressure was complete. Both Type 304 and 316 stainless steel tubes were tested in static sodium at 1200°F in the annealed state. The stress-rupture behavior of the control specimens and of the helium injected tubes is presented in Figures 11 and 12. As can be seen in Figure 11, the presence of helium from cyclotron injection reduced the life of 304 stainless steel from 400 to 300 hr. In the case of Type 316 stainless steel, helium reduced the stress rupture life by more than 50% for two stress levels; see Figure 12.

In conjunction with the testing of helium injected specimens in the retort containing Type 304 stainless steel specimens, a series of creep specimens of noninjected tubes was tested. In this case, seven tubes were stressed identically. At prescribed time intervals, the stress was removed. Subsequent profilometer measurements revealed the amount of creep strain as a function

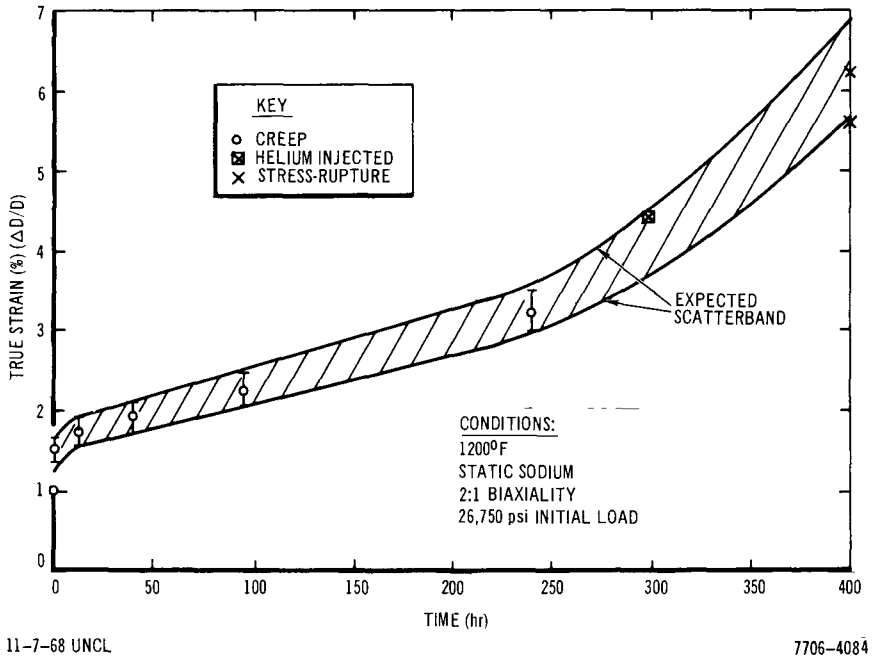

Figure 13. Creep Curve for a Biaxially Stressed Tube in Static Sodium

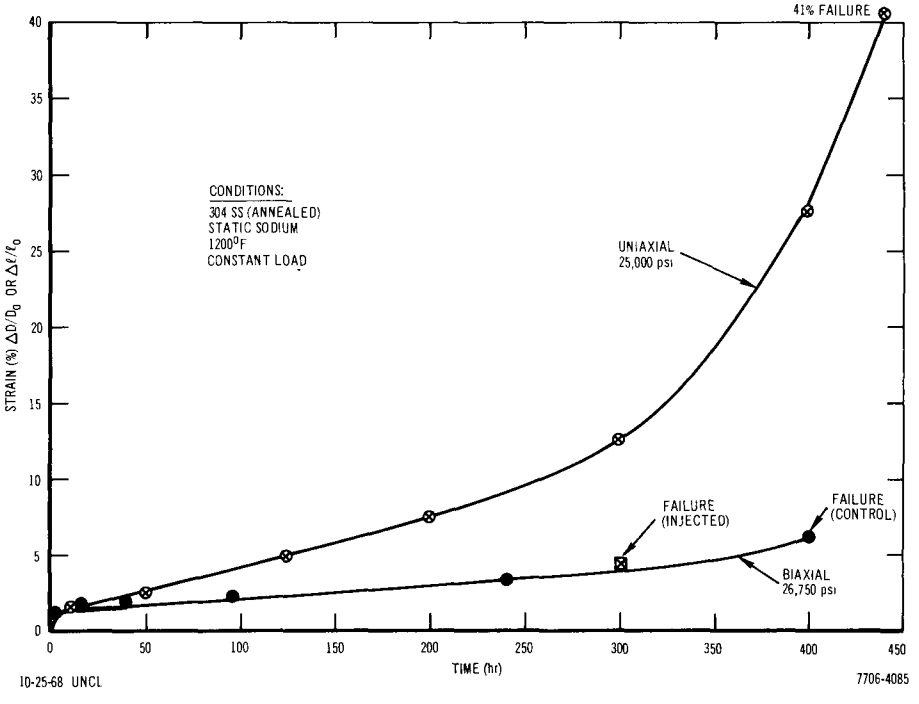

Figure 14. Comparison of Uniaxial and Biaxial Creep Curves in Static Sodium

of time of pressurization. The results of these measurements are displayed in Figure 13. Since these tubes were stressed identically to the stress rupture tubes, with and without helium, it is possible to make a comparison on the same graph of the strain at failure. It is interesting to note that the strain at failure of the control specimens lies on the extrapolated creep curve. There is less third stage creep associated with the biaxial stress condition than with uniaxial stress. For example, the amount of tertiary creep strain in a uniaxial test is a factor of 10 larger than the combined primary and secondary creep strain. The biaxial third stage creep strain is only a factor of 2 larger than the combined primary and secondary creep strain; see Figure 14. The strain at failure of the helium injected tubes fell on the creep curve for the noninjected tubes. If primary and secondary creep are unaffected by the presence of helium, it appears that helium reduces life by reducing the amount of third stage creep.

Helium has been suggested as favoring the rate or extent of grain boundary void formation. If this were the case, one would expect helium to be the most effective during a period of time when these voids are nucleated and grow. The microstructures of the noninjected and unfailed creep specimens do not exhibit evidence of void formation at grain boundaries. The control specimens which failed exhibited large grain boundary voids in the failure region. This conforms to earlier observations on annealed materials in static sodium. The helium injected tubes did not show large grain boundary voids; however, the number of voids was much greater. These observations imply that helium enables more voids to form at grain boundaries than would have formed without helium present. This could be expected to severely weaken the grain boundaries and promote early failure.

When the results of the tests on helium-injected tubes under internal pressure are compared to those under uniaxial tension, it appears that helium does not reduce the strain at failure as much in the biaxial stress state as it does in the uniaxial stress state. This, in part, could be expressed in terms of effects of biaxial stress on third stage creep. Stress-rupture under uniaxial produces a significant amount of third stage creep. If helium has its greatest effect on the amount of third stage creep, the relatively large reduction in ductility seen in uniaxial stress-rupture tests and tensile tests compared to biaxial tests is explained.

3. Mass Transfer Studies

The current test on Type 304 stainless steel is an extension of work initiated at the end of the last fiscal year. A piece of cladding was activated, and microhardness depressions were made on the surface. The test was run at conditions expected in the FTR with the exception of the core ΔT. In terms of the mass transfer analysis, this does not influence the value of the analysis, since the film drop between the cladding temperature and the bulk sodium temperature is believed to be equatable to the mass transfer mechanism driven by loop ΔT. Low pressure was used in the annulus between the cladding and the heater to prevent boiling of the NaK in the annulus. The stainless steel cladding was exposed for 387 hours to 1200°F sodium flowing at 20 ft/sec, while under a heat flux of 8×10^5 Btu/ft^2-hr.

The activation technique developed last year was employed to determine the rate of removal of individual alloying species. To date, the rate of removal of iron and chromium have been determined. In addition, the surface indentations were measured before and after exposure to provide a check on the calculated removal of surface layers.

In the activation method, the activities of individual species are counted before and after exposure to the sodium. A control sample which is not exposed to sodium is also counted to correct for the radioactive decay. The exposed samples exhibited an overall corrected activity loss in the heated zone of 0.946% which is due to loss of iron, chromium, and cobalt. The nickel half-life is too short to contribute to the total activity. The samples showed no change in activity in the unheated section of cladding just upstream. This indicates that the bulk sodium at the inlet to the heater test section is saturated with respect to iron, chromium, and cobalt.

The corrected activity decrease of chromium was 1.935% so that the activity decrease for iron and cobalt is the overall rate, less that of chromium, times the fraction of chromium present in the alloy.

To obtain the corrosion rate (flux of atoms across the surface of the cladding), the following relation was used:

$$Ji = (\text{wt }\%)\left(\frac{m}{A}\right)\left(\frac{\%\text{ activity decrease}}{\text{time}}\right)$$

For chromium, the total corrosion is 0.760 mg/cm^2 and for iron is 1.21 mg/cm^2; 0.94 mils/year for iron. The corrosion rate for chromium is 1.07 mils/year. Chromium is selectively removed however, and therefore does not contribute to surface recession by the amount indicated. The loss of activity from iron is related to surface recession. The average decrease in size of the small surface indentations showed a corrosion rate of 1.10 mils/year.

The activation analysis is by no means complete, particularly, the experimental error analysis. Activity decreases found in the heated zone were statistically significant, and led to reasonable corrosion rates. While it is premature to translate the above corrosion rates into a corrosion allowance, the feasibility and merits of this approach to mass transfer phenomena appear to be vindicated. The next test series will provide some information on the velocity, time, and heat flux dependence of mass transfer phenomena.

IV. EVALUATION OF EFFORT TO DATE

The program for the subtask continues to provide additional data on mass transfer and stress-rupture properties in flowing sodium under internal steady state and cyclic heating. The heater improvement phase has identified the problem areas for heater performance and life, and several design modifications were made to solve the problems. The completion of the stress-ruptures test with helium-injected tubes, coupled with a new method of obtaining biaxial creep data, has opened an avenue toward new thoughts on irradiation embrittlement.

The task has built and tested four Model C heater assemblies, and has built four Model B heater assemblies. The latter were modified so that cladding which is not pressurized can be tested to obtain more mass transfer data. This modification represents a decrease of 25% in cost of performing the flowing sodium exposures, so that more data can be obtained in this area. More important, the corrosion work can go on simultaneously with heater improvement tests, thus avoiding a delay in data acquisition. This places the entire program of mechanical properties and mass transfer studies about eight weeks ahead of schedule.

The program of this subtask continues to focus on the design implications of the work and analytical methods for describing the phenomena under study.

V. NEXT REPORT PERIOD ACTIVITIES

The following major activities are expected to take place during the next report period:

1) Test four Model B heaters,
2) Build and test four additional Model B heaters,
3) Build four Model C heaters,
4) Provide creep data on cold worked 304 stainless steel in support of the analysis,
5) Determine metallographic and strain profiles of the helium-injected Type 316 stainless steel tubes,
6) Begin work on a Topical Report on heaters,
7) Make additional mass transfer data analyses, and
8) Make a post-mortem study on heaters.

Program:	FBR Fuels and Cladding		
AEC Task:	Task 11-A, Mixed Carbide Fuels (Basic Properties)		
Project Manager:	J. L. Ballif		
Reporting Period:	July-September 1968		
General Order: 7707	Subaccount: 28210	AEC Category:	04-40-02-01.1

Principal Investigator: G. Ervin, Jr.

I. PROJECT OBJECTIVES

Objectives of the project are to: (1) determine selected microstructural attributes, and mechanical and physical properties of mixed carbide fuels, both to establish the potential for these materials as nuclear fuels, and to provide a basis for interpreting and understanding irradiation behavior in terms of atomistic transport phenomena, and (2) develop, where necessary, preparative techniques for polycrystalline mixed carbide materials of controlled structure and stoichiometry.

II. MAJOR ACCOMPLISHMENTS DURING FISCAL YEAR 1969

A report has been written which surveys the problem of cladding carburization in mixed carbide fuel elements and presents a plan for experimental study of carbon activities. The report also indicates the expected worth of various additive metals for broadening the permissible range of carbon content of carbide fuel.

III. PROGRESS DURING REPORT PERIOD

The problem of the compatibility of sodium-bonded mixed carbide fuel with stainless steel cladding has been studied in detail, and a report has been written. The problem may be stated in terms of the thermodynamic function, the carbon activity, or the closely related function, the carbon potential

$$\mu_c = RT \ln a_c$$

When the fuel has a carbon activity greater than that of the cladding, there will be carburization of cladding by transfer of carbon through the sodium bond. On the other hand, there is a lower limit of carbon activity in the fuel at which free metal is formed, and free metal also reacts adversely with cladding. With unmodified fuel, the change from the lower activity limit to the upper one occurs over a very small change in carbon content; therefore, some control of carbon activity is needed. Analysis of existing data on phase diagrams and thermodynamic properties indicate that a significant broadening of the allowable carbon range may be achieved by the addition of small percentage amounts of one of several metals. This conclusion, however, is based on limited and controversial data, and there is a serious need for direct carbon activity measurements on cladding and on modified fuel.

The data on additives shown in Table 1, are taken from published phase diagrams plus assumptions about some of the phase relations and activities.

TABLE 1

ESTIMATES OF ALLOWABLE RANGES IN CARBON CONTENT OF MIXED CARBIDE FUEL FOR 5% ADDITION OF VARIOUS METALS

Additive Metal	Minimum and Maximum Carbon (%)	Range (% C)	Solid Phases [besides (U, Pu)C]
Ti	5.52 to 5.71	0.19	$TiC_{0.81 \rightarrow 0.97}$
V	5.12 to 5.52	0.40	$VC_{0.5} + VC_{0.78 \rightarrow 0.85}$
Nb	4.86 to 5.14	0.28	$NbC_{0.5} + NbC_{0.72 \rightarrow 0.90}$
Cr	4.56 to 5.03	0.47	$Cr + Cr_{23}C_6 + Cr_7C_3$
Mo	4.56 to 4.86	0.30	$Mo + UMoC_2 + Mo_2C$
W	4.56 to 4.72	0.16	$W + UWC_2 + W_2C$
Re	4.56 to 4.71	0.15	$Re + UReC_2$

First, it was necessary to assume a value for the limiting carbon activity in stainless steel, above which the carbon makes it brittle. This was chosen as 10^{-2} which is an approximation from thermodynamic data on the stabilities of $Cr_{23}C_6$ and Cr_7C_3. It is assumed that the equilibrium between these two phases represents the carbon limit. According to this analysis, chromium is the best choice from the standpoint of carbon range, although vanadium may be equally good within the accuracy of the estimates.

Most of the conventional methods for obtaining carbon activities are saddled with serious drawbacks. As mentioned, activities may be calculated from thermodynamic functions obtained from thermal property measurements; i.e., heats of reaction plus specific heats. Such data are available in varying degree for all of the compounds in question; but with few exceptions, the accuracy is rather poor. Also, there are no data on mixtures. Some methods are suitable for obtaining metal activities from which carbon activities can be obtained by using the Gibbs-Duhem relationship. The most common of these methods is vapor pressure, but data can be obtained only at quite high temperatures, such as above 1800°C; and extrapolation to temperatures of interest for fuel-cladding interactions is not warranted. A good method for determining metal activities at the lower temperatures is that of emf measurements on cells with carbide electrodes, and such studies are in progress at Argonne and at Los Alamos. There is some question, however, as to the interpretation of results from cells with mixed carbide electrodes.

Simple, static, out-of-pile compatibility studies between pairs of compositions will not give actual activity numbers but will be a means for placing the compositions in an order of increasing activity for a given temperature. The most logical carbon transfer medium is sodium. Many such studies have already been made, and this is a very practical approach. The times for equilibrium are rather long. The results are not as useful, in that actual quantitative activities are not obtained, and nothing can be said about the effects of a temperature gradient.

Some work in progress at United Nuclear uses an empirical nonequilibrium method that obtains comparative carbon activities from the comparative carbon fluxes from samples contained in thin-walled iron capsules bonded with sodium

and swept by H_2O/H_2 mixtures which convert carbon to CO which is then analyzed in the gas stream. This method has been giving reasonable values of activities. Their significance, however, in an absolute sense, seems clouded by possible effects of kinetic factors such as depletion of carbon at the sample surface.

Equilibration with an analyzed CH_4/H_2 mixture would seem to be a straightforward method, but methane contents in the low parts per million range would have to be measured accurately. A method in which samples are equilibrated with CH_4/H_2 but does not require analysis of the gas is proposed. The method is patterned after that of Markin, Wheeler, and Bones (AERE-R 5562, October 1967) which they applied to oxygen potentials of UO_2 and which uses H_2O/H_2 mixtures. Applied to carbides, the carbide sample is held at one temperature in CH_4/H_2 gas whose carbon potential is fixed by contact with a reference carbon-containing sample held at another temperature in the same enclosure. The carbon potential is related to the carbon activity by the expression

$$\mu_c = RT \ln a_c \quad .$$

The reference material is conveniently graphite for a high range of carbon potentials and can also be metal/carbide mixtures or carbide/carbide mixtures whose carbon potentials are known. The application of the method is explained by Figure 1, on which the constant ratio $P_{CH_4}/P^2_{H_2}$ lines are plotted as carbon potential vs temperature. Shown as dashed lines, are carbon potentials of U/UC mixtures, from data of Storms (The Refractory Carbides, Academic Press, New York, 1967); and $PuC_{0.9}/Pu_2C_3$ mixtures, from data of L. M. Atlas (private communication). The carbon potential of graphite is zero at all temperatures, by definition, and it is seen that graphite held at high temperatures (1300 to 2600°K) will generate CH_4/H_2 mixtures with $P_{CH_4}/P^2_{H_2}$ ratios between 10^{-2} and 10^{-4} which at lower temperatures will be in equilibrium with $PuC_{0.9}/Pu_2C_3$ and probably also with mixed carbide, as well as with stainless steel.

It has been calculated that the times required to reach equilibrium, if limited by the methane flux through the gas phase, will be only a few hours under the above conditions in argon - 10% H_2 mixtures. Diffusion through the

3

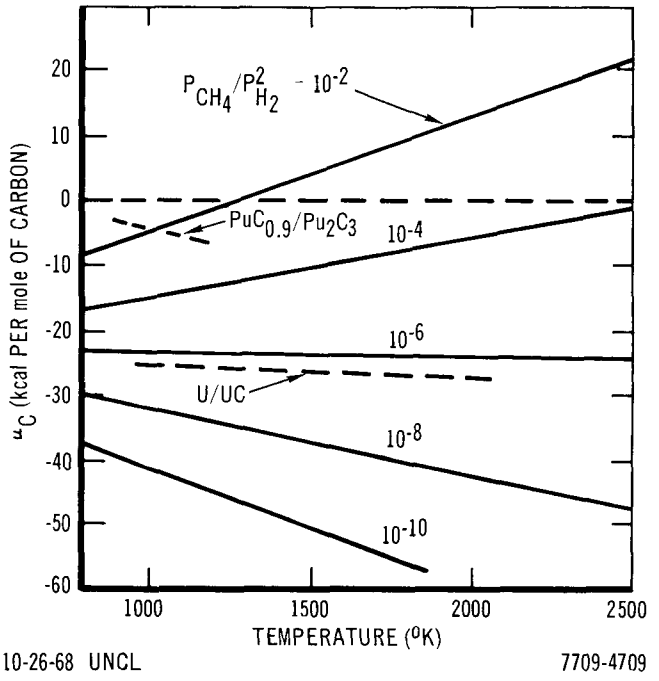

Figure 1. Carbon Potentials for Carbides and CH_4H_2 Mixtures

solid phase is more likely to be the slow process at temperatures below 1000°C unless the particle size of the carbide samples is quite small, such as <200 mesh. An alternative procedure is to determine the direction of carbon flux metallographically on pelleted samples.

A laboratory facility is now ready for operation with plutonium carbide. Some plutonium oxide is on hand for preparing mixed carbide, and some additional mixed carbide has been ordered as backup material. Appropriate nuclear safety analyses have been prepared, and the reports are awaiting approval.

IV. EVALUATION OF EFFORT TO DATE

A survey has been made which shows the importance of carbon activity for the cladding compatibility problem and the need for precise measurements, and which evaluates various methods for determining activities. A relatively new method has been selected which appears to be simple to use and which will give direct and absolute values on all types of samples including mixtures. The

details of application of the method have been considered and potential problems anticipated. A plutonium laboratory facility has been completed, some plutonium oxide is on hand for preparing carbide, and experimental work can now be started.

V. NEXT REPORT PERIOD ACTIVITIES

Because of the need for establishing priorities for a limited budget, and in the light of current activities at other laboratories on compatibility problems, plus indications of a successful swelling control experiment on UC at our laboratory, the basic properties work will be redirected toward swelling control in mixed carbides. The work will include cyclotron injection of helium bubbles into UC-W samples containing particulates, followed by heat treatment in a thermal gradient to observe (by electron microscopy) the motion of the bubbles and the effect of the particulates on the motion. Also included, will be the development of methods for the preparation of (U, Pu)C samples with particulates, by addition of tungsten and similar elements.

E

Program:	Fuels and Cladding		
AEC Task:	11-B, Mixed Carbide Fuels (Irradiation Studies)		
Project Manager:	J. L. Ballif		
Reporting Period:	July-September 1968		
General Order: 7707	Subaccount: 28220	AEC Category:	04-40-02-01.1

Principal Investigator: G. Ervin, Jr.

I. PROJECT OBJECTIVES

To apply fundamental technology toward the reduction and control of swelling in mixed carbide fuels and to demonstrate the effectiveness of fine dispersion tungsten doping in improving the high temperature irradiation stability of UC, are the objectives of this project.

II. MAJOR ACCOMPLISHMENTS DURING FISCAL YEAR 1969

The experimental setup on irradiation swelling of UC-W fuel (EXP-NRX-9-101) was shipped to the AI Hot Laboratory, disassembly has been completed, and examination of the fuel is in progress. Each fuel slug was retained in its niobium basket, and these have now been separated and placed in individual vials. Thus, we are assured of being able to obtain all the desired data. Substantial swelling of the control samples has been observed, indicating that another major objective of the experiment was achieved. It now seems certain that the experiment will be a good evaluation of fine particle dispersions for control of fission gas swelling in carbides.

III. PROGRESS DURING REPORT PERIOD

The irradiation experiment, NRX-101 was terminated at the end of June after a total peak burnup of 18,280 Mwd/MTU. The average peak centerline fuel temperature during the irradiation period is estimated to be 2550°F (1400°C) while the fuel at the ends of the string ran about 600°F colder. The capsule was shipped to the AI Hot Laboratory where it arrived July 18.

Disassembly of the capsule and observations at each stage proceeded without special difficulty. Gamma scan and pinhole camera photography were used to locate the fuel. It was found that the entire fuel string was free to slide; and, due to tipping of the capsule, had moved to within 6 in. of the top end. Knowledge of the position of the fuel was made use of in cutting open the inner encapsulation, and it was then possible to slide the entire fuel string intact out into a large tray where it was digested in Dowanol liquid to remove most of the NaK. No damage to any part of the capsule of the fuel string was noted.

The gamma scan which was performed on the Zr-95 peak showed a broad maximum which was displaced to a point somewhat below the center of the string. This is consistent with the flux in the reactor which was skewed toward the lower end, particularly during the first day or so of each startup, because of the low moderator level.

The pinhole camera photographs showed each slug in place in the string; Figure 1 is a typical photograph. All 120 fuel slugs were photographed in this way. Note that there are two slugs which are enlarged and distorted. The only slugs showing this characteristic are the 19 zone-melted control samples; i.e., UC with no tungsten added. All other slugs appeared to have the original slug shape, including five other controls which were arc cast instead of zone melted. At this point, having seen most of the fuel, after removal from the niobium baskets, it is known that the appearance of the control samples is due primarily to fracturing of the carbide. This observation is not of itself significant with regard to the comparative swelling of UC-W samples and control samples.

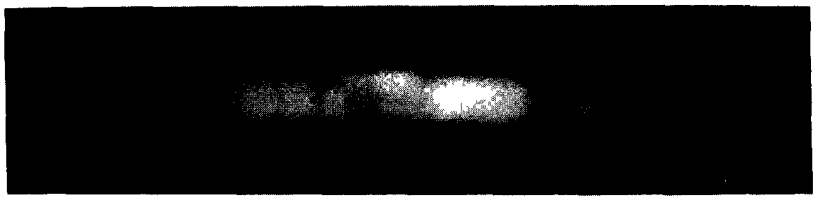

10-25-68 UNCL 7707-4705

Figure 1. Pinhole Camera Photograph of a Typical Portion of the 101 Fuel String

After digestion in Dowanol, the niobium baskets containing the fuel slugs were separated, placed in separate vials, and stored in vacuum desiccators. Then the fuel slugs were removed from their baskets, one at a time, to avoid any confusion of samples, and put through a furnace vacuum distillation to ensure complete removal of the NaK. This is important because of the density determinations. NaK distillation was performed at 600°F for one hour in a vacuum of about 1 micron. There was some problem in separating 15 or 20 baskets near the center of the string which had become stuck together (adjacent lids were stuck to each other) apparently due to diffusion bonding. They were pried apart, in most cases without much strain, but at the expense of some rough handling of the fuel. A portion of the string of baskets before removal of the fuel is shown in Figure 2. Although the pinhole camera photographs showed all the slugs except the controls to be nearly intact, by the time the NaK was removed and the slugs taken out of their basket, they were cracked and in most cases broken into many small pieces. Apparently they were delicately held together by the centering dimples of the baskets, but they were actually three dimensional jigsaw puzzles which fell apart once taken out of the containers. The breakage of the fuel was expected, and this expectation was the reason for the use of the baskets to maintain sample identity. Photographs of typical fuel samples are shown in Figures 3 and 4. The more complete fragmentation of the controls is evident by comparing Control Slug No. 8 with Nos. 7, 9, and 10; and by comparing Control Slug No. 60 with Nos. 56, 57, 58, and 59.

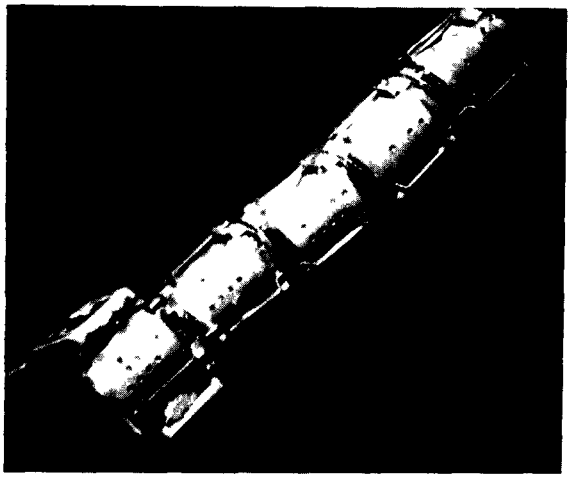

Figure 2. Part of Fuel String

10-25-68 UNCL 7707-4706

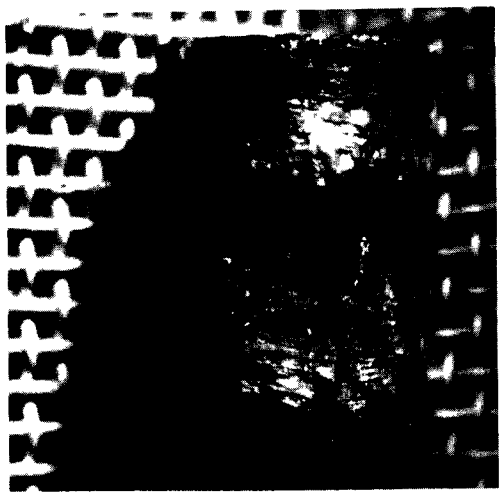

Slug No. 7

Slug No. 8

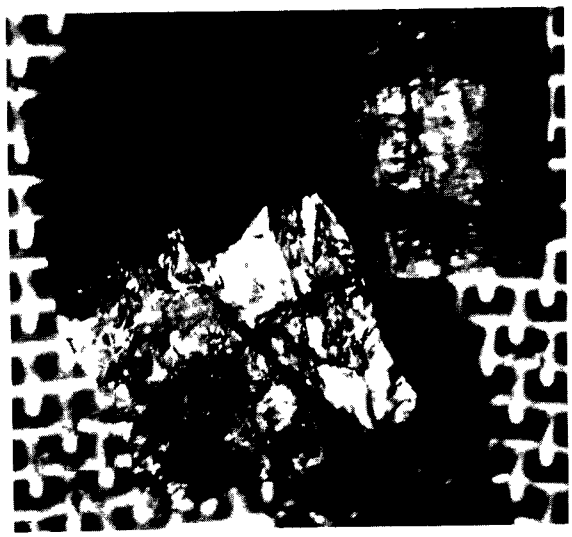

Slug No. 9

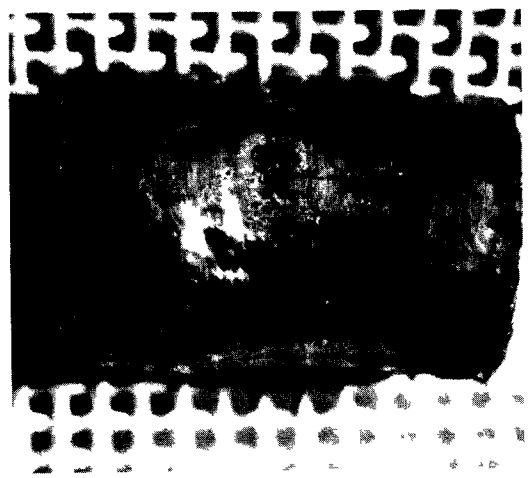

Slug No. 10

10-25-68 UNCL

7707-4707

Figure 3. Macrophotographs of Fuel Slugs (4.3X)

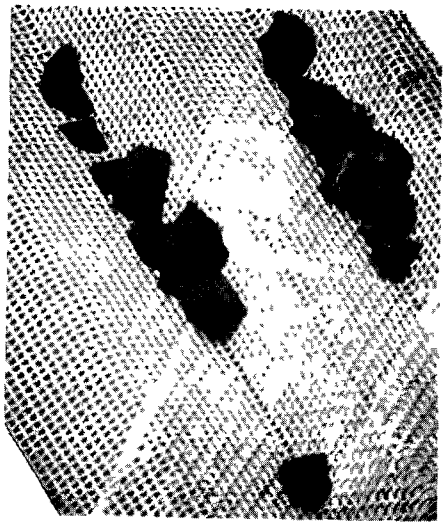

Slugs No. 56 and 57

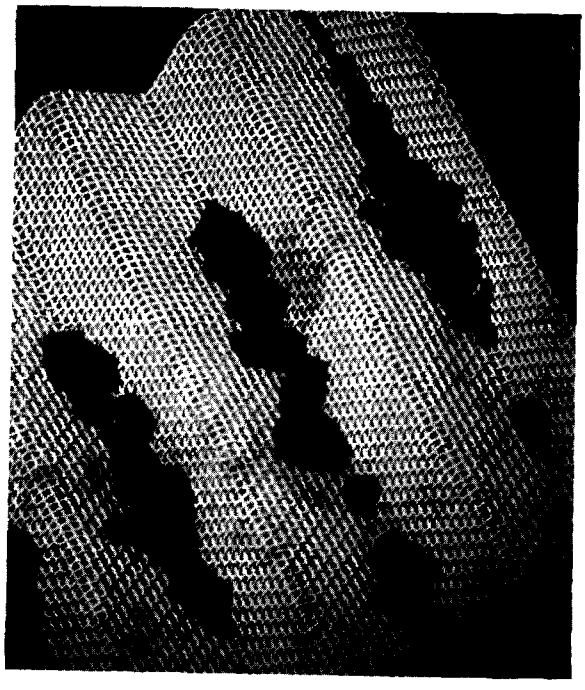

Slugs No. 58, 59, and 60

Slug No. 60

10-25-68 UNCL

7707-4708

Figure 4. Fuel Slugs Near the Middle of the Fuel String

Density measurements have been started at this writing. It is planned to measure densities on as many slugs as possible (with the funds available) in order to make statistical comparisons between types of samples. The measurements are being performed with great care to achieve the most precision that the method allows. Chunks of slugs are put in fine-screen baskets and weighed dry in air and again in Elox liquid, to determine density by immersion. The density of the liquid is determined each time by weighing a stainless steel cylinder in it. At this stage, the only statement that can be made with assurance is that some of the controls show swelling of about 10 vol %. This is an important finding because it means that the experiment will be successful in getting a good comparison of swelling behaviors between controls and tungsten-doped samples.

IV. EVALUATION OF EFFORT TO DATE

Experiment 101 was beset with design and construction problems which caused delays and high cost; however, all of these problems were surmounted, and it is now clear that the design was a good one and that the capsule was properly constructed; it survived the irradiation and handling without detriment. There were no instrument failures. Significant data are now being obtained which permit sound conclusions on the value of fine particle dispersions for control of fission gas swelling in carbides. Density measurements supplemented by metallography on these well-documented samples are expected to make substantial contributions to our understanding of the swelling phenomenon.

V. NEXT REPORT PERIOD ACTIVITIES

Density determinations will be completed within less than a month. The samples will be encapsulated, and a representative portion will be shipped to Los Alamos Laboratories where metallography will be performed. This is expected to occur early in November, but it is not known at this time what schedule will be followed at Los Alamos. If there is no priority problem, a significant portion of the optical metallography and a start on electron microscopy should be completed during the next quarter. Organization of the material for a final report will be started.

Program: FBR Fuels and Cladding
AEC Task: 11-C, Mixed Carbide Fuels (Casting Studies)
Project Manager: J. L. Ballif
Reporting Period: July-September 1968
General Order: 7707 Subaccount: 28230 AEC Category: 04-40-02-01

Principal Investigator: J. W. Carroll

I. PROJECT OBJECTIVES

The objectives of this task are to (1) establish optimum fabrication parameters, by calculation, for the melting and casting of mixed carbides, (2) utilize the calculated parameters in practice by producing laboratory quantities of mixed carbide, and (3) design, procure, and pilot run a furnace for the production of melted and cast mixed carbide fuel.

II. MAJOR ACCOMPLISHMENTS DURING YEAR 1968

Two studies were completed on the theoretical aspects of arc melting and casting mixed carbide. The first dealt with the loss of plutonium by volatilization during the melting operation, and the second dealt with the optimization of a melting-crucible design. A report has been written and issued titled, "Optimization of Melting Parameters for Fabrication of (U-Pu)C," which deals with methods of controlling volatilization loss of plutonium during melting.

III. PROGRESS DURING REPORT PERIOD

The crucible design optimization study was completed and a report has been written of the results. Data from the study are being used in the design of a crucible for developmental work on the arc melting and casting of mixed carbides

IV. EVALUATION OF EFFORT TO DATE

The data required for the proper design of a melting crucible and for the establishment of parameters to be used during the arc melting and casting of mixed carbide have been obtained. The theoretical data show that arc melting of mixed carbides should be feasible without high losses of plutonium due to volatilization during melting.

V. NEXT REPORT PERIOD ACTIVITIES

The installation of equipment in the NMDF for the mixed carbide development activity will continue.

Program:	General Chemistry and Chemical Engineering		
AEC Task:	12-A, Sodium Chemistry, Fundamental Studies		
Project Manager:	J. L. Ballif		
Reporting Period:	July-September 1968		
General Order: 7708	Subaccount: 36110	AEC Category: 04-40-04-04.1	

Principal Investigators: R. L. McKisson, R. L. Eichelberger, D. C. Gehri, J. Guon

I. PROJECT OBJECTIVES

The objective of this project is to advance the understanding of the chemistry of liquid sodium as a solvent for metals and nonmetals through study of the following:

1) The equilibrium solubility and the rate of solution of selected metals and nonmetals in liquid sodium, as a function of temperature, by using the highest purity materials available to minimize the perturbations caused by unwanted side reactions,

2) The nature of solute entities and their interactions in liquid sodium, from which thermodynamic properties of the solutions may be deduced, and

3) The analytical chemistry of solutes in liquid sodium at very low concentrations, in order that the data developed under 1) and 2) above may have the greatest possible reliability.

II. MAJOR ACCOMPLISHMENTS DURING FISCAL YEAR 1969

Assembly of the Sodium Chemistry Loop has been completed.

III. PROGRESS DURING REPORT PERIOD

A. SODIUM PURIFICATION

A sixth sodium distillation has been completed, and an extruder filled with the purified product, by using the gettering and distillation procedures described in NAA-SR-12444. The extruder being used as the source of sodium for

experiments is nearly empty, and the new extruder will be needed by early October. A sample of the final product from Extruder No. 5 will be taken for chemical analysis just before removing it from the system and installing the newly filled extruder. Only after installation on the ion-pumped vacuum system can the new product be sampled for analysis. No problems were encountered in the purification process, and the usual high quality product is expected.

B. SODIUM CHEMISTRY LOOP

Assembly of the Sodium Chemistry Loop has been completed. Welds have been inspected to AI Specification NA0107-023, Grade A. Heaters and thermocouples have been attached to the loop. The heater and thermocouple junction panels and wiring to the control console have been completed. The sodium reservoir has been filled with sodium and installed. The waste receiver has been helium leak tested, and heaters and thermocouples attached. The argon-vacuum manifold has been helium leak tested.

Welding of the Nickel-270 parts for the loop was done in an inert atmosphere box. The necessity for this procedure was dramatically demonstrated when a leak developed in one of the gloves and the box atmosphere became contaminated with approximately 500 ppm air. In spite of a high argon purge rate through the welding torch, it was not possible to make sound fusion welds. This observation prompted closer examination of the welds made by the vendor on the bellows sealed, Nickel-270 valves. In accordance with the material supplier's recommendation, Nickel-61 filler rod was used. Prior to acceptance by AI, the valves had to be helium leak tight to meet AI Specification NA0115-012, Rate I. Radiographs of the welds indicated considerable porosity in the root pass (or passes). Sound welds were obtained only after a substantial amount of filler rod had been added. The effect of this porosity on loop performance is not known; some leaching of impurities from these pores may be experienced.

In accordance with the quality control provisions of our contract with the USAEC, calibration of temperature, diagnostic voltage and amperage meters, and mass standards has been completed. A book for materials traceability records has been organized and a file of archive specimens prepared.

C. CARBON-IN-SODIUM SOLUBILITY STUDIES

The equation for the solubility of carbon in sodium as reported in the FY 1968 Annual Report, AI-AEC-12721, has been modified as a result of additional experiments at 700 and 900° C. When these data are included with those already reported, a least squares fit of all the data yields the equation

$$\log_{10} S(\text{wppm}) = 1.55 - \frac{360}{T(°K)} \quad ;$$

from which, a ΔH (soln) of 1700 cal/mole is calculated. A complete discussion of this equation, the data from which it is calculated, and the experimental procedures used in obtaining the data may be found in AI-AEC-MEMO-12686.

Efforts are continuing to refine these data and to discover the reasons for the apparent disagreement between carbon solubilities as calculated from this equation and those determined by using ^{14}C at the Argonne National Laboratory. A series of experiments designed to study the suitability of the dry combustion technique for the determination of carbon concentrations below 10 wppm has been completed. These results are being analyzed to establish the optimum conditions for obtaining both a low analytical blank and complete carbon recovery. The carbon content of the sodium used in this series is being independently measured by Dr. G. J. Lutz of the National Bureau of Standards by using activation analysis based on the $^{12}C(\gamma,n)^{11}C$ reaction. A new carbon solubility capsule design has also been developed and tested. Ten of these capsules which allow sampling of a center cut of the sodium phase have been fabricated out of a new supply of high purity Ni-270 stock. The new capsule design permits sampling the center portion of the sodium, independent of possible concentration gradients resulting from settling or flotation of (particulate?) carbon.

A series of experiments employing a ^{14}C tagged solute material is underway. The solute material has been prepared by carburizing small pieces of electron-beam zone-refined iron with ^{14}C tagged amorphous carbon at 1000° C. The new capsule design will be used, and each experiment will therefore consist of three analyses: (1) an analysis of the center cut, (2) an analysis of the remaining sodium, and (3) an analysis of the carbon produced by etching the Ni-270 capsule which was in contact with the sodium. The distribution of ^{14}C

as determined from these experiments may provide insight into the reasons for the much lower carbon solubilities that have been reported as a result of previous ^{14}C studies at other laboratories.

In determining the nature of the program outlined above, careful consideration has been given to the experience and comments of a number of investigators. The introduction of the new sampling techniques, the more adequate definition of variables in the dry combustion analysis, the employment of activation analysis, and the specified use of ^{14}C tagged solute material reflect this consideration and form the basis for a rather complete study of the carbon solubility problem.

D. METALS-IN-SODIUM SOLUBILITY STUDIES

1. Chromium

The results of four chromium solubility experiments were reported in the previous report (AI-AEC-12721). The values given were all less than 5 wppm, as measured by an analytical technique using atomic absorption spectrometry. The same high purity chromium rods used as solute for those experiments were irradiated to a level of approximately 500 dpm/microgram and then used for similar solubility runs.

Four sets of experiments using the irradiated Cr rods have been completed. In the first group of experiments, equilibrated at 700 to 1000°C, the sodium was found to have small radioactive particles on the surface, and the Cr rods had all come loose from the threaded crucible during the opening of the outer capsule and the sample collector. It was necessary, therefore, to cut the collectors again, below the surface of the sodium, and to cut through the sodium, discarding the surface. The results for these four samples showed the presence of 6, 43, 208, and 10 micrograms of chromium. The high values are undoubtedly the result of particulate Cr in the "pipe" formed in the center of the collector as the sodium solidified. The low values may reflect the solubility of chromium; although, if the solute became more concentrated at the surface of sodium during cooling, a disproportionate amount of Cr may have been rejected with the surface portion of the sample. Nevertheless, the results showed the feasibility of the radiochemical technique for chromium solubility studies.

TABLE 1

CHROMIUM SOLUBILITY EXPERIMENTS
USING ^{51}Cr SOLUTE RODS

Series	Experiment No.	Temperature (°C)	Cr in Na (wppm)
II	531	700	1.2
	532	800	10
	533	900	3.4
	534	1000	6.9
III	537	700	0.8
	538	800	11
	539	900	114
	540	1000	12.8
IV	544	800	43*
	545	800	44*
	546	900	282*

*Micrograms total

Results of the three subsequent series of chromium solubility runs, by use of the same irradiated rods, but with refinements in technique which prevented the rods from coming loose from the crucibles, are shown in Table 1. The numbers listed for the fourth series are total micrograms of chromium, since the amount of sodium in the collector has not yet been determined. The sodium loading in the experiments, however, was undoubtedly close to 2 grams, so that the results, when reduced to ppm, are higher than the earlier ones. The sodium from the first and fourth series of experiments was submitted for chromium analysis by atomic absorption spectrometry. The results from the first series were very low, with only about a microgram of chromium found although gamma-spectrometry had indicated as much as 200 micrograms. The AAS results from the fourth series are not yet complete. It is not clear at this time what the solubility of chromium in sodium is.

1. Iron

Irradiation of three iron crucibles was completed, and the crucible-collector assemblies were loaded with sodium, welded, and equilibrated at 700, 800, and

900°C. The irradiation was done with high purity titanium sample collectors already welded to the crucibles. After irradiation, the assemblies were cleaned in acid to remove surface oxidation, and then put through the normal procedures of vacuum desorption and sodium filling.

3. Niobium

Seven niobium solubility experiments have been run. Both assemblies which were equilibrated at 1000°C failed because the titanium collector ballooned. It is obvious that further experiments at 1000°C will need to have some sodium added to the outer capsule to balance the pressure of the sodium inside the crucible-collector assembly. The five successful runs have been submitted for chemical analysis. Priority work in the analytical chemistry laboratory has delayed the completion of the analysis, however.

4. Bismuth

Three solubility experiments have been completed in the effort to corroborate the solubility expression of Walker, Pratt, and Mott (Birmingham University and UKAEA, Harwell) presented at the 1968 AEC Corrosion Symposium. Because of its low melting point (~270°C), metallic bismuth is not a suitable solute for experiments in which the solute is separated from the solvent by inverting the crucible-collector assembly. Since the compound Na_3Bi (m. p. ~840°C) is the solid phase in equilibrium with liquid sodium in saturated solutions containing less than 25 atom percent bismuth, this compound was chosen as the solute with which to begin the equilibration.

The first preparation of Na_3Bi was carried out by heating appropriate amounts of the elements to about 500°C in a purified argon atmosphere while holding the reaction mixture in an aluminum cup between stainless steel plates. The purple Na_3Bi which formed was found to be too friable for use in a capsule experiment in which fine particles of solute might become distributed in the sodium phase.

Additional quantities of Na_3Bi were prepared by heating the reaction mixture to ~900°C, thereby fusing the Na_3Bi. The Na_3Bi was contained in a stainless steel foil cup within a stainless steel capsule. Five such capsules were prepared, with compositions of 75.40, 76.64, 76.68, 76.72, and 81.58 wt% Bi (Na_3Bi contains 75.19 wt% Bi). The contents of the first of these listed will be

TABLE 2

RESULTS OF BISMUTH-IN-SODIUM SOLUBILITY EXPERIMENTS USING Na_3Bi SOLUTE

Run No.	Temperature (°C)	Bi in Na (wppm)
664-8	200	36
664-11	300	150
664-12	400	2500

used to characterize the solute. Fused particles from the second one were used in solubility experiments. The solute was prevented from transferring to the sample collector with the solvent by means of a 150-micron stainless steel screen. Analysis for bismuth was by AAS. Results of the three experiments run are shown in Table 2. These three points were compared to the solubility expression of Walker, Pratt, and Mott, which is

$$\log_{10}(\text{at. \% Bi}) = 5.0038 - \frac{4188.9}{T(°K)} \quad .$$

The comparison shows general agreement with the British work, within the scatter of the data from which their expression was derived.

5. Analytical Chemistry Research

The Spark Source Mass Spectrometer has been undergoing improvement. A screen over the beam outlet hole in the source has resulted in much improved resolution. The data digitizing system was delivered and installed. A binocular microscope has been installed to allow the operator to observe the position of the spark during analysis. An oscilloscope has been added to the system, enabling the waveform of the spark to be observed. These refinements in the SSMS system will permit observation and control of previously unknown parameters in the use of the instrument.

6. Other Project Activities

Additional oxygen analyses in sodium were required for the recent ASTM-AEC Round Robin. These were performed and submitted as required to Atomic Power Development Associates.

Additional revision of the "Chemical Interactions" section of the Liquid Metals Handbook being prepared by the Liquid Metals Engineering Center was completed by Senior members of the project staff.

The topical report "The Solubility of Oxygen in Sodium – A Recommended Expression," AI-AEC-12685, was completed for final review.

IV. EVALUATION OF EFFORT TO DATE

Progress toward the objectives of the project has continued without any particular perturbation. The slowness in completing the irradiation of iron solubility crucibles was annoying, but the effort was usefully employed in other areas, and the problem is now resolved. The uncertainty in the determination of the solubility of chromium was not foreseen and must be resolved. Progress in the study of the carbon analytical method, and the solubility of carbon, is as planned, and the fabrication of the Sodium Chemistry Loop has maintained the schedule predicted several months ago, a fact which bears witness to careful and complete work during the planning stages of the facility.

V. NEXT REPORT PERIOD ACTIVITIES

All the activities reported will continue. Results of the iron solubility experiments with irradiated solute crucibles will be available and will be discussed in relation to the wet chemical results reported here and elsewhere. Other solubility work will proceed as planned. The evaluation of the high temperature combustion technique for analysis for carbon in sodium will be completed and will allow decisions to be made on the direction of future carbon solubility work. The first results of experiments using ^{14}C enriched solute material will be reported. The Sodium Chemistry Loop will be put into operation and evaluation experiments started with the oxygen probe.

Program:	Reactor Development
AEC Task:	12-B, Sodium Chemistry, Fission Product Contamination
Project Manager:	J. L. Ballif
Reporting Period:	July-September 1968
General Order: 7708	Subaccount: 29410 AEC Category: 04-60-10-01.1

Principal Investigators: M. Silberberg, J. Guon, G. Zwetzig

I. PROJECT OBJECTIVES

The objective of this program is to elucidate the behavior of fission products released to the coolant in a fast, sodium-cooled, LMFBR reactor during normal operation, in order to provide information necessary for the development of fission product trapping techniques in such systems. The disposition of fission products during normal operation must also be known in order to assess the consequences of potential accidents. Information is required on the extent of fission product retention in sodium coolant, the rate and extent of release to the cover gas, and the rate and extent of plate-out on surfaces.

II. MAJOR ACCOMPLISHMENTS DURING FISCAL YEAR 1969

Characterization of the Fission Product Behavior Loop (FPBL) was completed.

III. PROGRESS DURING REPORT PERIOD

A. SOURCE TERM

1. Corrosion Products

The term corrosion products refers to either core structural materials (such as fuel cladding or fuel element hardware) which are activated by the core neutron flux and subsequently enter the coolant stream by corrosion, or to materials which are corroded from the ex-core surfaces of the primary loop to the coolant and are subsequently activated as they pass through the core.

The previously reported study of corrosion product activities produced by core structure activation by the (n,γ) reaction was extended to include production of radioisotopes by the (n, p), (n,α) and (n, 2n) reactions. As before, the cross sections were averaged over a typical LMFBR neutron spectrum. The activity released to the coolant was then calculated based on the following assumptions.

Average neutron flux = 5×10^{15} nv

Operating time = 1 year

Corrosion rate = 2 mils/year

Number of fuel pins = 10^5

Fuel pin dimensions = 0.25-in. OD x 72-in. long

Structural material = Type 304 stainless steel with 0.05% Co^{59} impurity

The results are summarized in Table 1.

TABLE 1

CORROSION PRODUCT ACTIVITIES

Isotope	Production Reactions	Curies Released at 1 Year	Total Curies Released at 1 Year
41.9m Cr^{49}	Cr^{50} (n, 2n)	5.93×10^{-4}	5.93×10^{-4}
27.8d Cr^{51}	Cr^{50} (n, γ) Fe^{54} (n, α) Cr^{52} (n, 2n)	5.54×10^{4} 6.25×10^{3} 7.46×10^{2}	6.24×10^{4}
300d Mn^{54}	Fe^{54} (n, p) Mn^{55} (n, 2n)	2.12×10^{5} 3.24×10^{2}	2.12×10^{5}
2.94y Fe^{55}	Fe^{56} (n, 2n)	2.15×10^{3}	2.15×10^{3}
45.1d Fe^{59}	Fe^{58} (n, γ)	1.33×10^{4}	1.33×10^{4}
72d Co^{58}	Ni^{58} (n, p) Co^{59} (n, 2n)	5.31×10^{5} 7.38	5.31×10^{5}
5.3y Co^{60}	Co^{59} (n, γ) Ni^{60} (n, p)	8.54×10^{3} 1.36×10^{4}	2.21×10^{4}
37h Ni^{57}	Ni^{58} (n, 2n)	0.37	0.37

Examination of the above results shows that the most important corrosion products are Mn^{54} and Co^{58}, and that these are primarily produced by the (n,p) reaction. The corrosion products considered previously, Cr^{51}, Fe^{59}, and Co^{60}, produced by the (n,γ) reaction, are seen to be of secondary importance. Because of its long half-life, Co^{60} would of course, become increasingly important for longer operating periods.

2. Source Term Computer Program

a. Fission Product Inventory

It was previously reported that the fission product inventory for the Source Term would be computed by using the CURIE code modified by the substitution of fission yields characteristic of fast fission in plutonium* for the present yield values which are based on thermal fission in U^{235} These substitutions were made, and the results of test problems using the two sets of yield values were compared. The comparison indicated that the plutonium case yielded a fission product inventory about two-thirds that of the U^{235} case. Investigation revealed that this gross difference was due to faulty manipulation of the new yield values by the CURIE code. Additional study of the CURIE code relative to its application in the Source Term Program indicated the desirability of abandoning it in favor of a fission product generation routine specifically designed for the Source Term Program. This special routine would conserve computing time and core storage space by limiting the isotopes to be considered to those in the fifty most important mass chains, by eliminating some of the extensive and time-consuming output edits available with the CURIE code, and by providing a truly integrated program which permits optimum logic and intercommunication between the various code routines.

The equations necessary for this calculation were assembled and incorporated in the preliminary draft of the Source Term Program.

In line with the above, all the fission product chains from mass number 72 to mass number 159 were examined, using as a basis, a CURIE estimate of the fission product inventory for one year of reactor operation at 2120 Mwt and U^{235} thermal fission yields. This examination revealed that after one week of decay, only 47 mass chains contained isotopes having activities in excess of

*Taken from LA-3383

100 curies. Since the isotopes in these chains would have the greatest biological and residual radiation significance, these chains were selected for inclusion in the fission product generation routine. Three additional chains were selected for inclusion on the basis of their lower activity level but long half-life.

The selected chains were then examined in detail, and the latest values of half-lives and branching ratios were determined for inclusion in the program input data. Short-lived precursors (half-lives less than 20 minutes) were eliminated from the chains to save computation time, and their fission yields were added to the first long-lived isotope in the chain. Fission yields were based on fast fission in plutonium and were taken from LA-3383.

b. Fission Product Distributions

Analytical models for treating the various processes affecting fission product distribution in the primary system were developed and reviewed. Among the processes considered are release of fission products to the coolant from the fuel cladding; removal of fission products from the coolant by "plating" on surfaces, trapping and vaporization; and reintroduction of fission products into the coolant by corrosion of plated deposits. The present models for these processes are as follows.

1) Fraction of fuel pins with clad failure, f(t)

$$f(t) = f_1 + f_2 t + f_3 \exp(t/f_4) + f_5(t - t_r) \quad ,$$

where: t = time, f_1 to f_5 are constants, and $f_5 = 0$ for $t < t_r$.

2) Removal by "plating"

$$\left(\frac{dC_i}{dt}\right)_{plating} = -K\left(C_i - \frac{S_i}{\Delta}\right)$$

where:

C_i = concentration of isotope "i" in coolant,

S_i = surface concentration of "i" on adjoining surface,

Δ = characteristic length (e.g., hydraulic diameter or surface film thickness), and

K = reaction rate constant.

3) Removal by Trapping

$$\left(\frac{dN_i}{dt}\right)_{trapping} = -\mu F\left[C_i - C_i^o(T)\right] \quad ,$$

where:

N_i = atoms of "i" in primary system,

F = flow rate through trap,

$C_i^o(T)$ = solubility limit for chemical form of "i" at temperature, T, in trap,

μ = 1.0 for $C_i > C_i^o(T)$, and

μ = 0.0 for $C_i < C_i^o(T)$.

4) Removal by vaporization

$$\left(\frac{dN_i}{dt}\right)_{vap} = -\alpha_i \left[N_{i,eq}^v - \bar{N}_i^v(t_{i-1})\right] \quad ,$$

where:

$N_{i,eq.}^v$ = atoms of "i" in vapor space at equilibrium,

$\bar{N}_i^v(t_{i-1})$ = average number of atoms of "i" in vapor space during preceding time interval, and

α_i = vaporization rate constant for "i,"

also,

$$N_{i,eq}^v = \frac{W_c k_D^i PVC_i}{V_c \rho RT} \quad ,$$

where:

W_c = atomic weight of coolant,

k_D = distribution coefficient for "i" in coolant relative to vapor and liquid phases,

P = coolant vapor pressure,

V = volume of vapor space,

V_c = volume of coolant,

ρ = density of coolant,

T = local temperature in vapor space, and

R = gas constant.

5) Reintroduction by corrosion of deposits

$$\left(\frac{dN_i}{dt}\right)_{corr.} = \lambda A S_i \quad ,$$

where:

λ = fraction of monolayer removed per unit time,

A = surface area, and

S_i = surface concentration.

Equations were also prepared to account for generation of corrosion products and their removal by "plating" and trapping, for generation of fission products in the coolant by fission of plutonium contamination, and for generation of Na^{22} and Na^{24} activities.

3. Code Preparation

All of the foregoing equations have been incorporated in a preliminary draft of the Source Term Program. This draft includes the bulk of the logic and FORTRAN statements needed to test the operation of the program.

B. DEPOSITION AND TRAPPING STUDIES, FISSION PRODUCT BEHAVIOR LOOP (FPBL)

The first phase of loop testing has been completed. This phase was intended to characterize the loop by providing operating data to compare with design values. The loop is operating as predicted with two exceptions. One, lower heat transfer rates were obtained through the trap coolers, as a result of computational error (an improper dimension was used). When corrected, the predicted heat transfer rate is within 10% of the measured rate. The second is related to an abnormal temperature distribution within the trap heat exchangers. The

traps were radiographed. The measured axial misalignment was inadequate to explain the observed distribution. The resolution on the x-ray film was insufficient to accurately measure radial misalignment. The experimental capability of the loop is not adversely affected by these differences.

Testing of the sodium level gauge has been completed. The gauge response is such as to resolve changes in liquid level of less than 1/8 in.

The first sodium loading was discharged and a second load added. A sample was taken for chemical analysis. No problems in loading, unloading, or sampling were encountered. The cesium to be used during the initial set of experiments has been received (one month late). Equipment to be used to prepare stock solutions of cesium and sodium has been completed. Purification of the atmosphere in the inert atmosphere box to be used for the preparation of stock solutions has started.

The surge tank which contains 90% of the sodium in the FPBL was designed to operate either as a well-stirred vessel (using the by-pass pump to provide mixing) or as an unstirred vessel. An analysis was made to determine the better mode for the development of kinetic data. For cold trapping, it was assumed that two deposition mechanisms might apply, deposition of particulate due to the solubility limit being exceeded, or adsorption onto activated surfaces. Assuming a constant outlet composition in the solubility limited case, the applicability of the Langmuir Adsorption Isotherm, and adequately slow rates for the adsorption case, the expressions in Table 2 were developed.

Results indicate that for the stirred mode, the fission product buildup in the trap will vary as an inverse exponential with time for both depletion mechanisms. For this mode, distinguishing between the two mechanisms may be difficult. This is not the case for the unstirred mode. If the surge tank operates as it was designed to, the deposition mechanisms should be identifiable.

For hot trap tests, the deposition mode should be related to diffusion into the stainless steel surfaces. These rates should be sufficiently slow so that the operating mode of the surge tank should not affect system kinetics. Diffusion data* indicate that the count rate of isotopes diffused into the trap surfaces

*H. Keil, H. L. Scherff, R. Lindner, "Fission Product Transfer in the System UO_2/Liquid Sodium/Stainless Steel," Atomkeinenergie 12, 96-100 (1967)

TABLE 2

EXPRESSIONS FOR DETERMINING KINETIC DATA

Deposition Mechanism	Stirred Vessel	Unstirred Vessel
Solubility-Limited	$N = w(C_o - C_{out})\left(1 - e^{-t/t_1}\right)$	$N = w(C_o - C_{out})t/t_1;\ 0 < t \leq t_1$ $N = w(C_o - C_{out});\ t \geq t_1$
Surface Adsorption	$N = wC_o(1 - e^{-kt})$	$N = KwC_o\left\{(1 - kt_1)^n(t - nt_1) + t_1\sum_{i=1}^{n-1}(1 - kt_1)^i\right\};$ where: $(t - nt_1) < t_1$ and, when $n = 0$ $\sum_{i=1}^{n-1}(1 - kt_1)^i = 0$

N = mass of isotope in the trap, gm

C_o = initial concentration of isotope, gm/gm

C_{out} = concentration of isotope at the outlet of the trap, gm/gm

t = time, sec

t_1 = inventory change-over time (mass of sodium in the loop divided by the mass flow rate), sec

w = mass of sodium in the loop, gm

k = Langmuir adsorption rate coefficient (rate constant times equilibrium constant), sec^{-1}

should be twice the count rate of the isotope dissolved in the sodium in from 3 to 30 hr. A verification of the diffusion coefficients to within several factors should be practical in the FPBL.

IV. EVALUATION OF EFFORT TO DATE

Progress in formulation and preparation of the Source Term computer program is considered satisfactory. The number of isotopes to be considered in the program has been reduced to keep the program within manageable size. This should not affect the usefulness of the program, however, since all of the isotopes eliminated were either of very short half-life or very low yield. This reduction in the number of isotopes considered will assist in reducing the running time required for the program. Some question remains, however, as to the required running time for a "typical" problem. This can only be resolved after the code is operating and a determination is made as to the largest permissible time step consistent with code stability. The integration method used in the program was selected with a view toward minimizing stability problems.

With the exception of the one still unexplained temperature anomaly, the FPBL is a well characterized system. If tests with fission products indicate proper operation of the surge tank and no appreciable channeling in the traps, results should be obtained on not only several deposition properties, for which the loop was designed, but also on mechanism identification and kinetic data.

V. NEXT REPORT PERIOD ACTIVITIES

Necessary constants for use in the Source Term Program will continue to be assembled. The draft of the Source Term Program will be placed on computer cards to form a program deck. Test problems will be run and the program will be modified as necessary to provide proper operation.

Work using radioactive cesium will be well in progress. Preparations for work with radioactive barium will start.

Program:	HNPF				
AEC Task:	13, HNPF Retirement				
Project Manager:	B. F. Ureda				
Reporting Period:	July-September 1968				
General Order:	7709	Subaccount:	11400	AEC Category:	46-01-00-00.0

Principal Investigator: B. F. Ureda

I. PROJECT OBJECTIVES

The project objective is the accomplishment of AEC-designated tasks in the retirement of the HNPF. During the past quarter, these tasks were as follows. (1) Support the implementation of the discrete activities comprising the HNPF retirement by providing design and analysis assistance as required. (2) Coordinate the disposal of HNPF excess property to other AEC contractor users or to storage in accordance with AEC direction. (3) Assist in the determination of the economics of HNPF buildings disposition by performing engineering and cost studies as necessary. (4) Assist CPPD in the disposition of the irradiated fuel. (5) Assist CPPD in the preparation of the detailed procedures as needed to define the tasks outlined in the Activity Specifications. (6) Continue producing a motion picture record of the principal activities of the retirement program. (7) Prepare special reports of the retirement activities and a safety analysis of the HNPF retirement program end product.

II. MAJOR ACCOMPLISHMENTS IN FISCAL YEAR 1969

Accomplishments during fiscal year 1969 are: (1) completion of the shipment of the irradiated fuel to Savannah River Plant, (2) off-site shipment of the major portion of the HNPF excess property, (3) preparation of the HNPF building demolition technical specification to be used first to determine the cost of demolition and second to guide the demolition contractor in his work, (4) completion of engineering and cost studies to aid in determining the economics of building disposition, and (5) initiation and continuation of special report preparation and the recording of principal activities on motion picture film.

III. PROGRESS DURING THE REPORT PERIOD

A. SPENT FUEL SHIPMENT

Fuel shipping cask No. 1 containing the last shipment (25th) of spent fuel from the HNPF left the site on July 24, 1968. After the last fuel shipment, the empty railroad car was returned to the HNPF site and the moderator element shipping cask was welded to the car bed. This cask and the spent fuel shipping cask appurtenances and spare parts were shipped to storage at the SRP. The empty railroad cars were returned to the Rock Island Roads Kansas City shops. This action completed all the activity associated with the HNPF spent fuel.

B. ACTIVITY SPECIFICATION DEVELOPMENT

Eleven of the twelve Activity Specifications have been approved by the AEC. The remaining specification, No. 10, "Securing of the Isolation Structure," was rewritten so that it consisted of two distinct parts. Part A, deals with the sealing of the penetrations to the Isolation Structure and has been approved by the AEC. Part B, deals with the placement of the protective covering over the Isolation Structure, and has been revised again based on the recent agreements in regard to the demolition of the buildings; this revised version is now awaiting concurrence of CPPD prior to submittal to the AEC.

C. EXCESS PROPERTY DISPOSAL

Removal and shipment of excess property continues. Shipments of AEC-HNPF equipment to storage has been completed. All but a few of the large items such as pumps, valves, and control panels, have been shipped to other AEC contractors. Twenty more purchase orders are yet to be filled. The items involved are small such as fire extinguishers, air masks, instrumentation, and office furniture.

The building demolition package which contained the revision of the building demolition technical specification, drawings, and photographs of the building, and a list of excess property not destined for other AEC use was compiled and forwarded to the AEC-CH for distribution to likely contractors. Supporting engineering and cost studies on various approaches to building demolition were prepared so that an evaluation of the economics of demolition operation could be made by the AEC.

Special large sodium valves were shipped to AI Santa Susana where they were cleaned and packaged for storage for ultimate use by the Liquid Metals Engineering Center. Both primary and secondary valves were sent to AI; however, only the large (above 14-in.) primary sodium valves were cleaned since it became difficult to remove the radioactive contamination to acceptable limits. The valves that could not be cleaned with a reasonable effort were sent to burial.

D. CPPD

CPPD was given assistance in preparing the detailed procedures for the sealing of the reactor and the sealing of the isolation structure penetrations. Two isometric drawings showing the location of the isolation structure penetrations were drawn.

E. DOCUMENTATION

1) The report "Potential Effects of Sodium Hydroxide on the HNPF Reactor Vessel" was prepared and issued on August 9, 1968. This report was written to assure interested parties that the sodium hydroxide residue remaining in the reactor vessel after completion of the sodium reaction process would not detract by some corrosion mechanism from the long-time containment capability of the reactor vessel.

2) The HNPF sodium disposition report has been prepared and printed; copies are available for distribution. This report covers all the activities in the HNPF retirement dealing with sodium disposition. The two major activities reported are the disposition of the bulk sodium and the reaction of the residual sodium in the reactor vessel and the coolant loops.

3) The Safety Analysis report which will document the Health and Safety aspected of the HNPF retirement end product has been outlined and reviewed by the AEC. Preliminary work in completing this report is continuing.

4) The portions of the final summary report covering the completed HNPF retirement activities have been prepared.

5) Motion picture records of the principal activities have been taken. The existing film footage has been edited and the narration that will explain the action is being prepared.

IV. EVALUATION OF EFFORT TO DATE

Shipment of the irradiated fuel from the site was accomplished a few weeks ahead of schedule. Disposal of excess property was accelerated during this reporting period. If the shipment of excess property had had a higher priority in HNPF retirement, most of the excess property would have left the site earlier.

Disposal of the HNPF buildings and the placement of the protective covering over the isolation structure are the two important remaining tasks in the retirement program. The engineering and cost studies performed by AI have aided significantly in the determination of the building disposal.

Preparation of the reports that will be required by DRL and other AEC departments in assessing the work, and the remaining HNPF end product has proceeded sufficiently far so that preliminary informal reviews can be made. These early reviews will more likely permit simultaneous completion of the work and acceptance of the reports.

V. NEXT REPORT PERIOD ACTIVITIES

Approval of the one remaining Activity Specification will be obtained in the next report period.

The remainder of the excess property will be shipped off site except for the few items required during the placement of the protective covering over the isolation structure. The demolition of the HNPF buildings by an AEC-selected contractor is expected. A motion picture record of portions of this operation will be made.

Report preparation will continue; however, completion is not expected during the next reporting period since it now appears that the final placement of the protective covering over the isolation structure will not be made until the spring of 1969.

C

Program: Advanced Development Program		
AEC Task: 15, High Temperature Chemistry		
Project Manager: S. J. Yosim		
Reporting Period: July-September 1968		
General Order: 7711	Subaccount: 53020	AEC Category: 05-05-01-00.1

I. PROJECT OBJECTIVES

The project is divided into two general areas; namely, the study of fused salts and the study of metal - metal-salt solutions. The objective of the study of fused salts is to achieve an understanding of ionic melts (halides, oxides, oxy-salts and glass systems) by (a) establishing the nature of the species existing in ionic melts, (b) determining the physicochemical interactions between species, and (c) formulating systematic relationships between the physicochemical properties of fused salt systems and the molecular parameters of the species.

The objectives of the metal - metal-salt study are to determine phase diagrams for, and the nature of interactions between metals and their salts at high temperatures, to determine the species in these solutions and, finally, to predict the solubilities in metal salt systems.

II. MAJOR ACCOMPLISHMENTS DURING FISCAL YEAR 1969

A. PUBLICATIONS

The following paper was published.

S. J. Yosim and H. Reiss, "Fused Salts," Ann. Rev. Phys. Chem., 19, 59 (1968)

The following papers are in press.

1. L. F. Grantham, "The Electrical Conductivity of Molten Mercuric-Mercurous Halide Systems," J. Chem. Phys.
2. L. F. Grantham and S. J. Yosim, "Electronic Conduction in Fused Salts," in a book published by Marcel Dekker, Inc.
3. Milton Blander, "Some Fundamental Concepts in the Chemistry of Molten Salts," in a book published by Marcel Dekker, Inc.

B. TALKS

The following papers were presented.

1. An invited paper, "Some Fundamental Concepts in the Chemistry of Molten Salts," was presented by M. Blander at the symposium of Characterization and Analysis in Molten Salts at the 156th American Chemical Society Meeting.
2. An invited paper, "Electronic Conduction in Fused Salts," by S. J. Yosim and L. F. Grantham was presented by S. J. Yosim at the symposium on Characterization and Analysis in Molten Salts at the 156th American Chemical Society Meeting.
3. "The Electrical Conductivity of Molten Mercuric-Mercurous Halide Systems," was presented by L. F. Grantham, at the 156th American Chemical Society Meeting.

C. TECHNICAL ACCOMPLISHMENTS

1. The study of the electrical conductivities of the molten CuCl-$CuCl_2$ system was completed. Electron exchange was established as the most likely mechanism of electronic conductivity.

2. The study of the electrical conductivities of aluminum-halide - alkali-halide mixtures has been completed.

3. A review of some of the concepts important in molten salt chemistry was completed by Blander.

III. PROGRESS DURING REPORT PERIOD

A. SOME FUNDAMENTAL CONCEPTS IN THE CHEMISTRY OF MOLTEN SALTS

A review of some of the concepts important in molten salt chemistry was carried out at the North American Rockwell Science Center. Special emphasis was placed on those concepts which are an aid to physical intuition as well as those concepts which have a bearing on chemistry and chemical reactions. This review has been accepted for publication.

B. ELECTRICAL CONDUCTIVITY OF CuCl-$CuCl_2$ SOLUTIONS

The electrical conductivity of pure $CuCl_2$ was measured from the melting point (625°C) to 800°C. Since the void volume of the conductivity cell in this

determination was less than in the previous measurement, less $CuCl_2$ decomposition to Cl_2 and CuCl could occur. As expected, under these conditions, the conductivity was less than reported previously. These results suggest that a considerable portion of the measured conductivity in "pure" $CuCl_2$ is due to semiconduction (electron transfer between Cu^{++} and the Cu^{+} formed by the decomposition of $CuCl_2$). To take this into consideration, the compositions in the $CuCl_2$-rich melts were corrected for thermal decomposition. The logarithm of the exchange frequency calculated from the conductivity data was a nearly linear function of the exchange distance at constant temperature and was a linear function of reciprocal temperature at constant exchange distance, as predicted by the exchange model. This is the first salt system studied in which a conductivity maximum was observed as a function of composition, and where the evidence for electron exchange is so complete. The work has been completed and a paper describing these results is in press.

C. ELECTRICAL CONDUCTIVITIES OF ALUMINUM-HALIDE - ALKALI-HALIDE MIXTURES

Activation energies for conduction were calculated for the $AlCl_3$-KCl and $AlBr_3$-NaBr systems by plotting the log of the specific conductance vs 1/T. Values ranging from approximately 1 to 4 kcal/mole were obtained. When these activation energies were plotted vs composition, minima occurred near 30 to 40 mole % AlX_3. This was also the region where minima occurred in the conductance vs composition plots. The experimental phase of this work has been completed. A paper describing these results will be published.

D. IONIC SALT VAPORS

In a previous experiment, the conductivity of a fused silica cell containing CsCl + LiCl (1:5 mole ratio) vapor was measured over the temperature range 800 to 950°C. The magnitude of the conductivity and its variation with temperature were in accord with the presence of conducting species in the vapor. After the run, however, the tungsten electrodes were etched and appeared greyish, indicating that some reaction between the electrode and salt vapor may have occurred. A similar cell with platinum foil electrodes welded to tungsten rod leads was run over the temperature range 850 to 1100°C. The specific

resistances at these temperatures were about 1.1×10^6 and 41×10^3 ohm-cm, but the exact temperatures are in some question since the thermocouple was found to have moved out of contact with the cell. After the experiment was terminated, the cell was cut open and inspected. Although the platinum foil electrodes were smooth, they were a uniform grey throughout. The cause of this change on the electrodes must be determined before further measurements are made.

E. SOLID STATE GALVANIC CELLS

Conductivity measurements on single crystal CaF_2 samples at temperatures from 500 to 750°C have indicated that impurities are reacting with the samples. The conductivities were found to be greater than those reported in the literature [Ure, J. Chem. Phys. 26, 1363 (1957)] and also increased with time. These impurity effects were more pronounced in vacuum than in purified He, and when carbon (from "aquadag") electrodes were used. Other electrodes employed have been pressed pellets of $Y + YF_3$, $Al + AlF_3$ or $Dy + DyF_3$ and vacuum deposited gold. The CaF_2 specimen removed from the $Dy + DyF_3$ cell was examined with a probe spectrograph. It was found to have carbon on its edges and some oxygen on its faces. The latter would appear to be due to oxide impurities in the Dy electrodes. Since the cell employed in these measurements had electrical lead seals of epoxy, a possible source of contamination, a new cell with all glass-to-metal seals was fabricated and tested. When aquadag-coated carbon electrodes were used, increasing conductivities were again found. These results suggest that either diffusion of the electrode materials in the CaF_2 is occurring or impurities in the aquadag or the He atmosphere have not been eliminated.

F. A THEORETICAL STUDY OF TERNARY SALT SYSTEMS

A study has been initiated at the North American Rockwell Science Center to calculate the theoretical phase diagrams for additive ternary systems utilizing the quasi-chemical calculations published by Hagemark. From these calculations, it is hoped that it will be possible to characterize the shapes of liquidus isotherms and the appearance of miscibility gaps in terms of the deviations from ideal solution behavior of the binary subsystems. In addition to this, it

is planned to relate the thermodynamic properties of additive ternary systems to structural concepts in dilute solution and to the more generalized concepts of nonrandom mixing in concentrated solution. These calculations should aid in quantifying our present qualitative understanding of additive ternary molten salt systems and in understanding problems of the molten salt reactor. Specifically, this theoretical work should be an aid in fuel reprocessing and in predicting the thermodynamic properties of solutes in the molten salt reactor fluid, ($LiF-BeF_2$) and of fluids such as the fluoroborate coolants proposed at Oak Ridge.

IV. EVALUATION OF EFFORT TO DATE

The emphasis in the experimental approach continues on high pressure and transport experiments; however, consideration is being given to emphasize fluoride systems rather than the other halides. Although the experimental studies will be more difficult and time consuming, it is felt that such studies are necessary to further increase our understanding of fused salts.

V. NEXT REPORT PERIOD

Some definitive experiments on ionic salt vapors will be run. Emf's of solid fluorides will be measured by using solid state galvanic cells. A study of the physicochemical properties of SnF_2 (M.P. = 219°C) will be initiated. The theoretical study on ternary phase diagrams will be well underway. The high pressure studies on $AlCl_3$ will be resumed.

Program:	Advanced Development, Physical Research		
AEC Task:	16, Radiation Chemistry		
Project Manager:	R. A. Holroyd		
Reporting Period:	July-September 1968		
General Order: 7712	Subaccount: 53050	AEC Category: 05-05-02-00.1	

I. PROJECT OBJECTIVES

The objectives of this project are to delineate the fundamental physico-chemical processes occurring in the radiolysis of organic systems and to study these processes in separate experiments designed to increase our understanding of their nature and their role in radiolysis.

II. MAJOR ACCOMPLISHMENTS DURING FISCAL YEAR 1969

A. PAPERS PUBLISHED

1. R. A. Holroyd, "Radical Yields of Hydrocarbons," pp 1-32, in "Aspects of Hydrocarbon Radiolysis," edited by T. Gauman and J. Hoigne, Academic Press, London (1968)
2. R. A. Holroyd, "The Reaction of Nitrous Oxide with Excited Molecules in the Radiolyis and Photolysis of Liquid Alkanes," in Adv. in Chem. Series 82, 488 (1968)

B. PAPERS PRESENTED (at the International Conf. on Rad. Chem. Argonne, August 1968)

1. R. A. Holroyd, "Reactions of Nitrous Oxide, Carbon Dioxide and Carbon-Tetrachloride with Excited Molecules in the Photolysis of Liquid Alkanes"
2. R. A. Holroyd, "Nanosecond Pulse Radiolysis of Molten Aromatic Liquids"

III. PROGRESS DURING REPORT PERIOD

A. NANOSECOND PULSE RADIOLYSIS OF LIQUID NAPHTHALENE

The pulse radiolysis of naphthalene was studied to determine the relative yields of excited molecules in triplet and singlet states, and to assess the role of intersystem crossing in triplet state formation. The excited singlet state was observed both by emission and by absorption spectroscopy. The emission

spectrum showed that the singlet was present to an extent as excimers. A short lived absorption, which peaked at 395mμ, was observed, and the decay of this absorption was correlated with that of the fluorescence. This absorption was attributed to the naphthalene excimer. The yield of singlets was shown to be G = 4-7. The yield of naphthalene triplets as determined from the absorption at 415 mμ was found to be G = 1.6. The formation of this number of triplets by intersystem crossing which is ~40% efficient is consistent with the results. When 1,2-benzanthracene was added to the naphthalene, singlet-singlet transfer occurred. The rate of transfer exceeded the diffusion controlled rate and is attributed to an excimer-migration mechanism. A manuscript describing this research has been prepared.

B. STUDY OF ESR SPECTRA OF NEGATIVE IONS

In the radiolysis of aromatic compounds, the anion is often formed by electron attachment. Elucidation of the mechanism of radiolysis depends on a knowledge of the reactions of anions. An ESR study of anions of purines, pyrimidines, and aromatic hydrocarbons has begun. The anions are prepared either electrolytically or by alkali metal reduction. Our work on hydrocarbons has begun with diphenylfulvene which has been reduced to its anion by alkali metal and electrolytic techniques. Diphenylfulvene anion yields a well resolved spectra (line width ca. 0.15 G) extending over 23 G. Preliminary interpretations of these spectra have been made and are being compared to results from the spectrum simulation program GLAD. Hyperfine coupling constants obtained from this analysis will be compared to those predicted by Huckel and McLachlan molecular orbital theories which are currently being programmed for the IBM 360 computer. A better understanding of the molecular electronic structure of anion radicals is anticipated from this study.

IV. EVALUATION OF EFFORT TO DATE

The pulse radiolysis studies have demonstrated that in the radiolysis of naphthalene, the primary processes such as excitation and ion neutralization lead predominately to the formation of excited singlet states. A significant yield of triplets is formed apparently by intersystem crossing. Singlet-singlet

energy transfer in liquid naphthalene is extremely rapid as a result of an excimer migration mechanism.

Studies of electron reactions with hydrocarbons and nitrogen containing heterocycles are underway. The electrolytic generation technique is working quite well, and several new anion radicals have already been discovered. The computer program necessary to analyze the ESR spectra of radical ions and to determine the location of unpaired spin has been completed.

V. NEXT REPORT PERIOD ACTIVITIES

The reaction of electrons with other substituted fulvenes will be investigated to determine the effect of substitution on spin density. Anion radicals of some purine and pyrimidine derivatives will be prepared and their structure determined. The reaction of hydrogen atoms with organic compounds will be studied as a function of temperature from -196 to +100°C. The radiolysis of substituted tetrahydrofurans will be investigated.

Program:	Physical Research Program			
AEC Task:	17, Electronic Structure of Metals and Alloys			
Project Manager:	R. G. Breckenridge			
Reporting Period:	July-September 1968			
General Order:	7713	Subaccount:	54010	AEC Category:

Principal Scientists: R. G. Breckenridge, L. J. Barnes, H. J. Fink and S. L. Wipf

I. PROJECT OBJECTIVES

This effort is devoted to the acquisition of knowledge regarding the electronic structure of metals and alloys (configuration of electronic energy states in momentum space) and the role of this structure in determining electrical, thermal, magnetic, vibrational, and alloying characteristics. Detailed information on the shape of the Fermi surface is provided by de Haas-van Alphen studies in magnetic fields up to 200 kilogauss, and the density of electronic states at the Fermi level is deduced from low-temperature specific heat measurements. The latter also yield information on lattice vibrational modes and on the interactions involved in superconductivity and magnet ordering. Further characterization of magnetic interactions is accomplished by means of conventional magnetic susceptibility techniques. Considerable effort is devoted to the exploration of high-field superconductivity with emphasis on thermodynamic and transport characteristics, and on the electron energy spectrum as deduced from thin-film electron-tunneling measurements. These experimental investigations are correlated with current theory, and attempts are made to characterize quantitatively the relationship between superconductivity and the normal-state electronic structure.

II. MAJOR ACCOMPLISHMENTS DURING FISCAL YEAR 1969

Publications

1) H. J. Fink, "Vortex Nucleation in a Superconducting Slab near a Second Order Phase Transition and Excited States of the Sheath Near H_{c3}," submitted to Phys. Rev.

2) H. J. Fink, "Nucleation of Superconductivity above H_{c3}," accepted for publication, Phys. Rev.

3) A. G. Presson and H. J. Fink, "Analog Relaxation Solution of the Non-Linear Ginzburg-Landau Equations," Proceedings of International Conf. on Analog and Hybride Computations Applied to nuclear Energy, France (1968)

4) Technical Publications to be published in a Brookhaven National Laboratory report as the Proceedings of the "Brookhaven Summer Study on Superconducting Accelerators" are

   a) S. L. Wipf, "AC Losses in Superconductors," A Review,

   b) S. L. Wipf, "Comments about Instability,"

   c) S. L. Wipf, "Instabilities and flux Annihilation," and

   d) S. L. Wipf, "Summary of the 4th Week (July 1-3) on AC Losses, Instabilities and Flux Pumps."

5) S. L. Wipf, "Review on AC Losses and AC Critical Currents," Invited paper given at the Conference on AC Properties of Superconductors and their Applications at the University of Warwick, England (1968).

III. PROGRESS DURING REPORT PERIOD

A. NUCLEATION OF SUPERCONDUCTIVITY ABOVE H_{c3}, H. J. FINK

The recent calculations of van Gelder concerning an upper critical field $H_{c4} > H_{c3}$ for a wedged-shaped specimen are discussed in the light of the surface nucleation field of a slab of finite thickness. It is shown that H_{c4} is not a new critical field and that it is related to the size dependent surface nucleation field.

B. VORTEX NUCLEATION IN A SUPERCONDUCTING SLAB NEAR A SECOND ORDER PHASE TRANSITION AND EXCITED STATES OF THE SHEATH NEAR H_{c3}, H. J. FINK

We have calculated as a function of slab thickness d the critical field at which a second order phase transition occurs, the point at which vortices nucleate in the slab ($d/\xi = 1.84$), and the size of the unit cell which contains one flux quantum (ξ is the coherence length). When $1.84 < d/\xi < 2.33$, there are two current loops of opposite circulation in one unit cell; and when $d/\xi > 2.33$, one of

the current loops splits into two loops each of which moves towards one of the surfaces as d/ξ is increased. The generalization of the order parameter H_{c3} leads directly to Abrikosov's Ansatz for the order parameter near H_{c2} when applied to bulk nucleation. The energies of the excited states of the surface sheath and the matrix elements for the transitions between the excited states and the ground state have been calculated.

C. ANALOG RELAXATION SOLUTION OF THE NONLINEAR GINZBURG-LANDAU EQUATIONS, A. G. PRESSON AND H. J. FINK

Boundary value solutions of the nonlinear Ginzburg-Landau equations have been obtained on the analog computer for both cylindrical and infinite slab geometry. A relaxation technique was used to solve the sensitive two-point boundary problem. Parametric studies were made for the transition between the superconducting and normal state in a continuous manner for a fixed number of fluxoids when the applied magnetic field was used as an independently acting variable. The relaxation technique was automated on the computer to obtain a continuous input-output operation which was controlled by the applied magnetic field. Current, energy, order parameter, and other variables of interest were computed as a function of the applied magnetic field while the latter was varied continuously.

D. SUPERCONDUCTING POINT CONTACTS, L. J. BARNES

During this period, we have carried out more studies of the superconducting point contacts. We are now in a position to write a reasonably comprehensive report for publication and this is presently being done. One of the fruitful recent studies concerns the effects of temperature variations upon the differential conductance of point contacts exhibiting tunneling behavior. The expected change of energy gap values with temperature was observed as well as changes in the sums and differences of the gaps involved. In addition to these clear cut features, considerable addition structure in the differential conductance was observed not to change with temperature. This structure is most probably associated with some form of electromagnetic geometrical resonance in or around the point contact. Most of these features are harmonically related (that is, $V_f = n V_o$, n an integer, for example) which further points to some form of geometrical resonance. We have not yet determined the precise nature

of these resonances. This is further good evidence that these junctions are behaving as weak links; that is, they are probably emitting electromagnetic radiation (AC Josephson effect) proportional to the voltage drop (V) across the junction ($w = 2\ eV/n$). When a resonant condition is reached, more power is fed into the junction; hence, the applied DC current must increase giving DC current peaks at the various resonant values of the voltage.

The actual structure of the differential conductivity is somewhat better understood by us now. Often the differential conductance exhibits a series of rather well defined peaks (as opposed to being simply oscillatory). It is not immediately obvious whether the peak itself or for example the inflection point on either side is the particular feature to index or take note of. It appears now that both situations arise. If there is a current step in the I-V characteristics, the peak itself locates the position of maximum slope; and in this case, is certainly the feature of interest. In other cases, there is obviously a peak in the current centered about some voltage value. The I-V curve is generally rising so rapidly compared to the amplitude of the peak that the I-V curve only shows a small bump. In this case, the inflection point on the side of the peak toward higher voltage is the feature of interest, since it locates the maximum in the current peak. One can convince oneself of this quite easily with some simple arithmetic or drawings. In some straight-forward cases, inspection of the I-V curve shows whether a peak or step in the current is present; and, in these cases, they index appropriately. There is almost always a step in the current at the sum of the energy gaps $[eV = (\Delta_1 + \Delta_2)]$ which is expected. At the individual gap values, Δ_1 and Δ_2, there is generally a step although at times there appears to be a peak superimposed on it. At the subharmonics of the gaps Δ/n ($n \geq 2$), a <u>peak</u> in the current distribution appears to be the rule which indicates that these features are probably due to some resonant condition of the weak link rather than multiparticle tunneling which indeed should be very small for $n > 2$. The Δ_1 and Δ_2 steps probably indicate two particle tunneling; whereas, the $\Delta_1 + \Delta_2$ step is the start of ordinary single particle tunneling.

At present, we think we have enough experimental work to present a reasonably good picture of what does take place in a superconducting point contact. We will shortly submit a report of this work for publication in the Physical Review.

E. THERMAL PROPERTIES OF SUPERCONDUCTORS, S. L. WIPF

A program to measure the thermal diffusivity of selected superconductors below the critical temperature and if possible in a magnetic field has been started. Until now, the method to be employed has been used extensively at room temperature and to over 1000°C. The adaptation of the measuring equipment to work at cryogenic temperatures has been designed.

A knowledge of the thermal diffusivity is essential in order to calculate the occurrence of magnetic instabilities. It is also interesting to compare the data with existing specific heat and thermal conductivity measurements which are very few and unreliable. The thermal diffusivity is the ratio of specific heat and thermal conductivity but is easier to measure than either of these quantities.

Comparison with theories for short mean free path effects in superconductors are also expected to produce new insights. The superconductors to be investigated are mainly Nb-Ti alloys and Nb-Zr. Pure Nb with well known specific heat and thermal conductivity may be used for testing and calibration.

IV. EVALUATION OF EFFORT TO DATE

This program has been in a somewhat transitional period involving changes in research tasks and personnel but this phase is drawing to a close. The tunneling studies on thin films has been replaced by work on tunneling and other phenomena at point contacts. It has taken some time to get oriented in this new task but by now a substantial amount of information is available and being prepared for publication. This work is proving extremely productive and, if anything, almost embarrassingly so. It seems likely that work on point contacts in superconductors will assume the same importance that they did in the field of semiconductors.

The theoretical studies continue to make excellent progress in elucidating many details of the behavior of superconductors.

The addition of Dr. Wipf to the program also adds a new topic for investigation which is just getting under way. Dr. Wipf has for some time been interested in problems of flux migration and thermal stability in superconductors. This interest combined with the availablility of some unusual apparatus has suggested a study of thermal diffusivity in superconductors. It is anticipated that interesting and useful results will be obtained from this work.

V. NEXT REPORT PERIOD ACTIVITIES

The three major tasks are expected to continue without any major changes in emphasis. Now that the preliminary learning period is over in the work in point contacts, this work should proceed at a rapid pace. The equipment and instrumentation for the thermal diffusivity studies should be operational in the next report period.

Program:	Physical Research Program			
AEC Task:	18, Radiation Damage in Crystalline Solids			
Project Manager:	R. G. Breckenridge			
Reporting Period:	July-September 1968			
General Order:	7714	Subaccount:	54040	AEC Category: 05-06-02-03.0

Principal Scientists: W. Bauer, D. W. Keefer, H. H. Neely, A. Sosin, K. H. Thommen and D. D. Vawter

I. PROJECT OBJECTIVES

The materials requirements of modern technology demand an increased understanding of the effects of lattice defects on the physical properties of crystalline solids, and on their behavior when subjected to various kinds of radiation. Studies of radiation damage in solids not only directly yield information on the effects of radiation, but also provide a means of investigating defects in solids. It is the objective of this project to study the production of defects in crystalline solids by radiation, and to attain an understanding of their structure, their interactions with each other and with impurities and dislocations, their effect on the physical properties of solids, and their recovery kinetics. Comprehension of these points should assist in the understanding of lattice defects produced in solids by other means, and help make possible the development of materials of superior properties as the ability to better control their defect structure is developed. The materials chosen for study are metals, metal alloys, and semiconductors.

II. MAJOR ACCOMPLISHMENTS DURING FISCAL YEAR 1969

Publications were as follows.

1. W. Bauer, "Stage III Recovery of Electron Irradiated Alumimum," Proceedings of International Conference on Vacancies and Interstitials in Metals, Julich, West Germany (September 1968)

2. H. H. Neely, D. W. Keefer and A. Sosin, "Electron Irradiation and Recovery of Tungsten," Phys. Stat. Sol. 28, 675 (1968)

3. K. Thommen, "Energy and Orientation Dependence of Electron-Irradiation Induced Damage in Undoped GaSb," accepted for publication in Phys. Rev.

4. D. W. Keefer, J. C. Robinson and A. Sosin, "Modulus Effects in Metals after Low Temperature Electron Irradiation - III. Aluminum," Acta Metallurgica 16, 927 (1968)

5. D. W. Keefer, "Temperature Dependence of Dislocation Pinning in Electron Irradiated Copper," a paper presented at the Symposium on the Interactions Between Dislocations and Point Defects held at A. E. R. E. Harwell, England (July 8-11, 1968) The paper will appear in a forthcoming A. E. R. E. Report.

6. D. W. Keefer, "Effects of Temperature on Dislocation Pinning in Electron Irradiated Copper," submitted to Acta Metallurgica

III. PROGRESS DURING REPORT PERIOD

A. THE STAGE III RECOVERY IN ELECTRON IRRADIATED ALUMINUM, W. Bauer

A paper entitled, "The Stage III Recovery in Electron Irradiated Aluminum" has been accepted in the Proceedings of the International Conference on Vacancies and Interstitials in Metals at Julich, Germany, KFA Conference Report, p. 275. The abstract and summary of the paper is included below.

1. Abstract

We have studied the irradiation-produced resistivity recovery of 99.9999% pure annealed and prequenched aluminum foils. The prequenched specimen exhibited two distinct recovery peaks, at 245°K and 320°K (Stage IV), whereas the unquenched specimen exhibited only one peak at 255°K (Stage III). The activation energy of the Stage III recovery, analyzed by the Meechan-Brinkman method, was found to be 0.58 eV. The order of reaction kinetics was found to be a function of the recovery. The implications of these results on existing recovery models are discussed.

2. Summary

In this paper we have presented new results and reviewed other data which bear on two recovery models for the near room

temperature recovery in aluminum. The first model considered (Model i) allows interstitial migration, restricted by impurities, in the lower temperature portion of Stage III and the beginning of vacancy migration in the higher temperature portion of Stage III. The second model (Model v) attributes the Stage III recovery solely to the migration of single vacancies.

The recovery results of the irradiated and prequench samples presented here are in good qualitative agreement with Model i. Whereas considerably different sink configurations with interstitial clusters nucleating at impurities have to be invoked for Model v. The activation energy measurements in Stages III and IV indicate similar results (necessary for Model v) but there is enough spread not to rule out a small difference. The order of kinetics are shown to be a function of recovery. The dependence being similar to what is expected from a diffusion limited bimolecular reaction. In the case considred the initial concentration of reactants differs by only 10% - - further evidence for Model i. More detailed investigations of the reaction kinetics promise to be fruitful, especially in resolving the problem of the temperature difference of Stages III and IV.

B. RESISTIVITY RECOVERY OF ELECTRON–IRRADIATED TITANIUM, W. Bauer

We have irradiated Ti near 10°K and found a recovery spectrum consisting of a number of well defined peaks located at 34, 67, 85, and 130°K. The resistivity ratio of $\rho_{4.2°K}/\rho_{0°C}$ of the material used in these experiments was only $\approx$20. This low ratio reflects the relatively high dislocation density and possibly hydrogen impurities. Unfortunately, the temperature for preirradiation annealing is limited to below that of the phase transition near 890°C. We have observed a considerable amount of super-recovery starting as low as 190°K in successive irradiations. These results are in good qualitative agreement with as yet unpublished work of Jackson and Herschbach using deuteron irradiation.

Experiments have also been conducted to ascertain whether free migration takes place in titanium near 140°K. This temperature coincides with the high temperature side of the major peak at 130°K and is thus, in analogy with the

well understood recovery spectrum of copper, a likely temperature where free migration of the interstitial occurs. By using a combination of differing dose and preirradiation at 180°K, we found evidence for the beginning of free migration near 130°K; however the effect was small. The top value on a "serpentine" plot was only 1.2 as compared to typical values of 2 for metals such as platinum, copper, and iron. The effect could be almost entirely suppressed by heating the specimens through the phase transition before the irradiation. A similar suppression of the effect was observed after deuteron irradiation when the specimens were cold-worked prior to irradiation. Both pretreatments result in larger dislocation densities and possibly more vacancies. That vacancies can suppress the free migration effect discussed above is clear, and evidence for this although not entirely unambiguous, may be found in the experiments of Jackson and Herschbach on platinum. Whether vacancies are sufficiently immobile below the phase transition temperature in titanium remains to be shown. Another interesting area of investigation is the possible connection of the low temperature super-recovery and the precipitation of dissolved hydrogen.

C. ATOMIC DISPLACEMENT PROCESSES IN GOLD, W. Bauer

We have recently reexamined results of experiments and calculations (done by Allan Anderman) designed to elucidate the displacement processes during electron irradiation of gold at low temperatures.

The major experimental result is that the energy dependence of the damage production rate in the three low index directions is similar. As a result of this, the extrapolated threshold displacement energy in the three directions is nearly the same, being approximately 36 ev.

This value of the energy is in good agreement with the results of computer calculations of $T_d(100) = 36 \pm 2$ ev. The calculations made use of a Born-Mayer potential empirically derived by Andersen and Sigmund. Dyanmic events in the (110) direction were also carried out, but due to efficient energy propagation were not carried to conclusion. Nevertheless, these incomplete results demonstrated a remarkable similarity to results of earlier calculations by the Brookhaven group on copper. Their conclusionswere that the threshold energy in copper in the (110) and (100) directions were nearly the same. Thus, in analogy, one may also conclude the same is the case in gold.

The implications of these results on existing recovery models in copper and gold are being currently investigated. Another problem currently under consideration is the question of why the experimentally measured threshold energies in the (111) direction in copper and gold are considerably lower than is indicated on theoretical grounds.

D. RECOVERY OF ELECTRON IRRADIATED ZIRCONIUM, H. H. Neely

Following the preliminary study of the recovery of electrical resistivity after electron irradiation, a more detailed study of various aspects of the annealing spectrum are being investigated. The concentration and radiation doping dependences upon the recovery of two identical high purity samples have been investigated employing the "Sosin serpentine" technique, and measuring the temperature shifts and the enhanced recovery. As was predicted in the preliminary study, a difference of concentration of a factor of ~5 shows a ratio of ~1 through 110°K; the serpentine plot then increases to ~1.6 peaked at ~123°K, then swings through 1 to bottom out at 0.3. The radiation doping study was accomplished by preirradiating then annealing the sample after the presumed free migration peak, to leave an excess concentration of vacancies. The doping temperature was 165°K. The samples in this case were then irradiated to an equal dose of ~4.1 x 10^{-8} Ω cm. The recovery of the doped sample is enhanced by about 6% in substage I_f (110 - 140°K). The serpentine plot backs up the recovery plot in that it shows a peak with a ratio of 1.5 centered at 130°K. These data strongly indicate long range interstitial migration in this temperature range and close pair recovery processes responsible for the recovery below 110°K.

The stage at 280°K exhibits a peak in the serpentine plot after the concentration dependence irradiation, indicating an order of reaction of >1. This stage is being studied in further detail.

E. SEMICONDUCTOR IRRADIATIONS

1. Semiconductor Irradiation, GaSb, K. Thommen and D. D. Vawter

Little information is available on the interaction between radiation produced defects and chemical impurities in III-V compound semiconductors. We believe that intercomparison of radiation effects in undoped and doped materials will aid

a better understanding of this important subject matter. As a first step, we have studied the effects of low temperature electron irradiation on the electrical properties of GaSb doped with Zn. From the room temperature carrier concentration, we estimate the Zn-concentration as $2 \times 10^{17} cm^{-3}$. Irradiations were performed with 1.0 Mev electrons while the sample temperature was held below 15°K. The radiation induced changes of the carrier concentration and the mobility and the recovery of these quantities upon isochronal annealing were essentially the same as those in the undoped material with the following notable exceptions:

1) A small reverse recovery state (5% of the total radiation induced change) occurred between 50 and 60°K, and

2) The center temperature of stage IV was 25°K higher in the Zn-doped material.

The results indicate that the defects which are removed in Stages I, II, and III do not interact with the Zn atoms; whereas, the Stage IV defects do. The fact that only the temperature location but not the size of Stage IV is affected by the presence of the Zn atoms suggests that the interaction occurs during annealing in the Stage IV temperature range. The origin of the small reverse recovery stage at 55%K in the Zn doped material is not understood at the present time, and further work is required before an interpretation can be attempted.

A preliminary isothermal annealing study revealed that stage II recovery obeys first order kinetics in the Zn-doped material. First order kinetics was not observed for Stage II in the undoped material. This may be due to the fact that the Fermi level remains essentially fixed during the annealing in the Zn-doped material but moves somewhat towards the middle of the gap in the undoped material. First order kinetics of the Stage II recovery supports the interpretation of this stage as recombination of close Ga interstitial vacancy pairs. If the recombination rate is charge state dependent (as has been found for stage II recovery in InSb), a change of the Fermi level position during the recovery will affect the recovery kinetics.

2. Semiconductor Irradiations, GaAs, K. Thommen and D. D. Vawter

Careful isochronal annealing studies with n-type GaAs after low temperature 1 Mev electron irradiation revealed a small recovery of the resistivity

(1% of total radiation induced resistivity change) in the range 80 to 100°K, followed by an equally small reverse recovery between 100 and 130°K. If a sample is annealed isochronally from 80 to 130°K, then illuminated with white light, and subsequently subjected to a second isochronal annealing from 80 to 130°K, the 1% "dip" in the resistivity recovery is observed again during the second annealing. It is therefore attributed to "reversible" electronic processes, and does not correspond to irreversible recovery of atomic defects.

Preliminary isothermal annealing studies were made of the recovery stages which peak at 237 and 280°K. A new technique was employed, in which the electrical properties are measured at the annealing temperature. This allows frequent measurements of the defect monitoring quantities, and avoids errors due to the finite temperature rise and cool down times which are unavoidable when the measurement are made at a reference temperature different from the annealing temperature. If the change of the defect monitoring properly which occurs in a given recovery stage is small compared with the value after completion of the recovery, it can be hoped that in the expression

$$q(\eta_i) = q_o + q_1 \eta_i + q_2 \eta_i^2 + \ldots,$$

quadratic and higher order terms can be neglected. Here, q stands for the defect-monitoring quantity, and η_i is the concentration of the defects, which are removed (or relocated) in the i^{th} recovery stage. In our isothermal annealing experiments, $(q - q_o)/q_o$ was ≤ 0.07. The results indicated that both for the 237 and the 280°K stage, the recovery obeyed first order kinetics with the exception of an initial period being about 0.3 life times long. During this initial period, the recovery proceeded slightly faster so that extrapolation of the exponential decay observed for long annealing times intersected the ordinate $t = 0$ at a value $\sim$10% smaller than the actual initial value. A computer executed least square fit revealed that the experimental data can not be represented satisfactorily by the sum of two exponentials. The reason for the initial deviation from first order kinetics remains unclear at the present time.

F. MODULUS CHANGES AT LOW TEMPERATURES DISLOCATION PINNING IN METALS, D. W. Keefer AND J. C. Robinson

1. Dislocation Pinning in Copper

A paper titled, "Effects of Temperature on Dislocation Pinning in Electron Irradiated Copper" has been submitted to Acta Metallurgica. The abstract is as follows.

A study has been made of the effect of temperature on the number of dislocation pinners produced in copper by electron irradiation. The electron doses were kept low so that very small numbers of point defects were produced. Two irradiation techniques were employed. One (the "direct" procedure) simply involved irradiation at 77, 125, or 150°K. In the other (the "alternate" procedure), the sample was alternately irradiated at 77°K and annealed at either 125 or 150°K. In both procedures, modulus and internal friction measurements were made at 4.2 and/or 77°K.

If the alternate procedure is employed, measurements at 77°K show that the number of pinners is less following an anneal than it was immediately after the 77°K irradiation. On the other hand, measurements at 4.2°K show that a net increase in pinner occurred during this same anneal. It is suggested that these results are evidence that different portions of the dislocation population are being used at 77 and 4.2°K to monitor the pinner density and that the behavior of point defects on these dislocation groups is different.

An enhancement of pinning at 77°K is observed after an anneal or irradiation at 125 or 150°K. These enhancement effects are observed only in samples exhibiting a well-defined relaxation peak at 80°K (frequency ~300 cps) and can be observed at measuring temperatures between 40 and 150°K. This is the temperature range over which the relaxation peak occurs. These results are discussed in terms of a model in which enhanced pinning occurs because of a distribution of Stage I interstitials on dislocations.

Enhancement of modulus Stage III (200 - 250°K) is observed following irradiation at 150°K over that after irradiation at 77°K.

This result is discussed in terms of the possible conversion of Stage I to Stage III type interstitials.

2. Dislocation Pinning in Silver

The study of dislocation pinning in silver is continuing. A sample of 6 9's purity has been irradiated at 4.2°K with 1.5 Mev electrons. Isochronal annealing results obtained up to about 200°K are virtually identical to those obtained on a sample of 5 9's purity: a pinning stage between 30 and 50°K followed by a series of three pinning stages between 60 and 200°K. Since one or more of these latter stages may be due to dislocation pinning by defects released from impurity traps, a careful analysis of the impurity content in the samples will be made. These results are of considerable interest since in no other metal have we observed pinning effects which could be ascribed to defects released from traps.

IV. EVALUATION OF EFFORT TO DATE

This program is making unusually satisfactory progress at present. A new level of understanding of the fundamental aspects of the radiation damage in the previously studied fcc metals is being attained largely through an interaction between theory and experiment. The application of the calculations of the displacement behavior in gold done previously by A. Anderman on this program (also supported by Cambridge Air Force Research Lab) to an interpretation of the experimental results is proving very instructive and apparently will aid in the interpretation of the results for other metals. The extension of the experimental work to the bcc and hcp metals is also progressing satisfactorily. The results tend to be more complex than in the fcc metals but it is anticipated that the analysis of the results will proceed rapidly based on the information previously obtained.

The mechanical property studies are making steady progress on the complex problem of dislocation pinning. A reasonably satisfactory model for the situations in copper has been produced and it is anticipated that similar results will be obtained for silver.

The semiconductor studies are also progressing well. The work on GaSb is now concerned with the interactions of the electronic properties of the material with the radiation produced defects and is proving very illuminating. This

work has been extended to GaAs. In view of the technical importance of GaAs in solid state devices of various types this work may have considerable practical significance.

V. NEXT REPORT PERIOD ACTIVITIES

In general no major changes in the program are planned. The studies on radiation effects in metals will continue with increasing emphasis on the bcc and hcp metals. The mechanical property studies will continue on silver and this work may be completed during the next period. The semiconductor studies will be continuing with a possibility of completing the work on GaSb during this period.

Program:	Advanced Development		
AEC Task:	22, Radiation Chemistry of Chromosomes		
Project Manager:	R. A. Holroyd		
Reporting Period:	July-September 1968		
General Order: 7724	Subaccount: 17001	AEC Category:	06-04-00-00.0

I. PROJECT OBJECTIVES

The long range objective of this study is to obtain information which will correlate molecular alterations with biological damage to mammalian chromosomes, caused by radiation. The immediate objective is a better understanding of the radiation chemistry of chromosomes and their main constituents, nucleic acids and proteins.

II. MAJOR ACCOMPLSIHMENTS DURING FISCAL YEAR 1969

The paper by R. A. Holroyd and J. W. Glass, "Radicals Formed by Electron Transfer to Pyrimidine Derivatives," International J. Rad. Biol., has been accepted for publication.

III. PROGRESS DURING REPORT PERIOD

A. TRITIUM LABELING OF RADICAL SITES IN IRRADIATED CHROMOSOMES

Studies have begun to determine radical sites in irradiated chromosomes by tracer techniques. The radical sites will be labeled by reacting tritium-labeled H_2S with the chromosome sample subsequent to exposure to ionizing radiation or atom bombardment.

$$R. + H_2S \rightarrow RH + HS \qquad \ldots(1)$$

Prior ESR studies had indicated that gamma irradiation as well as hydrogen atom bombardment of chromosomes, cell nuclei, and nucleoprotein resulted in radical formation in the protein component. Preliminary tests with nonradioactive H_2S have shown that radicals formed in nucleohistone samples react

readily with H_2S, Reaction 1, and that 75% of the radicals are destroyed rapidly in a period of about 4 min. Construction of special vacuum equipment necessary for handling tritium-labeled H_2S is complete, and the tagged material has been ordered.

B. REACTION OF HYDROGEN ATOMS WITH DEOXYRIBOSE-5-PHOSPHATE

The reaction of hydrogen atoms with deoxyribose-5-phosphate was investigated for comparison with deoxyribose, and to evaluate the extent of sugar attack in DNA. The deoxyribose-5-phosphate is a better model compound since it has the same 5-membered ring as is present in DNA; whereas, pure deoxyribose has a 6-membered ring. This structural change could affect the ESR spectrum of the radicals formed. Deoxyribose-5-phosphate was found to be reactive toward hydrogen atoms, and the ESR spectrum obtained indicated that the same radicals were formed as in deoxyribose but in different proportions. In the former compound, the principal radical, which accounts for 70% of the spectrum, is one in which the unpaired electron interacts strongly with only one proton; this radical accounts for only 40% of the radicals in deoxyribose. Most probably, a hydrogen atom is abstracted from the 1 or 5 position.

C. REACTION OF HYDROGEN ATOMS WITH DNA

A new analysis of the ESR spectrum obtained by bombardment of DNA with hydrogen atoms has been made, into which the deoxyribose-5-phosphate results have been incorporated. The spectrum was analyzed by a computer method which determined the percentage of radicals formed on each base and on deoxyribose in DNA. The results showed that at room temperature hydrogen atoms react 40% of the time with the purine bases, 25% of the time with thymine, and approximately 15% with cytosine. Thus, hydrogen atoms react 80% of the time by addition to bases and 20% by abstraction from deoxyribose groups. A paper describing these results is being prepared.

The reaction of hydrogen atoms with DNA is being studied as a function of temperature. Results to date indicate that thymine base attack becomes of minor importance, but other bases are attacked at -80°C. At -196°C, the DNA is unreactive.

D. REACTIONS OF ELECTRONS WITH NUCLEIC ACID BASES

The existence of the electron as an intermediate in gamma radiolysis is well established. In the case of compounds containing DNA, it is also expected that electron attachment to the nucleic acid bases to form anions will occur. It is therefore of interest to elucidate the reactions of such anions. One such reaction, the rapid protonation of the thymine anion, has been demonstrated (R. A. Holroyd and J. W. Glass, Internatl. J. Rad. Biol., in press). The reactivity of anions can be predicted from the electronic structure; i.e., the location of the electron in the anion. To determine this structure, we are studying the anions of nucleic acid bases by ESR spectroscopy under conditions of high resolution. An electrolytic technique is being used to generate the anions. Results obtained so far show that purine can be electrolytically reduced to its anion in dimethylformamide. The ESR spectrum of the purine anion is being analyzed. Anions of other purine and pyrimidine bases will be investigated by this technique.

IV. EVALUATION OF EFFORT TO DATE

The tritium labeling experiments are underway. Initial tests showed that the titration with H_2S is feasible and that labeling can be accomplished with the tritiated reagent. The study of the reaction of hydrogen atoms with DNA at 25° is now complete. It is shown that bases react more readily than deoxyribose; the DNA bases are attacked to an extent which is roughly proportional to the percentage of each base present. The ESR studies of DNA base anions, which are now underway, look very promising and should provide insight into the role of electron reactions in the radiolysis of DNA.

V. NEXT REPORT PERIOD ACTIVITIES

During the next report period, chromosomes and cell nuclei will be exposed to ionizing radiation and hydrogen atom bombardment. The radicals thus formed will be titrated with T_2S and the samples analyzed to determine the percentage of damage in the various components.

The reaction of electrons with the various DNA bases will be investigated by the electrolytic technique. From this study, predictions about the modes of reaction of the anions can be made.

Further studies of the interesting temperature effect in the reaction of hydrogen atoms with DNA will be made. A study of the reaction of hydroxyl radicals with DNA and its components will be made.

Program: LMFBR Component Development
AEC Task: 25, Noise Analysis Instrumentation
Project Manager: C. W. Wheelock
Reporting Period: July-September 1968
General Order: 7757 Subaccount: 53100 AEC Category: 04-40-03-01

Principal Investigator: R. L. Randall

I. PROGRAM OBJECTIVES

The objective of the program is demonstration of the feasibility of liquid metal flow rate measurement by use of noise analysis techniques, and development of an operating instrument for use in calibration of, and as an alternative to, other flow measurement methods. The technique involves detecting small temperature variations (thermal eddies) at two points in the flowing stream. The two signals are cross-correlated with a variable delay time. The delay time which gives maximum correlation is the transit time of the fluid between the sensors.

Two methods for detecting the thermal eddies are being investigated, thermocouples with matched response time, and electrical conductivity probes. The latter technique has the advantages of simplicity and fast, localized response.

The first phase of the development program is the experimental demonstration of the conductivity cell cross-correlation method in a water loop. The objective of this phase is to establish the accuracy of the method in cylindrical flow sections and to determine variations of uncertainty with flow rate, fluid density, viscosity, and channel size.

The second phase of the program is similar to the first phase except that water flow rates will be measured by the use of thermocouples.

The third and fourth phases are extensions of Phases 1 and 2 to a liquid metal system.

II. MAJOR ACCOMPLISHMENTS DURING FISCAL YEAR 1969

One test run was completed in the water loop with the 2-in. diameter test section instrumented with conductivity sensors at five axial locations, and thermocouples at two radial positions and two axial locations. Auto-correlation plots were obtained for four thermocouples and five conductivity

sensors for each of 25 test runs. Cross correlation plots were obtained relating 7 sensor pairs for each of these tests. Factors relating amplitude decay and bandwidth of signals created by thermal eddies as they pass thermocouples and conductivity sensors have been obtained as functions of flow, temperature, and sensor position from autocorrelation measurements. Transit time measurements obtained by cross correlation of sensor signals were related to average flow velocity measurements obtained by volumetric measurement as functions of sensor pair position, flow, and temperature. The data reduction and analysis of this test is approximately 50% completed.

The second test section instrumented with 26 thermocouples arranged on two moveable fins was installed, and testing was started. Cross correlation plots have been obtained relating selected fin thermocouples from 20 tests conducted to date with the second test section. The data reduction effort for this test is approximately 10% complete at this time.

The following tentative conclusions are implied from cross correlation of signals from single and dual electrodes and in-stream TC's, used with the 2-in. diameter test section and a single wall injection port located about 10 pipe diameters up-stream from the first electrode.

1) No significant difference was detected between signals from dual or single electrodes with regard to correlation, transit time, amplitude or bandwidth.

2) Changes in the ratio of measured to average flow velocity with temperature, were not detectable within the measurement precision of these tests.

3) Measured to average flow velocity (averaged over all electrodes) showed some tendency to decrease with flow, 2 to 4%, due to a flow increase of 800%.

4) The ratio of measured to average flow velocity appears to show an essentially linear increase, with distance from the injection port, varying from about 0.98 to 1.068 over a distance of about 15 pipe diameters. The cause of the effect is being investigated.

Test sections with 1-1/2-in. and 1-in. diameters have been fabricated for later use in determining effects of cylinder size on sensor and measurement parameters.

III. PROGRESS DURING REPORT PERIOD

Work began on parametric testing with conductivity sensors and thermocouples. Detailed descriptions of test sections, instrumentation, and the test loop are given in Reference 1. Test parameters planned include flow velocities ranging from about 1.5 to 16 ft/sec; water temperatures of 86 and 120°F; several types of conductivity sensors at five axial positions; in-stream thermocouples at various radial and axial positions; and pipe diameters of 2, 1-1/2, and 1 in., respectively. Sensor signals are tape recorded for later replay: (1) for autocorrelation or power spectra to study amplitude decay and decay time constants versus sensor position and hydraulic conditions, and (2) for degree of correlation and transit time relating various sensors to study eddy propagation, deterioration, size, and velocity versus sensor positions and hydraulic parameters.

Parametric tests were to have been conducted first with test sections instrumented with conductivity sensors, and later with test sections instrumented with thermocouple fin assemblies. Some of the electrodes, however, were removed and replaced by TC's which permitted simulatneous testing with conductivity and temperature sensors. Temperature sensors were fabricated by inserting 20-mil thermocouples into 20-gauge hypodermic needles to provide mechanical support for the TC's. The TC junction extends 3/32 in. beyond the end of the needle. Solder was used to seal the outer end, and Conax Packing Glands are used to permit installation of the sensors at desired in-stream depth which makes it possible to map the velocity profiles.

Results from a loop demonstration test on 7/29/68, using the dump tank system to measure flow rate, indicated that a measured transit time of 12.2 ms/ft corresponds to a flow rate of 1.432 gal./sec (about 86.0 gpm). For the particular sensors and test conditions, the measured to average flow velocity was determined from the preliminary data to be 1.01. This slightly higher than average eddy velocity is a function of the "effective" cross sectional area of the flow channel and the range of sensitivity of the sensor. The parametric tests are designed to relate this factor to various pipe sizes, sensor configurations, flow rates, and temperatures.

Parametric testing with a 2-in. test section was initiated on 8/2/68, with a series of tests designed to provide data relating: temperature sensors at selected radial positions, four types of conductivity sensors at each of five axial positions, four different flow velocities, and two temperature conditions. Flow conditions were set up by using the CRT display of the Signal Correlator output as a flow meter. Signals from two sensors, one foot apart, were correlated, and the transit time relating them was determined from the CRT display. Signals from conductivity sensors at five axial locations, and four thermocouples at two in-stream depths were recorded in both filtered and unfiltered form by using two FM tape recorders. Hot water injection was used to induce signals for both condductivity and temperature sensors. Tests were conducted at nominal flow velocities of 16, 8, 4, and 2 ft/sec, and at water temperatures of 86 and 120°F. This corresponds to variations in Reynolds number from 40,000 to about 400,000. This series comprised a total of 25 tests.

The signal correlator was used to obtain autocorrelation plots from tape recorded signals from the 4 thermocouples and 5 conductivity sensors for each of the 25 test runs. Cross correlation plots were also obtained relating 2 thermocouple pairs and 5 electrode pairs for each test. The autocorrelation plots were used to determine the mean square amplitude of the sensor output and the decay time constant of the sensor signal. The latter is related to the half power bandwidth of the signal. The analysis and evaluation of these data have been about 50% completed.

The following observations have been made from autocorrelation analyses of signals from dual and single in-stream electrodes and from in-stream thermocouples for a 2-in. diameter test section and a single wall injection port located about 10 pipe diameters upstream from the first electrode.

1) The amplitude of signals from electrodes extending across the diameter of a test section decreases with distance at a rate of approximately one decade per 13.5 pipe diameters; whereas, the amplitude of signals from in-stream TC's decreases at a rate of approximately one decade per 40 pipe diameters. This difference reflects the averaging effect of the electrode, with its larger feeling range.

2) The decay time constant increases (bandwidth decreases) at a rate of approximately one octave per 17 pipe diameters for electrode signals, as compared to approximately one octave per 36 pipe diameters, for thermocouple signals.

3) With electrodes spaced over a range of 22 pipe diameters apart, the half power bandwidth of signals varies from about 1.5 Hz at the last electrode at a flow velocity of 1.9 ft/sec, to about 17 Hz at the first electrode at a flow velocity of 14.3 ft/sec. For center-of-stream thermocouples separated about 6 pipe diameters apart, the half power bandwidth of signals varies from about 1.8 Hz at the last TC at a flow velocity of 1.9 ft/sec, to about 3.6 Hz at the first TC at a flow velocity of 7.9 ft/sec.

4) If it is assumed that the measured decay time constant represents the average time for eddies to pass a given sensor, the product of flow velocity and decay time constant should indicate the average length of thermal eddies. For electrode signals, this product approximately doubles each 13.5 pipe diameters for any given flow rate. For a given electrode, this product varies at a rate approximately proportional to the one-fourth power of flow. Similarly, the average length of thermal eddies varied from about 0.75 in. at the first electrode at 1.9 ft/sec, to about 4 in. at the last electrode at 14.3 ft/sec with about a 22-pipe diameter distance between electrodes. Studies of eddy length and width at various axial and radial positions are planned by use of data from the thermocouple fin assemblies in the second test section.

The delay times corresponding to the peak in the cross correlation plots from five electrode pairs and two pairs of TC's were obtained manually by using a graphical method. The resolution of this manual technique varies from 0.2 to 2%, depending on the ratio of decay time constant of sensor signals to distance between sensors. The lower the ratio, the higher the resolution.

The partial evaluation of these data, which has been completed to date, leads to the tentative conclusions given in Section II. With regard to Item 4, it was noted that the ratio of indicated to average flow velocity showed an

essentially linear increase with distance from injection port, from about 0.98 to 1.068 over a distance of about 15 pipe diameters. Relocation of the hot water injection point and changes in the injection characteristics did not appear to change this effect. Other causes for this effect will be investigated, including the possibility that the flow straightener near the test section inlet flattens the velocity profile, and that the observed effect may be due to the development of a new profile in the test section.

The second test section, instrumented with 26 thermocouples arranged on two movable fins, was installed, and testing was started before the anomilies with sensor positions were known. Preliminary cross correlation analysis of TC signals from these showed similar effects. Further tests are planned with geometrical changes in the test loop, including changes in relative position and construction of the flow straightener.

Design development of the prototype system for on-line transit time measurement was initiated. Three basic designs are being considered. One uses analog integrators and divider circuits to calculate the center of gravity of the cross correlation function. The second uses logic circuitry to simulate the graphical method of determining transit time. The third uses the method of the second design to locate and continuously track the peak of the cross correlation function and provides a continuous oscillator output signal whose frequency is proportional to fluid transit rate.

Work was completed on fabrication of 1-1/2- and 1-in. diameter test sections for conductivity sensors. Electrode configurations are identical on all three test section sizes. Provisions were made to install movable TC's in these test sections at 7 axial positions.

IV. EVALUATION OF EFFORT TO DATE

Parametric tests conducted to date have demonstrated the feasibility of the correlation flow measurement technique with both conductivity sensors and thermocouples. The signal correlator has been used to effectively set-up and monitor flow conditions on-line during tests. Results obtained indicate that the factor relating measured transit rate to average flow velocity for each pair of sensors is independent of temperature, flow conditions, injection methods, and that it is essentially constant. Data relating amplitude and bandwidth of sensor output versus flow and sensor position will be useful in designing future tests and applications.

V. NEXT REPORT PERIOD ACTIVITIES

Tests will be conducted to determine factors affecting measured to average flow ratios. Parametric tests with the thermocouple fin assemblies and the 1-1/2- and 1-in. diameter test sections will be completed. Work will begin on modification of the signal correlator to provide automatic readout of transit time or transit rate. Preliminary planning will be initiated for demonstration tests in an existing sodium or NaK test loop.

References

1. R. L. Randall, "Noise Analysis Instrumentation," Annual Technical Progress Report, AEC Unclassified Programs, Fiscal Year 1968, July 1968, pages 363, 381. AI-AEC-12721